

SIGNALING BY NON-CANONICAL RECEPTOR TYROSINE KINASES

ERBB3 AND RYK

Fumin Shi

A DISSERTATION

in

Biochemistry and Molecular Biophysics

Presented to the Faculties of the University of Pennsylvania

in

Partial Fulfillment of the Requirements for the Degree of Doctor of Philosophy

2012

Supervisor of Dissertation

Mark A. Lemmon

Professor and Chairman of Biochemistry and Biophysics

Graduate Group Chairperson

Kathryn M. Ferguson, Associate Professor of Physiology

Dissertation Committee

Kathryn M. Ferguson, Associate Professor of Physiology

Gregory D. Van Duyne, Professor of Biochemistry and Biophysics

Ronen Marmorstein, Wistar Institute Professor of Chemistry, Biological Chemistry

Marcelo G. Kazanietz, Professor of Pharmacology

Ravi Radhakrishnan, Associate Professor of Bioengineering

Jeffrey R. Peterson, Associate Professor at Fox Chase Cancer Center

ACKNOWLEDGMENT

This dissertation would not have been possible without the support of many people.

I would like to first express my deepest gratitude to my supervisor, Mark Lemmon, for his excellent mentorship over the years, for allowing me to freely pursue my research interest, and for all the encouragements and understanding.

To Sung Hee Choi, Katarina Moravcevic, Diego Alvarado, Jon Kenniston and Daryl Klein, for being excellent teachers at the beginning of my graduate research and tolerating my naivety.

To Jeannine Mendrola, for her instructions during my early rotation in the Lemmon lab, for her support, help and ear-penetrating laughter.

To Lemmon lab people: Pam Jones, Nick Bessman, Steve Artim, Scott Bresler, Jin Park, Neo Wu, Camilla Oxley, Jason Moore, for creating a wonderful environment and cheering me up when my experiments fail – which happens 90% of the time.

To Kate Ferguson, for being a great committee chair. To Yu-San Huoh, for all the help with my experiments in the Ferguson lab. And to Steve Stayrook and Karl Schmitz, for setting up the computer systems in the lab – over and over again.

To my thesis committee members: Greg Van Duyne, Ronen Marmorstein and Marcelo Kazanietz, for their guidance and support during my graduate study.

To my dear wife, Wenting Li, for her love that supports me every day. And to my parents, for believing in me at every step of my life.

ABSTRACT

SIGNALING BY NON-CANONICAL RECEPTOR TYROSINE KINASES

ERBB3 AND RYK

Fumin Shi

Mark A. Lemmon

Signaling by receptor tyrosine kinases (RTKs) typically involves binding of extracellular ligands and subsequent activation of intracellular kinase domain, which in turn mediates autophosphorylation and downstream signal transduction. However, several RTKs, such as ErbB3 (HER3) and Ryk/Derailed, lack key conserved (and catalytically important) residues in their intracellular kinase domain, and are thought to be inactive ‘pseudo’-kinases. Much less is known regarding how these receptor tyrosine ‘pseudo’-kinases mediate transmembrane signaling. The work described in this dissertation attempts to understand the non-canonical signaling by ErbB3 and Ryk/Derailed using a combination of biophysical, biochemical and cell biology methods.

ErbB3 is one of four members of the human epidermal growth factor receptor (EGFR) family. ErbB3 signals primarily by heterodimerizing with ErbB2 (HER2) and mediates resistance of tumor cells to EGFR/ErbB2-targeted therapeutics. We have investigated the role of ErbB3 ‘pseudo’-kinase domain in its signaling. *In vitro* enzymology study shows that, despite the sequence alterations, ErbB3 kinase domain binds ATP with high affinity and possesses weak kinase activity to *trans*-autophosphorylate its intracellular region. We also describe a crystal structure of ErbB3 kinase, which resembles the inactive EGFR and ErbB4 kinase domains. Whereas

mutations that destabilize this configuration activate EGFR and ErbB4 (and promote EGFR-dependent lung cancers), a similar mutation conversely compromises ErbB3's ability to activate downstream Akt signaling in our cellular studies. These findings suggest that ErbB3 kinase may be crucial for signaling and could represent an important therapeutic target.

Ryk and its *Drosophila* homolog Derailed (Drl) contain an extracellular Wnt Inhibitory Factor (WIF) domain and participate in non-canonical Wnt signaling. We attempt to understand, for the first time, the molecular mechanism of Ryk/Drl-Wnt interaction using Drl as a model system. We show that Drl binds directly to *Drosophila* Wnt5 (DWnt5) with submicromolar affinity using surface plasmon resonance (SPR). X-ray crystallography study has identified a conserved binding site of Drl for DWnt5. Mutating this site abolishes DWnt5 binding by Drl. This study serves as a starting point for our understanding of Wnt signaling by Ryk/Drl at a molecular level.

Table of Contents

Title Page.....	i
Acknowledgment.....	ii
Abstract.....	iii
Table of Contents.....	v
List of Tables.....	ix
List of Illustrations.....	x
Main Text	
Chapter 1: Characterization of ErbB3 Tyrosine Kinase Domain.....	1
1.1 Introduction to Receptor Tyrosine Kinase ErbB3.....	2
1.1.1 Overview of ErbB Family Receptor Tyrosine Kinases.....	2
1.1.2 Introduction to ErbB3 Signaling.....	4
1.1.3 ErbB3 in Cancer Development and Corresponding Therapeutics.....	5
1.1.4 Structure and Biochemistry of Tyrosine Kinase Domains.....	10
1.1.5 ErbB3, a Heretical Kinase with Changes at Conserved Catalytic Residues in TKD.....	14
1.1.6 Summary.....	16

1.2	<i>In vitro</i> Characterization of the Enzymatic Activity of ErbB3 TKD.....	17
1.2.1	Autophosphorylation of the Purified ErbB3 Intracellular Domain.....	17
1.2.2	ErbB3 TKD Fully Retains ATP Binding Ability.....	23
1.2.3	Inhibitor Profiling of ErbB3 Kinase.....	27
1.3	Structural Characterization of ErbB3 Kinase Domain by X-ray Crystallography.....	30
1.4	Cellular Studies to Investigate the Role of ErbB3 Kinase Domain in ErbB Signaling.....	39
1.4.1	Effect of ErbB3 mutations on Autophosphorylation of ErbB2/ErbB3 Heterodimers in BaF3 Cells	41
1.4.2	Mutations within the ErbB3 Kinase Domain Affect its Ability to Activate Akt Signaling in CHO Cells.....	44
1.5	Summary and Discussion of ErbB3 Studies	53
1.6	Experimental Procedures for Chapter 1.....	63
	Chapter 2: Characterization of Derailed-Wnt Interactions.....	68
2.1	Overview of Ryk/Derailed – Wnt Signaling Pathway.....	69
2.1.1	Introduction to Wnt proteins and Wnt Pathway.....	69
2.1.2	Introduction to Ryk/Derailed Family Receptor Tyrosine Kinases.....	73

2.1.3	Introduction to Human Wnt Inhibitory Factor-1 (hWIF-1)	75
2.1.4	Ryk/Drl Interact with Wnts and Mediate Wnt Signaling.....	78
2.1.5	The Pseudokinase Domains of Ryk/Drl Lack Kinase Activity but are Capable of Signal Transduction.....	81
2.1.6	Biophysical Characterization of Drl-DWnt5 Interactions as a Model System for Ryk/Drl Signaling.....	83
2.2	Biophysical Characterization of Derailed-DWnt5 Interactions.....	85
2.2.1	Expression, Purification and Characterization of <i>Drosophila</i> Derailed and DWnt5 Proteins.....	85
2.2.2	Analysis of Derailed-DWnt5 Interactions by <i>in vitro</i> Pull-down and SPR.....	91
2.3	Structure Determination of the Derailed-2 Extracellular Region.....	99
2.4	Structure-Guided Point Mutations in the Derailed Extracellular Region Disrupt its Binding to DWnt5.....	106
2.5	Summary and Discussion of Derailed-DWnt5 Studies.....	112
2.6	Experimental Procedures for Chapter 2.....	116
Appendices		
Appendix 1	List of Kinase Inhibitors Used in Chapter 1.2.3.....	123

Appendix 2	A Chemical Genetic Approach to Study ErbB Signaling in Cells.....	126
2.1	Using Bumped Inhibitors to Selectively Inhibit Cellular Signaling by Analog-sensitive ErbB Mutant.....	129
2.2	Using Bumped ATPs as Preferred Substrates for Analog-sensitive ErbB Kinase.....	136
	Bibliography.....	143

List of Tables

Table 1.1: ErbB3 TKD crystallographic statistics (molecular replacement).....	31
Table 2.1: SPR studies of different sDrl variants binding to DWnt5.....	95
Table 2.2: SPR studies of Drl homologs binding to DWnt5.....	98
Table 2.3: Derailed-2 extracellular domain crystallographic statistics (molecular replacement)	100
Table 2.4: SPR studies of DWnt5 binding property of Drl ectodomain proteins (residue 1-242) with single point mutation.....	110

List of Illustrations

Figure 1.1: Scheme of ligand induced ErbB activation.....	3
Figure 1.2: Structural features of tyrosine kinase domain.	13
Figure 1.3: Autophosphorylation of the ErbB3 Intracellular Domain <i>in vitro</i>	20
Figure 1.4: Quantitation of ³² P incorporation into ErbB3-ICD by the kinase domains from ErbB3 or EGFR.	22
Figure 1.5: Mant-ATP Binding to ErbB3-TKD ⁶⁴⁸⁻¹⁰⁰¹	25
Figure 1.6: Inhibitor Profiling of ErbB3 Kinase.	29
Figure 1.7: Cartoon representation of the crystal packing of ErbB3-TKD.	32
Figure 1.8: Crystal structure of ErbB3-TKD.	34
Figure 1.9: QM/MM simulations of phosphoryl transfer of ErbB3 and EGFR kinases...38	
Figure 1.10: Autophosphorylation of ErbB2 and ErbB3 in ligand-induced ErbB2/ErbB3 heterodimers in BaF3 cells.	43
Figure 1.11: ErbB3 mediates neuregulin induced Akt activation in CHO cells.	46
Figure 1.12: V836R and L839Q double mutation in ErbB3-TKD impairs its ability to activate Akt pathway in CHO cell.	48
Figure 1.13: V836R and L839Q double mutation impairs the ability of an EGFR/ErbB3 chimeric protein to activate the Akt pathway in CHO cells.	50
Figure 2.1: Overview of Wnt signaling.	72
Figure 2.2: Domain organization of Ryk and Derailed.	74
Figure 2.3: Reported structures of human Wnt Inhibitory Factor -1 (hWIF-1).	77
Figure 2.4: Sequence alignments of WIF domains.	79
Figure 2.5: Characterization of recombinant Derailed extracellular region.	86
Figure 2.6: Characterization of DWnt5 protein.	90
Figure 2.7: Drl ectodomains are capable of pulling down DWnt5 from conditioned medium.	92
Figure 2.8: SPR studies of sDrl proteins binding to DWnt5 variants.	94
Figure 2.9: SPR studies of DWnt5 binding to <i>D. melanogaster</i> Drl homologs.	97
Figure 2.10: Crystal structure of sDrl-2 extracellular domain.	103
Figure 2.11: Crystal packing of sDrl-2.	105
Figure 2.12: Surface conservation of Drl WIF domain homology model.	107
Figure 2.13: SPR studies to characterize the effect of point mutations in sDrl (1-242) on binding to immobilized DWnt5 wildtype protein.	109

Chapter 1

Characterization of ErbB3 Tyrosine Kinase Domain

1.1 Introduction to Receptor Tyrosine Kinase ErbB3

1.1.1 Overview of ErbB Family Receptor Tyrosine Kinases

Human ErbB receptor tyrosine kinases (RTKs), including ErbB1 (EGFR), ErbB2 (HER2), ErbB3 (HER3) and ErbB4 (HER4), are type I transmembrane proteins that mediate cellular responses to an array of extracellular ligands (Yarden and Sliwkowski 2001; Hynes and MacDonald 2009). Each receptor contains an extracellular ligand binding region, a single transmembrane helix, and an intracellular tyrosine kinase domain (TKD) that is flanked by juxtamembrane and C-terminal regulatory regions (Baselga and Swain 2009; Hynes and MacDonald 2009) (Figure 1.1, left). Upon ligand binding to the extracellular region, ErbB receptors undergo homo- or hetero- dimerization (Lemmon 2009), bringing their intracellular TKDs close to each other. The proximity of the intracellular domains (ICD) induces allosteric trans-activation of enzymatic activity, mediating the phosphoryl transfer of ATP γ -PO₄ to the side chain of multiple tyrosines on the receptor's C-tail (Zhang, Gureasko et al. 2006; Jura, Endres et al. 2009; Red Brewer, Choi et al. 2009). Phosphorylation of tyrosines creates docking sites for recruitment of various signaling molecules, which activates downstream signaling cascades (such as MAPK and Akt pathways) and ultimately triggers cell proliferation and survival (Yarden and Sliwkowski 2001) (Figure 1.1, right). In a pathological setting, aberrant ErbB signaling via either ErbB protein overexpression or mutation plays an important oncogenic driver role in the development of various cancers.

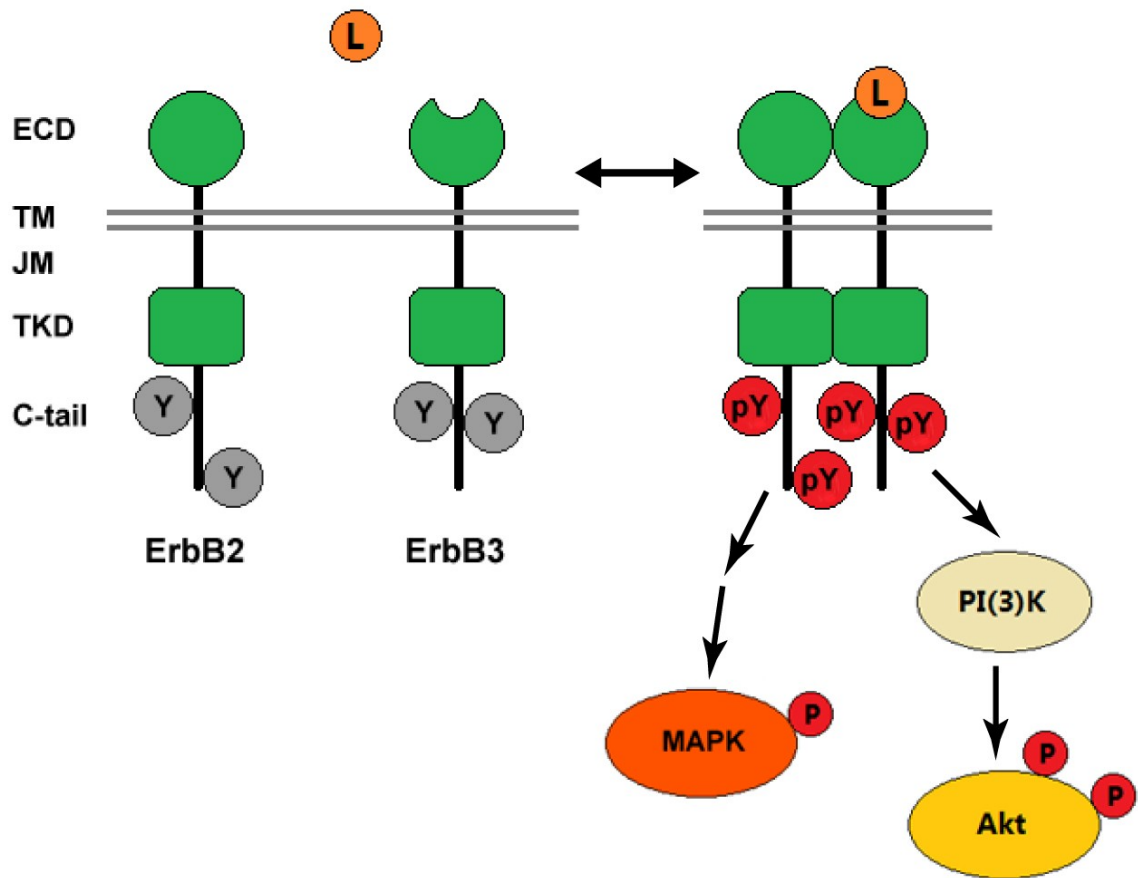


Figure 1.1: Scheme of ligand induced ErbB activation (shown in the figure is signaling of the ErbB2/ErbB3 heterodimer). ECD: extracellular domain; TM: transmembrane domain; JM: juxtamembrane domain; TKD: tyrosine kinase domain. Grey circles (Y): tyrosine residues; Red circles (pY): phosphor-tyrosines; Orange circles (L): ligand.

1.1.2 Introduction to ErbB3 Signaling

ErbB3 (HER3) stands out among the four mammalian ErbB receptors due to two special properties. Firstly, it is the only ErbB protein that contains an atypical kinase domain. When first cloned (Kraus, Issing et al. 1989; Plowman, Whitney et al. 1990), it was noted that ErbB3 contains amino acid substitutions at two particular sites that are highly conserved in other known kinases (Hanks, Quinn et al. 1988). Since these two residues are involved in maintaining the active conformation and mediating the phosphoryl transfer reaction, the ErbB3 kinase was suggested to be catalytically defective, and some evidence was reported to this effect (to be discussed further in the following sections) (Citri, Skaria et al. 2003).

Secondly, binding of neuregulin ligands to ErbB3 fails to induce ErbB3 homodimerization, and can only induce the formation of heterodimers between ErbB3 and other ErbBs (Ferguson, Darling et al. 2000; Citri, Skaria et al. 2003; Berger, Mendrola et al. 2004). Mixing neuregulin1 β (Nrg1 β) with recombinant ErbB3 extracellular domain protein failed to induce homodimerization of the latter (monitored by analytical ultracentrifugation) (Ferguson, Darling et al. 2000). Using an ErbB3 ECD/EGFR ICD chimeric protein, Berger et al. also showed that neuregulin cannot stimulate autophosphorylation of this chimeric protein (or downstream signaling when it is expressed in *Drosophila* S2 cells), unless ErbB2 protein is also expressed in the same cell (allowing heterodimerization). In contrast, neuregulin induces a robust signaling response in S2 cells expressing ErbB4 alone (Berger, Mendrola et al. 2004).

Among all ErbB heterodimers that ErbB3 can form, the ErbB2/ErbB3 heterodimer is generally considered to be the most potent mitogenic signaling complex in the ErbB receptor network (Citri, Skaria et al. 2003; Holbro, Beerli et al. 2003). In cells that contain only these two ErbB receptors, both ErbB2 and ErbB3 are extensively tyrosine phosphorylated upon neuregulin stimulation (Riese, van Raaij et al. 1995). Due to the presence of multiple C-tail phosphotyrosine binding sites for the p85 subunit of PI3K, ErbB3 is highly effective in activating the PI3K-Akt pathway that leads to cell survival and proliferation (Prigent and Gullick 1994; Soltoff, Carraway et al. 1994; Hellyer, Cheng et al. 1998), whereas ErbB2 is mainly responsible for activating the MAPK pathway through Grb2/Sos recruitment (Figure 1.1). When ErbB signaling is activated aberrantly, cancer results. The ErbB2/ErbB3 heterodimer has been proposed as an “oncogenic unit” due to its potency in eliciting mitogenic and transforming signals (Holbro, Beerli et al. 2003). Tumor mice models using transplantation of ErbB transfected NIH-3T3 cells have shown that overexpression of ErbB2/ErbB3 causes the most aggressive tumor growth compared with other ErbB combinations (Alaoui-Jamali, Song et al. 2003).

1.1.3 ErbB3 in Cancer Development and Corresponding Therapeutics

Numerous studies have demonstrated an important role for aberrant ErbB3 signaling in various cancers, including breast (Holbro, Beerli et al. 2003; Lee-Hoeflich, Crocker et al. 2008), prostate (Soler, Mancini et al. 2009), lung (Engelman, Janne et al. 2005), ovarian, colon and gastric cancers (Sithanandam and Anderson 2008).

The role of ErbB3 is best characterized in breast cancer. Data from *in vitro* and mouse models, plus clinical studies in humans, all argue that the ErbB2/ErbB3 heterodimer drives breast cancer progression (reviewed in (Hamburger 2008; Lee-Hoeflich, Crocker et al. 2008)). Overexpression of ErbB2 and/or ErbB3 in breast cancer has been reported to correlate with poor prognosis (Travis, Pinder et al. 1996; Ferretti, Felici et al. 2007), whereas knockdown of ErbB2 or ErbB3 can markedly suppress the growth of breast cancer cells (Faltus, Yuan et al. 2004; Lee-Hoeflich, Crocker et al. 2008). As a result of these observations, inhibition of ErbB2/ErbB3 signaling has become a very attractive goal in the clinical treatment of breast cancer. Current efforts to suppress this signaling pathway have been mostly focused on ErbB2, targeting either the extracellular ligand-binding and dimerization region using therapeutic antibodies or intracellular kinase activity with small molecule inhibitors. Some of these ErbB2-targeted drugs, such as Herceptin and Tykerb (lapatinib), are among the most famous breast cancer drugs (Park, Neve et al. 2008) and have proven to be effective in some patients with breast cancer characterized by ErbB2 overexpression (Nahta and Esteva 2006; Bedard, Cardoso et al. 2009).

Despite significant advances with ErbB2-directed therapies in breast cancer, effectiveness of these treatments is modest at best. These drugs work for only a small subset (<25%) of patients – even within the group showing ErbB2 gene amplification and overexpression (Chen, Xia et al. 2008), and development of resistance is a very significant problem (Chen, Xia et al. 2008; Bedard, Cardoso et al. 2009). ErbB3 has recently become a focus of attention, as it appears to play an important role in escape

from (or resistance to) therapeutic agents that target ErbB2 in cancer. Sergina et al. showed that the BT474 and SKBR3 breast cancer cell lines become resistant to gefitinib, an ErbB TKD inhibitor, within 24 hours of treatment, and this correlates with a recovery in ErbB3 (but not ErbB2) phosphorylation and corresponding Akt activation (Sergina, Rausch et al. 2007). Suppression of ErbB kinase activity with gefitinib also appeared to induce relocalization of the ErbB3 protein from intracellular compartments to the plasma membrane, which was proposed to facilitate its interaction with other ErbBs, contributing to inhibitor resistance. Similarly, breast cancer cell lines that are resistant to Herceptin (an ErbB2 antibody) can be inhibited by antibodies against ErbB3 (van der Horst, Murgia et al. 2005).

ErbB3 also plays a similar role in drug resistance of non-small cell lung cancer (NSCLC) associated with EGFR overexpression or mutation. In gefitinib-sensitive NSCLC cell lines, ErbB3 is found to be associated with the PI3K p85 subunit and mediates signaling from activated EGFR to the downstream Akt pathway via PI3K. Alternatively, ErbB3 can contribute to the development of gefitinib resistance in NSCLC cell lines through partnering with another receptor tyrosine kinase MET. MET amplification causes hyper-phosphorylation of ErbB3 even in the presence of gefitinib. Similar ErbB3-mediated EGFR activation of Akt signaling has been reported in erlotinib sensitive pancreatic and colorectal tumor cell lines (Buck, Eyzaguirre et al. 2006). Consistent with these observations, down-regulation of ErbB3 using RNA interference (RNAi) can restore the sensitivity of cancer cells to gefitinib or erlotinib – with associated reduction of activated phospho-Akt levels. Where MET is involved, small

molecule inhibitors of its tyrosine kinase can also restore gefitinib sensitivity (Engelman, Zejnullahu et al. 2007). By contrast with these observations, gefitinib-resistant NSCLC cell lines show no detectable association of ErbB3 with PI3K-p85 or Akt sensitivity to ErbB3 knockdown (Engelman, Janne et al. 2005).

Due to an increasing realization that ErbB3 is a key contributor to development of cancers and their drug resistance, many pharmaceutical companies are actively pursuing antibodies that specifically target ErbB3 in order to suppress its oncogenic signaling. One ErbB3 antibody called MM-121 (Merrimack Pharmaceuticals Inc.) has been developed to suppress ligand-induced ErbB3 phosphorylation in cancer cell lines and, when combined with the EGFR-targeted cetuximab antibody, it suppresses cetuximab resistance in a mouse lung cancer model driven by an EGFR T766M/L834R dual mutation (Schoeberl, Faber et al.). Multiple phase I&II clinical trials are currently being conducted to test the efficacy of this therapeutic agent in multiple settings. Other ErbB3-specific antibodies undergoing clinical trials include U3-1287 generated by U3 Pharma & Amgen and MP-RM-1 by MediaPharma (Sala, Traini et al.). Recently, a novel dual-specific ErbB3/EGFR antibody, MEHD7945A, has been developed by Genentech, and has shown promising result in studies of suppression of solid tumors (Schaefer, Haber et al.). MEHD7945A is currently in phase II clinical trials for squamous cell carcinoma of the head and neck and in a phase I clinical trial for epithelial tumors. Despite these developments, however, therapeutically inactivating ErbB3 through extracellular targeting with antibodies will be a challenging task, since the majority of ErbB3 has been reported to be located in intracellular compartments rather than at the cell surface (Sergina, Rausch et al. 2007).

Whereas much effort has been put into inactivating ErbB3 with antibodies that target its extracellular regions, the ErbB3 kinase domain has been ignored so far. The primary reason for this is that ErbB3 has been deemed “kinase-dead” due to the sequence alterations in its TKD mentioned above (Hanks, Quinn et al. 1988; Prigent and Gullick 1994). Based on this notion, it has been assumed that all tyrosine phosphorylation in the ErbB2/ErbB3 heterodimer arises from ErbB2’s kinase activity (Citri, Skaria et al. 2003; Holbro and Hynes 2004). This creates a problem, however, because studies of ErbB signaling mechanisms argue that autophosphorylation of ErbB receptors within ligand-induced dimers occurs *in trans*, with each ErbB kinase mediating tyrosine phosphorylation of its dimerization partner (Honegger, Kris et al. 1989; Honegger, Schmidt et al. 1990; Lammers, Vanobberghen et al. 1990). According to this model, it is unclear how ErbB2 could become phosphorylated in an ErbB2/ErbB3 heterodimer unless ErbB3 carries an active kinase. Consistent with this possibility, recent studies of some other presumed “pseudokinases”, such as Wnk, CASK, VASP and KSR, have revealed that they do retain kinase activity in spite of previous sequence-based assumptions that they are “kinase dead” (Min, Lee et al. 2004; Mukherjee, Sharma et al. 2008; Villa, Capasso et al. 2009; Brennan, Dar et al.). Similar to ErbB3, these presumed pseudokinases all contain sequence alterations at key conserved residues in their kinase domain, but can nonetheless catalyze the phosphoryl transfer reaction through non-canonical mechanisms. It is therefore important to take a closer look at ErbB3’s TKD, and to test the hypothesis that ErbB3, like other active pseudokinases, does in fact function as an active kinase to promote ErbB signaling. If this is the case, targeting the

ErbB3 kinase domain may be a promising and important novel therapeutic strategy in cancer treatment.

1.1.4 Structure and Biochemistry of Tyrosine Kinase Domains

To understand the special properties of ErbB3 kinase domain, we first need to discuss the general features of tyrosine kinase domains. The overall structure of protein kinase domains (both tyrosine kinases and Ser/Thr kinases) is highly conserved, comprising an N-lobe and a C-lobe (Figure 1.2A). The N-lobe contains five antiparallel β -strands and one α -helix (called α C), whereas the C-lobe is mostly α -helical. Binding sites for Mg-ATP and phosphorylation substrate are located between these two lobes, next to the activation loop that links these two lobes.

Several key regions and conserved residues around the active site have been implicated in kinase regulation and in catalysis itself (Figure 1.2B). For many protein kinases, trans-phosphorylation of key Ser/Thr/Tyr residue(s) in the activation loop prevents it from forming auto-inhibitory interactions and effectively stabilizes the active conformation of the kinase domain (Hubbard, Mohammadi et al. 1998). However, it should be noted that this is not the case for EGFR (discussed in the following paragraphs). Coupled with release of the activation loop from its auto-inhibitory position is a re-positioning of the α C helix in the N-lobe, which utilizes a Glu side-chain (replaced by His740 in ErbB3) to form an ion pair with the ϵ -amino group of a highly conserved Lys from the VAIK motif in β 3 strand. The latter also interacts directly with the ATP α - & β -phosphates and promotes ATP binding in the active conformation (Huse and Kuriyan

2002). A Lys to Met mutation at this position impairs the kinase activity of most kinases (Qian, Levea et al. 1994). A conserved Asp residue (replaced by Asn815 in ErbB3) from an also-conserved HRD motif is located between the ATP γ -PO₄ and the side chain of the substrate tyrosine, marked Asp1 in Figure 1.2B (Williams, Wang et al. 2000). Another key Asp from the conserved DFG motif (Asp2 in Figure 1.2B) is responsible for coordinating Mg²⁺ ions with ATP phosphate groups. Upon binding to the catalytic cleft of the TKD, the substrate peptide remains largely exposed to solvent. Consequently, unlike most enzymes, tyrosine kinases usually have low substrate specificity *in vitro* (Fan, Wong et al. 2005).

The catalytic process of tyrosine kinases is still not fully understood. Since the major sequence alteration in the ErbB3 TKD is the substitution of the Asp in HRD motif (Asp1 in Figure 1.2B) with Asn815, the catalytic role of this key Asp is discussed here. This Asp was initially thought to function as a general base, deprotonating the tyrosyl side chain of the substrate so that the latter becomes a good nucleophile to attack the γ -phosphate group of ATP in an associative manner (Stamos, Sliwkowski et al. 2002). In the associative mechanism, bond formation between the attacking nucleophile and the γ -PO₄ precedes the leaving of the ADP moiety (Cleland and Hengge 1995). Current enzymatic studies of tyrosine kinases, however, instead favor a dissociative mechanism, in which the reaction order at this stage is reversed and the ADP moiety leaves first. In this mechanism, the nucleophilicity of the phosphate acceptor is less important (Cleland and Hengge 1995; Cole, Courtney et al. 2003; Shen, Hines et al. 2005). In fact, a neutral Tyr sidechain seemed to be a better substrate than the negatively charged tyrosinate in

studies of the Csk tyrosine kinase (Kim and Cole 1997; Kim and Cole 1998) and the role of Asp1 was hypothesized to be stabilization of a preferred rotamer of the tyrosine hydroxyl to facilitate the reaction process (Adams 2001).

Catalytic activity of tyrosine kinases is tightly regulated in cells, and EGFR has been used as a model system for studying the activation of ErbB family kinases. Unlike most tyrosine kinases, although EGFR TKD contains a tyrosine in the activation loop, phosphorylation of this tyrosine is not required for EGFR kinase activation (Tice, Biscardi et al. 1999). Zhang et al. (Zhang, Gureasko et al. 2006) have shown that the EGFR kinase domain is activated through the formation of an asymmetric homodimer (Figure 1.2C) – in which the C-lobe of the activating kinase domain (yellow in Figure 1.2C) interacts with the N-lobe α C region of the activated kinase (blue in Figure 1.2C), inducing allosteric alterations and stabilizing the latter in the active conformation. Mutations in the crystallographically observed interface between the activating kinase and the activated kinase disrupt dimer formation and EGFR activation. In addition, the juxtamembrane region of EGFR is now known to contribute to stabilization of the asymmetric dimer shown in Figure 1.2C by wrapping around the C-lobe of the activating kinase domain as a so-called juxtamembrane ‘latch’ (Jura, Endres et al. 2009; Red Brewer, Choi et al. 2009). A similar allosteric activation mode through asymmetric dimerization has also been described for ErbB4 (Qiu, Tarrant et al. 2008).

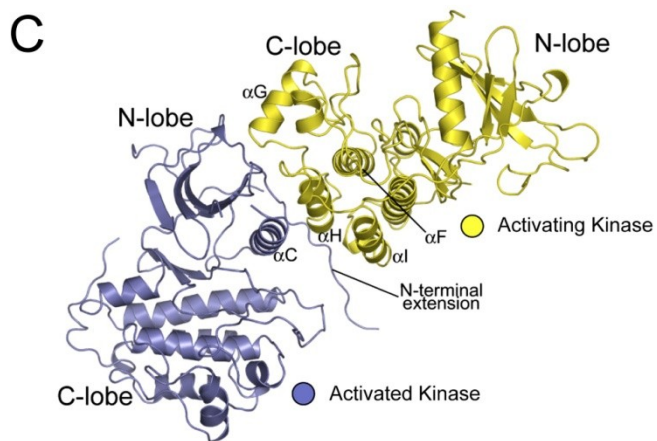
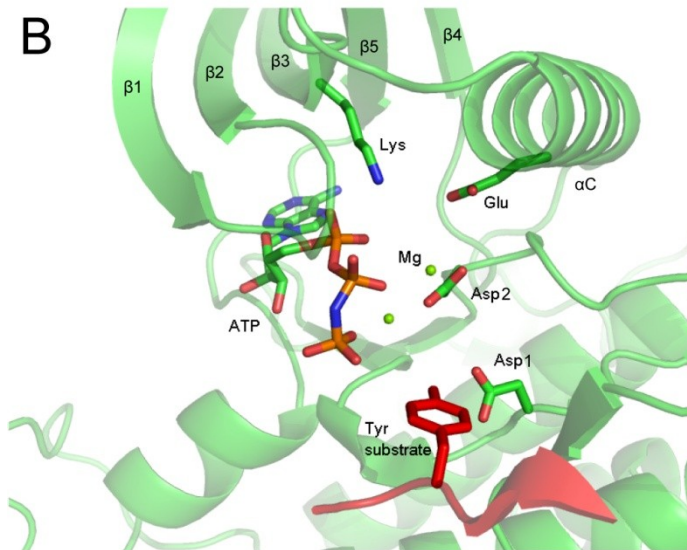
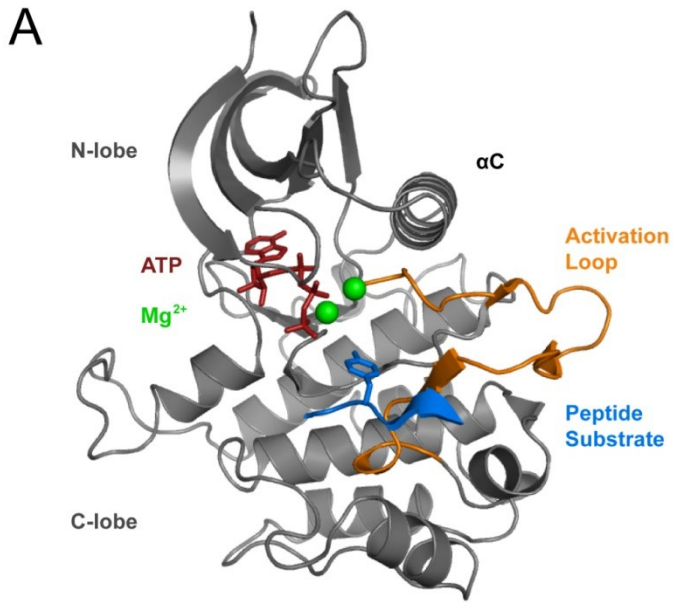


Figure 1.2: Structural features of tyrosine kinase domain. (A) Overall structure of tyrosine kinase domain in the active conformation (PDB 1IR3). Dark red: ATP; Orange: activation loop; Blue: peptide substrate (tyrosine sidechain is shown); Green: magnesium ion. (B) Close view of TKD active site. (C) Asymmetric dimer of EGFR TKD (adapted from (Zhang, Gureasko et al. 2006)). Yellow: activating kinase; Light blue: activated kinase.

1.1.5 ErbB3, a Heretical Kinase with Changes at Conserved Catalytic Residues in TKD

As mentioned in the previous section, the ErbB3 kinase domain harbors amino acid substitutions at two key conserved sites. First, an Asn (N815) replaces the conserved catalytic Asp in the HRD motif (Asp1 in Figure 1.2B) that lies near the γ -PO₄ of ATP and the side chain hydroxyl of the substrate tyrosine. Other than being important for full catalytic activity in other kinases, the exact function of this aspartate is the subject of much debate. Site-directed mutagenesis of this aspartate in protein kinase A (Gibbs and Zoller 1991) and the Csk tyrosine kinase (Cole, Grace et al. 1995) substantially reduces (but does not abolish) kinase activity. Moreover, a D813A EGFR mutant is still capable of mediating EGF-induced DNA synthesis (suggesting some residual kinase activity), whereas a K721R (kinase-dead) EGFR mutant cannot (Coker, Staros et al. 1994). These findings argue that replacement of this Asp with Asn815 in ErbB3 does not necessarily imply an absence of kinase activity.

The second amino acid substitution in ErbB3 TKD occurs at the conserved Glu site in the α C helix (Glu- α C in Figure 1.2B), which in other kinases forms a salt bridge

with lysine in the VAIK motif and contributes to stabilization of the ATP binding site in the active conformation. This Glu is replaced in ErbB3 by a histidine (H740). However, the effect of mutating this residue is not well understood. It should also be noted that the sequence of ErbB3 in the α C helix region is very different from that in other kinases, so that an alternative structural solution might exist to stabilize the active conformation. Apart from these two mutations, other conserved residues near the ATP binding pocket thought to be crucial for kinase activity are all “intact” in ErbB3.

Following the initial cloning of ErbB3, and realization that its kinase domain harbors these unusual differences from ‘canonical’ protein kinases, several early biochemical studies investigated ErbB3 kinase activity and concluded qualitatively that it is kinase-inactive (Guy, Platko et al. 1994; Sierke, Cheng et al. 1997). Insect cell-expressed recombinant ErbB3 intracellular domain was reported neither to bind ATP nor to become autophosphorylated *in vitro* (Sierke, Cheng et al. 1997). On the other hand, full-length ErbB3 protein expressed in insect cells could be affinity labeled with an ATP analogue through crosslinking (Guy, Platko et al. 1994), but was autophosphorylated only to a very small extent that was not increased by addition of ligand neuregulin – and was therefore ascribed to ‘background’ *trans*-phosphorylation by endogenous insect cell kinases (Guy, Platko et al. 1994). Based on these findings, the prevailing view in the literature is that the ErbB3 kinase domain is an inactive ‘pseudokinase’ (Citri, Skaria et al. 2003; Boudeau, Miranda-Saavedra et al. 2006). These initial studies should be interpreted with caution, however. The *in vitro* studies of the ErbB3 intracellular domain only investigated diluted protein in solution (Sierke, Cheng et al. 1997) – whereas the

EGFR precedent argues that dimerization is likely to be required for kinase activation. Moreover – although the authors did not realize this at the time – neuregulin binding does not induce ErbB3 homodimerization (Berger, Mendrola et al. 2004), so the cellular studies of full-length ErbB3 never actually subjected the protein to a treatment that may activate its kinase activity. Therefore, these prior studies failed to investigate ErbB3 kinase activity under conditions where activity (if present) would be manifest (i.e. following dimerization or oligomerization). Nonetheless, all proposed signaling mechanisms involving ErbB3 have assumed that it has no kinase activity.

1.1.6 Summary

ErbB3 is a unique member of the ErbB family RTKs. It contains an atypical kinase domain and an extracellular domain that exclusively forms heterodimers with other ErbBs. ErbB3 plays an important role in the development of cancers, especially when partnered with ErbB2. In oncology, current ErbB3 targeting therapeutic strategies only focus on developing specific antibodies for ErbB3 ectodomain. On the other hand, the ErbB3 kinase domain has not been pursued therapeutically as it is unclear whether ErbB3 is a functional kinase.

Other than the observation of amino acid alterations in ErbB3 TKD, few experimental studies have attempted to address the question of whether ErbB3 is able to function as a kinase, especially under the conditions similar to those necessary for other ErbB kinases to become activated. An increasing number of studies have discovered that many of the presumed-inactive pseudokinases actually retain significant activity.

Therefore, it is inappropriate to assume that ErbB3 is ‘kinase-dead’ simply based on these observations. If ErbB3 is an active kinase, targeting this activity would offer a novel and very promising treatment for ErbB2/ErbB3 expressing breast cancers that are resistant to Herceptin and Tykerb. My study aims to investigate, using updated knowledge of ErbB kinases, whether ErbB3 kinase retains catalytic activity and to understand the role of ErbB3 TKD in cell signaling.

1.2 *In vitro* Characterization of the Enzymatic Activity of ErbB3 TKD

1.2.1 Autophosphorylation of the Purified ErbB3 Intracellular Domain

N-terminally 6xHis-tagged ErbB3 intracellular domain (ErbB3-ICD, residues 665-1323) and isolated tyrosine kinase domain (ErbB3-TKD, residues 665-1001) were expressed in baculovirus-infected Sf9 cells and proteins were purified as described in Experimental Procedures. Neither ErbB3-ICD nor ErbB3-TKD showed any autophosphorylation activity when incubated with only Mg²⁺ and ATP in solution, consistent with previously published studies (Sierke, Cheng et al. 1997). However, robust tyrosine autophosphorylation could be seen in anti-phosphotyrosine Western blots (Figure 1.3A) when lipid vesicles containing DOGS-NTA-Ni (1, 2-dioleoyl-*sn*-glycero-3-([N(5-amino-1-carboxypentyl)iminodi-acetic acid] succinyl) nickel salt) were added to the reaction system, allowing 6xHis-tagged ErbB3-ICD to be clustered onto the vesicle surfaces (Figure 1.3A, two right-most lanes). This method was used previously to promote assembly of 6xHis-tagged signaling molecules on membrane surfaces for several receptors (Shrout, Montefusco et al. 2003), and was crucial for activity in earlier studies

of EGFR kinase activation by Kuriyan and colleagues (Zhang, Gureasko et al. 2006). Autophosphorylation is also dependent on the addition of Mn^{2+} or Mg^{2+} ions (Figure 1.3B), with Mn^{2+} slightly preferred. Consistent with the fact that ErbB3 phosphorylation sites are concentrated in the C-terminal tail, removing this region to give ErbB3-TKD is accompanied by a loss of detectable autophosphorylation.

To confirm that the autophosphorylation shown in Figure 1.3A arises from ErbB3-ICD protein, and not from other contaminating kinases, we assessed the ability of a K723M-mutated form of the protein to autophosphorylate under the same conditions. This conserved Lys is important for ATP-binding to the tyrosine kinase domain, and mutation of the analogous residue is well known to abolish the activity of many kinases, including EGFR (Honegger, Dull et al. 1987; Zhang, Gureasko et al. 2006). As shown in the second lane of Figure 1.3C, the K723M mutation greatly diminishes the degree of ErbB3-ICD autophosphorylation. However, the K723M-mutated ErbB3-ICD protein is *trans*-phosphorylated robustly on its C-terminal tail when the 6xHis-tagged isolated ErbB3-TKD is added, as shown in lane 3 of Figure 1.3C. On the other hand, the ability to *trans*-phosphorylate ErbB3-ICD is substantially diminished when the added ErbB3-TKD also harbors a K723M mutation (Lane 4 in Figure 1.3C and lane 5 of Figure 1.3D left). Similarly, a K723R mutation also disrupts the kinase activity of ErbB3-TKD (lane 4 of Figure 1.3D right). The ErbB3 TKD contains a tyrosine (Y849) in its activation loop. To test the hypothesis that phosphorylation of this tyrosine activate kinase activity, Y849 was mutated to Glu to mimic the negatively charged phosphotyrosine. This mutation impairs the ability of ErbB3-TKD to *trans*-phosphorylate the ICD's C-terminal tail (Lane

6 in Figure 1.3D left), arguing against this hypothesis, but nonetheless suggesting some role for this tyrosine in regulation of ErbB3's kinase activity. In addition, the Ala substitution of V836 at the beginning of the activation loop also showed diminished kinase activity (Lane 5 in Figure 1.3D right) and its implication will be discussed in sections 1.3 and 1.4. We also asked whether reintroduction of the Asp at the position occupied by the proposed catalytic base in other kinases (in the N815D mutant) can increase the *trans*-phosphorylation activity of ErbB3-TKD. As shown in Lane 7 of Figure 1.3D (left), the N815D mutation did not have a significant activating effect, consistent with a previous report (Prigent and Gullick 1994).

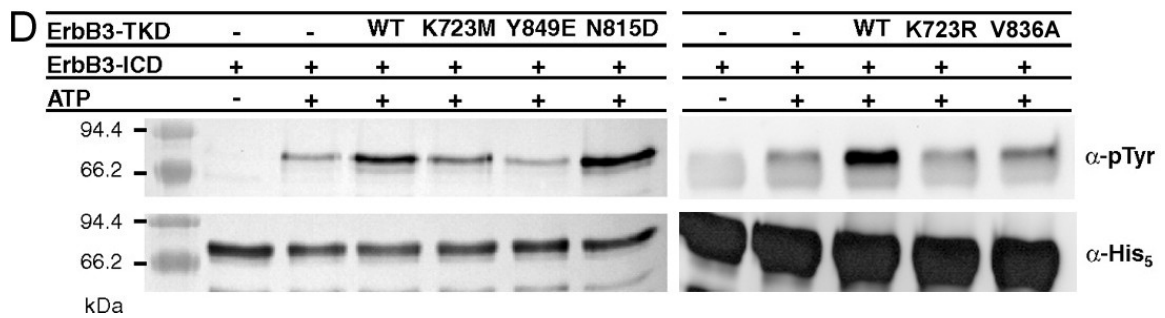
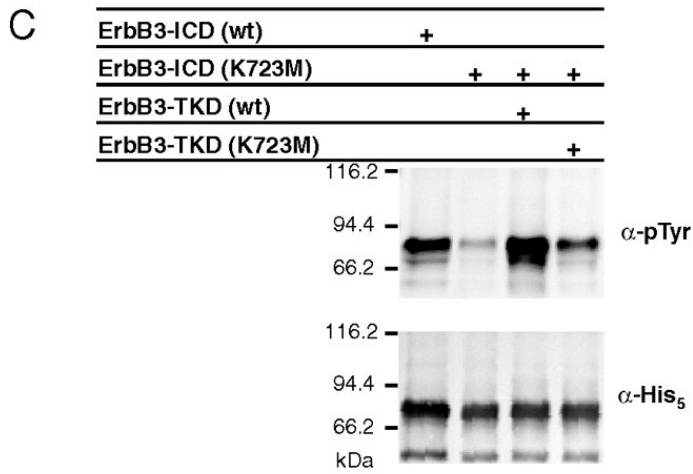
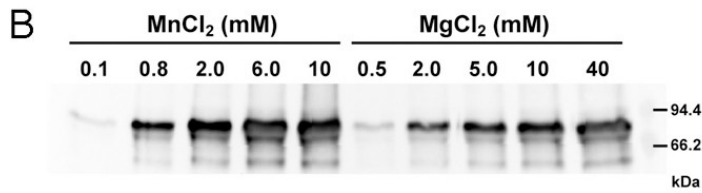
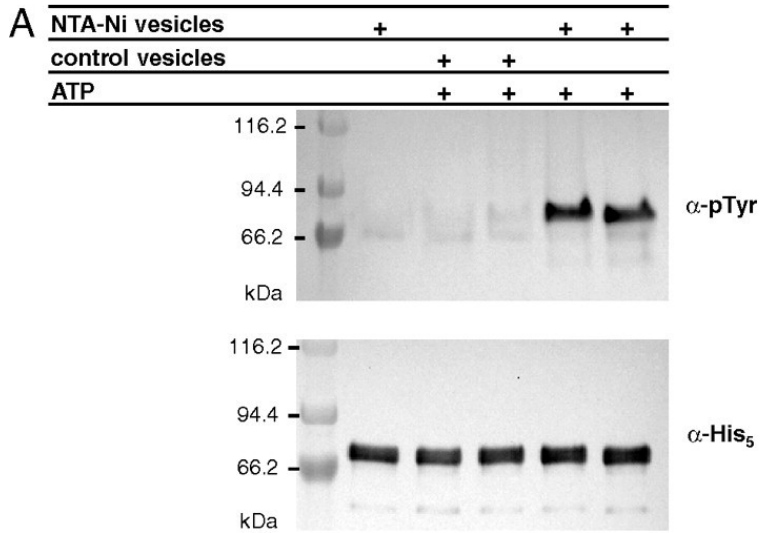


Figure 1.3: Autophosphorylation of the ErbB3 Intracellular Domain *in vitro*. **(A)** ErbB3-ICD autophosphorylation monitored by immunoblotting with anti-phosphotyrosine antibodies. ErbB3-ICD at 3 μM was incubated at 25°C in 100 mM MOPS, pH 7 containing 2 mM MnCl_2 , 5 mM MgCl_2 , 200 mM NaCl, 5 % glycerol, and 0.1 mM DTT. Lane 1 contained molecular weight markers. For lane 2, 125 μM phospholipid (in vesicles) containing 10% (mole/mole) DOGS-NTA-Ni was added to 3 μM ErbB3-ICD. Lanes 3 and 4 represent duplicate samples in which 1 mM ATP and control vesicles (lacking DOGS-NTA-Ni) were added to 3 μM ErbB3-ICD. In lanes 5 and 6, 1 mM ATP plus DOGS-NTA-Ni vesicles were added, and significant autophosphorylation was seen. Reactions were stopped after 30 mins by adding 50 mM EDTA and SDS-PAGE gel-loading buffer. Samples were subjected to SDS-PAGE and immunoblotting with anti-phosphotyrosine antibodies (upper panel) and an anti-pentahistidine antibody (lower panel) for loading control. **(B)** Dependence on divalent cation concentration of ErbB3-ICD autophosphorylation. Purified ErbB3-ICD (3 μM) was incubated for 30 minutes in 100 mM MOPS pH 7.4, containing 1 mM ATP, 125 μM phospholipid (in vesicles) with 10 % (mole/mole) DOGS-NTA-Ni, and the noted concentrations of MnCl_2 or MgCl_2 . **(C)** For lane 1, 3 μM ErbB3-ICD was allowed to autophosphorylate as in lanes 5 and 6 of **(A)**. K723M-mutated ErbB3-ICD was treated identically for lane 2, and little autophosphorylation was observed. Autophosphorylation of K723M-mutated ErbB3-ICD was recovered when the wild-type isolated ErbB3-TKD⁶⁶⁵⁻¹⁰⁰¹ was added at 6 μM (lane 3), and to a significantly lesser extent when K723M-mutated ErbB3-TKD⁶⁶⁵⁻¹⁰⁰¹ was added (lane 4). Thus, the isolated ErbB3-TKD can phosphorylate ErbB3-ICD in *trans*. **(D)** The ability of wild-type and mutated ErbB3-TKD⁶⁶⁵⁻¹⁰⁰¹ to *trans*-phosphorylate ErbB3-ICD was compared as described in the text.

Although these results demonstrate that ErbB3 is capable of catalyzing phosphoryl-transfer, we found that its catalytic efficiency is substantially lower than seen for EGFR activated in a similar manner. We have not been able to detect significant phosphorylation of added poly(Glu:Tyr) substrates or of short peptides modeled on phosphorylation sites within ErbB3 or ErbB2. Experiments in which the incorporation of ^{32}P into the ErbB3 intracellular domain was used to monitor rates of *trans*-phosphorylation (Figure 1.4) suggested that ErbB3-TKD phosphorylates ErbB3-ICD at a rate that is about 1000 fold slower than that seen for EGFR under similar experimental conditions. Nonetheless, the experiments in Figure 1.3 show that ErbB3 does contain an active kinase domain.

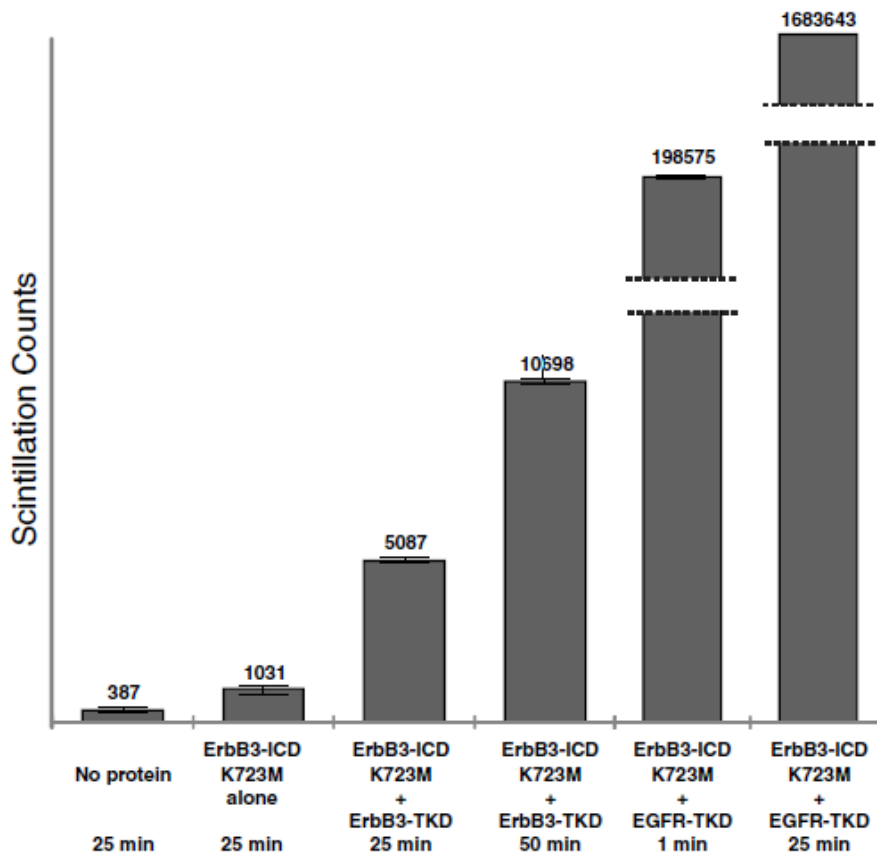


Figure 1.4: Quantitation of ^{32}P incorporation into ErbB3-ICD by the kinase domains from ErbB3 or EGFR. A final concentration of 3 μM wild-type ErbB3-TKD or EGFR-TKD was co-incubated with 6 μM 6xHis-tagged ErbB3-ICD (K723M) as substrate in 20 mM Tris-HCl pH 8.0, 200 mM NaCl, 5% glycerol, containing 0.1 mM DTT, 5 mM MgCl_2 , 2 mM MnCl_2 , 100 μM ATP (with 3 μCi [γ - ^{32}P]ATP) and 100 μM lipid (vesicles containing 10% DOGS-NTA-Ni with 90% DOPC). Reaction mixtures were incubated at room temperature for the times listed, and reactions were stopped by adding EDTA to a final concentration of 50 mM. Samples were spotted onto phosphocellulose paper to immobilize protein. After a series of washes, ^{32}P incorporation was measured by scintillation counting. Mean range of variation are plotted from at least two independent experiments. ^{32}P incorporation catalyzed by ErbB3-TKD occurred at approximately 209 cpm per minute (5,087 in 25 min; 10,698 in 50 min). ^{32}P incorporation catalyzed by EGFR-TKD was clearly saturating (or depleting substrate) by 25 min. On the basis of the 1-min time point, we estimate a maximum incorporation rate of 198,575 cpm per minute, suggesting a rate that is \sim 940-fold higher than that for ErbB3-TKD.

1.2.2 ErbB3 TKD Fully Retains ATP Binding Ability

Having detected kinase activity with our ErbB3 proteins, we next investigated the ATP-binding properties of ErbB3-TKD, since previous analyses have yielded conflicting results (Guy, Platko et al. 1994; Sierke, Cheng et al. 1997). We used mant [2'-(3')-*O*-(*N*-methylantraniloyl)]-ATP, a fluorescent analogue of ATP, for direct binding studies. As shown in Figure 1.5A, a solution of 1 μM mant-ATP (plus 5 mM MgCl_2) does not have significant fluorescence when excited at 280 nm. However, following addition of ErbB3-TKD at 3 μM there is a significant peak centered at 448 nm that reflects fluorescence resonance energy transfer (FRET) from tryptophans and/or tyrosines in the protein to the

mant-ATP. The peak at 448 nm is absent without mant-ATP, and the observed FRET requires that ErbB3-TKD, MgCl₂, and mant-ATP are all present in the sample (Figure 1.5B). Moreover, FRET is substantially diminished when 20 μM ATP is added (a 20-fold excess over mant-ATP), which should saturate the nucleotide-binding site in the kinase. These results argue that the ErbB3 kinase domain does indeed bind ATP.

To estimate the affinity of this binding, we monitored FRET from the kinase to mant-ATP upon titration of ErbB3-TKD into a solution containing 0.6 μM mant-ATP plus 5 mM MgCl₂. A simple hyperbolic binding curve was observed, as shown in Figure 1.5C, which suggested a K_D value of 1.1 μM for Mg²⁺/mant-ATP binding to ErbB3-TKD. This is lower than K_D values measured for Mg²⁺/ATP binding to EGFR (Cheng and Koland 1998) or protein kinase A (Iyer, Garrod et al. 2005). It is also smaller than apparent K_M values for (Mg²⁺ or Mn²⁺) ATP measured for EGFR (Qiu, Tarrant et al. 2009), ErbB2 or ErbB4 (Qiu, Tarrant et al. 2008). Consistent with the significant reduction in autophosphorylation activity seen for the K723M mutant in Figure 1.3, substitution of this lysine with methionine also greatly diminishes mant-ATP binding to ErbB3-TKD (Figure 1.5C). We have also performed some preliminary mant-ATP binding experiments with the K723R and V836A mutants of ErbB3 TKD, and the results suggested that the K723R mutant retains ATP binding affinity, while the V836A mutation disrupts ATP binding (Figure 1.5D).

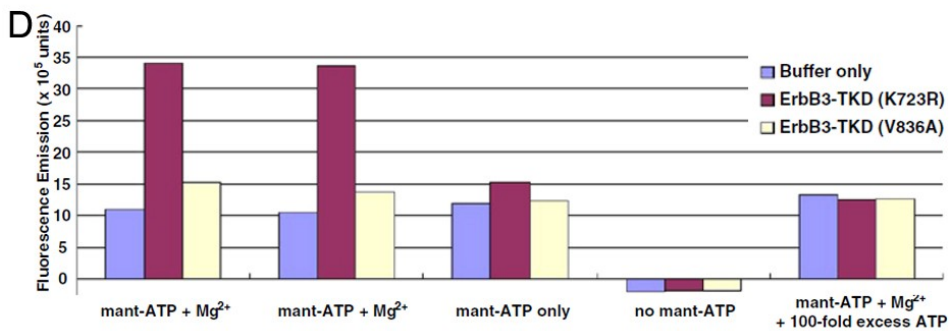
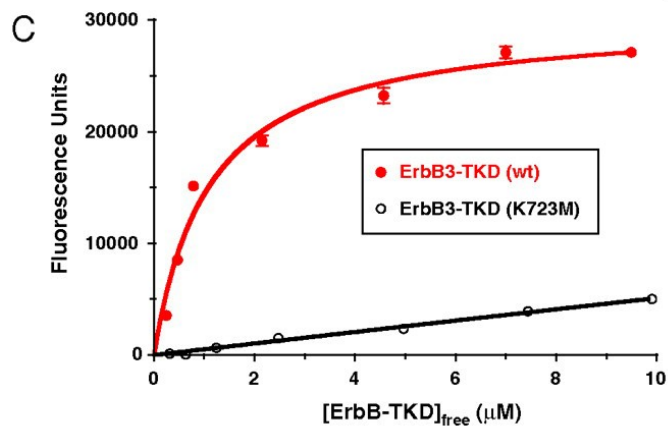
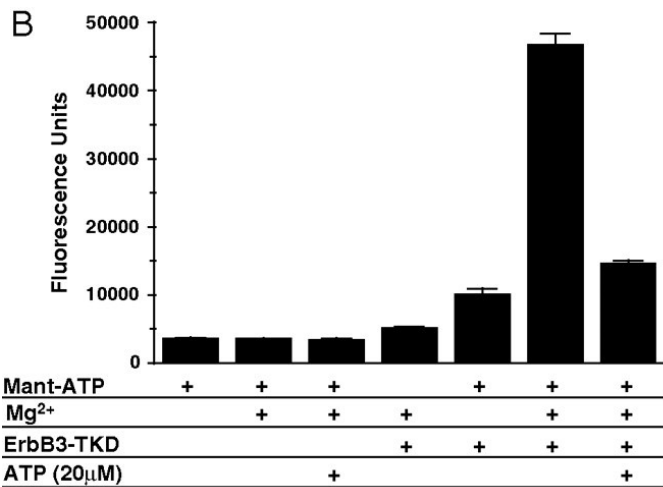
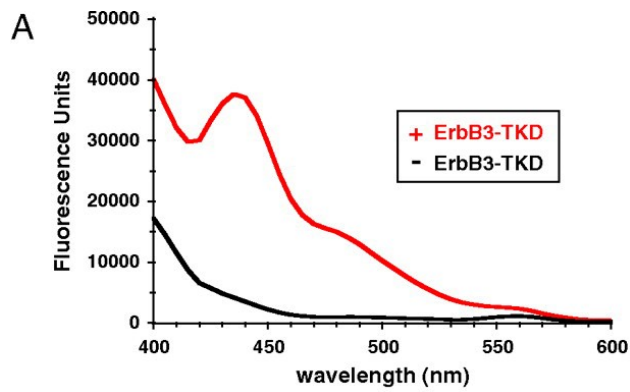


Figure 1.5: Mant-ATP Binding to ErbB3-TKD⁶⁴⁸⁻¹⁰⁰¹. **(A)** Fluorescence emission spectra (with excitation at 280 nm) are shown for 1 μ M mant-ATP (plus 5 mM MgCl₂) in the absence of ErbB3-TKD (black) and with 3 μ M added ErbB3-TKD⁶⁴⁸⁻¹⁰⁰¹, illustrating FRET between the protein and bound mant-ATP. **(B)** Fluorescence emission of 1 μ M mant-ATP at 450 nm under different conditions (with excitation at 280 nm). No significant protein-to-mant FRET is seen for 1 μ M mant-ATP alone, or any pairwise combination of 1 μ M mant-ATP, 5 mM MgCl₂, and 3 μ M ErbB3-TKD⁶⁴⁸⁻¹⁰⁰¹. However, when all three are added together, significant fluorescence emission is seen at 450 nm, signifying mant-ATP binding. The FRET signal is greatly reduced by adding 20 μ M ATP to saturate the nucleotide-binding site in the kinase (far-right column), indicating that FRET reflects specific binding to the ATP-binding site. **(C)** Titration of ErbB3-TKD⁶⁴⁸⁻¹⁰⁰¹ into a solution of 0.6 μ M mant-ATP containing 5 mM MgCl₂ causes an increase in fluorescence emission from mant-ATP at 450 nm (via FRET from the protein to which it is bound). The resulting hyperbolic binding curves were fit to a simple binding equation, yielding a best-fit K_D value of 1.1 μ M for wild-type ErbB3-TKD. A K723M mutation variant greatly diminished (but did not abolish) mant-ATP binding. **(D)** Mutating V836 in ErbB3-TKD⁶⁶⁵⁻¹⁰⁰¹ disrupts mant-ATP binding. Samples containing buffer alone or mutated ErbB3-TKD at 10 μ M were incubated alone (fourth set of bars), with 5 μ M mant-ATP (third set of bars), with 5 μ M mant-ATP plus 10 mM MgCl₂ (first and second sets of bars), or with 5 μ M mant-ATP, 10 mM MgCl₂ plus 500 μ M ATP (fifth set of bars). Assays were performed in 20 mM Tris pH 8.0, 200 mM NaCl, 5% glycerol. Fluorescence measurements were taken in triplicate using a Tecan SAFIRE II plate reader, with excitation wavelength of 340 nm and emission wavelength of 450 nm (10-nm bandwidth for both). The K723R mutant binds mant-ATP with an affinity similar to that seen for wild-type protein and shows a substantial increase in fluorescence emission from mant-ATP that can be competed away by addition of excess ATP. By contrast, the V836A mutant displayed little evidence of binding, consistent with the loss of the ability of V836A-mutated ErbB3-ICD to autophosphorylate as assessed in immunoblotting assays. Note that the first and second sets of bars are experimental repeats.

1.2.3 Inhibitor Profiling of ErbB3 Kinase

We next investigated whether currently available kinase inhibitors (especially those targeting ErbB kinases) can inhibit the kinase activity of ErbB3. This study serves two purposes:

- 1) Since these inhibitors all target the ATP binding pocket of kinases, an inhibitor sensitivity ‘profile’ will provide one view of the similarity between the ATP binding pocket of the ErbB3 TKD and that of other kinases (such as EGFR) using these inhibitors as probes.
- 2) The screen could potentially identify inhibitor(s) that can preferentially inhibit ErbB3 kinase but not other ErbB kinases. Such inhibitor could be applied in cellular studies to examine the role of ErbB3 kinase.

We first examined whether the current FDA-approved EGFR-specific inhibitors (gefitinib, erlotinib and lapatinib) can effectively inhibit ErbB3 kinase. Figure 1.6A shows that, at low micromolar concentration, none of the three inhibitors blocks the kinase activity of ErbB3, whereas all of them completely inhibit EGFR kinase. This result is not surprising since (1) these three inhibitors are optimized for EGFR and (2) the ErbB3 kinase is more homologous to ErbB4 kinase, which is also a much weaker binder of these inhibitors (Wood, Truesdale et al. 2004).

Next, using small inhibitor libraries containing commercially available ATP-competitive kinase inhibitors, we examined the inhibition profile of ErbB3 kinase, to compare it with that of EGFR kinase. Since no available inhibitor has been optimized for

ErbB3 kinase, these experiments were performed at a higher concentration of inhibitor (50 μ M) and lower concentration of ATP (100 μ M) in order to identify inhibitor candidates that are likely to have relatively weak binding of ErbB3 kinase. The results showed that, although the EGFR and ErbB3 kinases share fairly similar inhibition profiles, most inhibitors that did block their activities appear to have less potency towards ErbB3 than EGFR, represented by a smaller degree of ErbB3 inhibition in this qualitative assay. In addition, some of the EGFR kinase inhibitors failed to block ErbB3 activity at all. The work of our collaborators in the laboratory of Kevan Shokat at U.C.S.F. has shown similar results. Therefore, we conclude from this study that, although the overall ATP binding site of ErbB3 TKD is structurally similar to that of EGFR kinase, it is targeted less effectively by current kinase inhibitors. One reason for this may be the relatively stronger ATP binding of ErbB3 TKD compared to other kinases as determined in our mant-ATP assay. Another reason could be that the structural configurations of ErbB3 kinase (and its most populated states in the conformational ensemble) are weaker binders for these inhibitors.

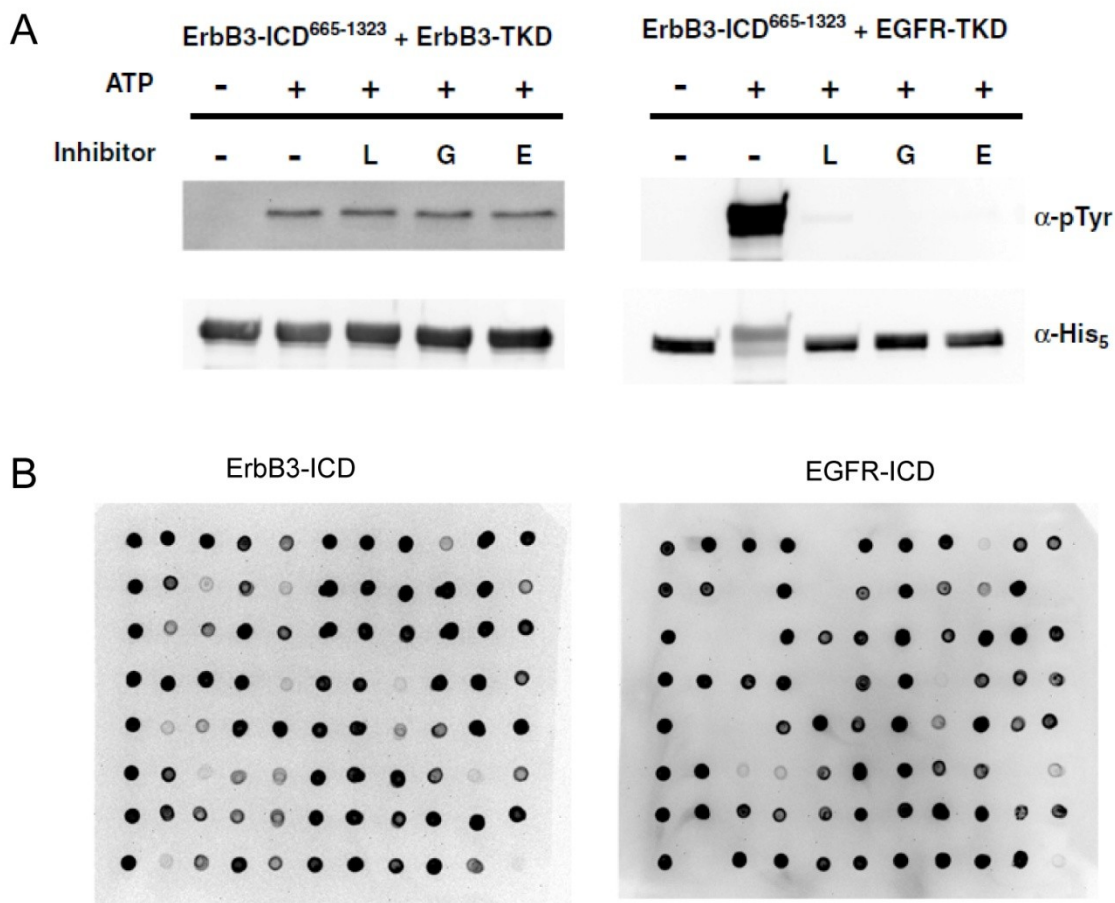


Figure 1.6: Inhibitor Profiling of ErbB3 Kinase. (A) Western blot analysis to assess the effect of EGFR or EGFR/ErbB2 inhibitors on ErbB3-TKD activity (left) and EGFR-TKD activity (right). ErbB3-ICD (0.3 μ M) was mixed with 0.3 μ M ErbB3-TKD (left) or 0.3 μ M EGFR-TKD (right) in 1 mM ATP (except in the first lane), 5 mM MgCl₂, 2 mM MnCl₂, 10 μ M lipid (10%NTA-NiDOGS + 90%DOPC in vesicles), 20 mM Tris-HCl pH8.0, 200 mM NaCl, 5% glycerol and 0.1 mM DTT for 1 hr (left) or 1min (right) at 25 °C. Phosphorylation was monitored by Western blotting with pY20 antiphosphotyrosine (Upper) and anti-His5 antibody for normalization (Lower). To assess inhibitor specificity, experiments were performed in the presence of 4 μ M lapatinib (L), 4 μ M gefitinib (G), 4 μ M erlotinib (E), or without inhibitor (DMSO only: “-”). All three inhibitors blocked EGFR activity, but left trans-phosphorylation by ErbB3-TKD unaffected.

(B) Western blot analysis to assess the effect of a commercially available kinase inhibitor library (EMD#1) on ErbB3 kinase activity (left) and EGFR kinase activity (right). 1 μ M ErbB3-ICD or 0.1 μ M EGFR-ICD is incubated with 50 μ M inhibitor and 100 μ M ATP in kinase assay buffer (same as in A) for 1 hour (for ErbB3) or 5 minutes (for EGFR) at 25 °C. Reactions were quenched with EDTA (100 mM final concentration) and 2 μ l of each sample was spotted onto nitrocellulose paper. After drying, phosphorylation was monitored by Western blotting with pY20 anti-pTyr antibody and corresponding anti-mouse HRP secondary antibody. Samples in the first column of each blot (8 samples on the left) represent kinase reaction without inhibitor (DMSO only). Kinase inhibitors in the EMD#1 library are listed in Appendix 1.

1.3 Structural Characterization of ErbB3 Kinase Domain by X-ray

Crystallography

To gain insight into how the ErbB3 tyrosine kinase domain retains activity despite substitutions at key residues, we determined its crystal structure. Crystals of ErbB3-TKD grew only in the presence of 5 mM MgCl₂ and the non-hydrolyzable ATP analogue adenylyl-imidodiphosphate (AMP-PNP), and diffracted X-rays to 2.8 Å resolution (Table 1.1). The structure was solved by molecular replacement using an inactive EGFR TKD structure as search model. The asymmetric unit contains two ErbB3-TKD molecules, which are almost identical to one another and pack in the crystal lattice in an N-lobe to N-lobe, C-lobe to C-lobe manner (Figure 1.7).

Table 1.1: ErbB3 TKD crystallographic statistics (molecular replacement).

ErbB3 TKD	
Data collection	APS (GM/CA CAT)
Space group	C2
Cell dimensions	
<i>a</i> , <i>b</i> , <i>c</i> (Å), β (°)	193.4, 48.0, 82.2, $\beta = 108.1^\circ$
Resolution (Å)	50.00 - 2.80 (2.85-2.80) *
R_{sym} or R_{merge}	0.083 (0.499)
$I / \sigma I$	17.1 (2.2)
Completeness (%)	90.0 (55.3)
Redundancy	6.3 (3.4)
Refinement	
Resolution (Å)	50.00 – 2.80
No. reflections	14406
$R_{\text{work}} / R_{\text{free}}$	25.2/28.5
Model	
Protein amino acids	aa A680-728, 732-844, 854-959
	aa B680-711, 713-729, 732-845, 854-959
No. atoms	4316
Protein	4245
Ligand/ion	64
Water	7
R.m.s. deviations	
Bond lengths (Å)	0.006
Bond angles (°)	1.099

*Values in parentheses are for highest-resolution shell.

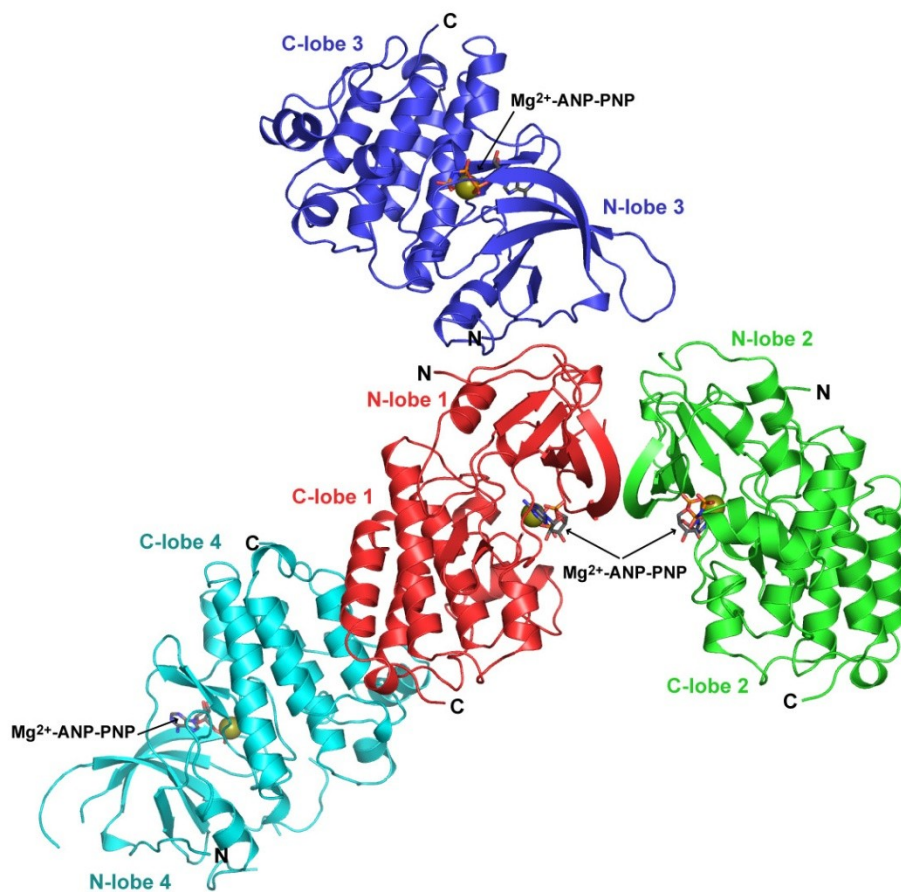


Figure 1.7: Cartoon representation of the crystal packing of ErbB3-TKD. The green structure is molecule A in the asymmetric unit, and the red structure is molecule B. These associate in the crystals through N-lobe mediated interactions. In addition, interaction partners in the crystal are shown for molecule B (red) that associate through alternative N-lobe mediated (dark blue) and C-lobe mediated (cyan) contacts. The packing of ErbB3-TKD molecules in our crystals appear to be the same as those described and discussed in detail by Jura *et al.* (Jura, Shan et al. 2009).

As shown in Figure 1.8A, the overall structure of ErbB3-TKD closely resembles that of the inactive conformation of the EGFR kinase (Zhang, Gureasko et al. 2006), and in turn that of the inactive ErbB4 and Src kinase domains (Zhang, Gureasko et al. 2006; Qiu, Tarrant et al. 2008). Although reduced in length as described below, the α C helix of ErbB3-TKD is displaced away from the active site, in the ‘out’ position typically seen in structures of inactive kinases (Huse and Kuriyan 2002). The activation loop of ErbB3-TKD also retains the characteristic short α -helix that abuts the α C helix in inactive EGFR and ErbB4 (green in Figure 1.8A), and is the site of key mutations that activate EGFR in non-small cell lung cancer (NSCLC) (Sharma, Bell et al. 2007). One particularly notable difference between ErbB3-TKD and the other ErbB kinases is the length of the α C helix, the amino-terminal half of which (\sim 1.5 turns in EGFR) is unraveled in ErbB3-TKD. This region forms a well-defined loop (residues 732-739) in ErbB3-TKD that appears to be anchored by backbone-mediated interactions with the β 4/ β 5 loop and the projection of the F734 side-chain into a hydrophobic pocket formed largely by side-chains from β 3 (I725), β 5 (L764), α C (M741), and the activation loop (L839 and L840) (Figure 1.8B).

Consistent with our mant-ATP binding studies shown in Figure 1.5, we could see clear electron density for both AMP-PNP and Mg^{2+} in the ErbB3-TKD structure (Figure 1.8C). The bound Mg^{2+} ion is coordinated by the side-chains of N820 and D833 (from the DFG motif), plus the α - and β -phosphates of AMP-PNP. The ϵ -amino group of the highly conserved K723 residue (in strand β 3) interacts with both the α -phosphate of AMP-PNP and the D833 side-chain, thus playing a key role in nucleotide binding as seen for inactive EGFR, and indicated by the substantially reduced kinase activity (Figure 1.3)

and mant-ATP binding (Figure 1.5) in the K723M variant of the ErbB3 intracellular domain or TKD.

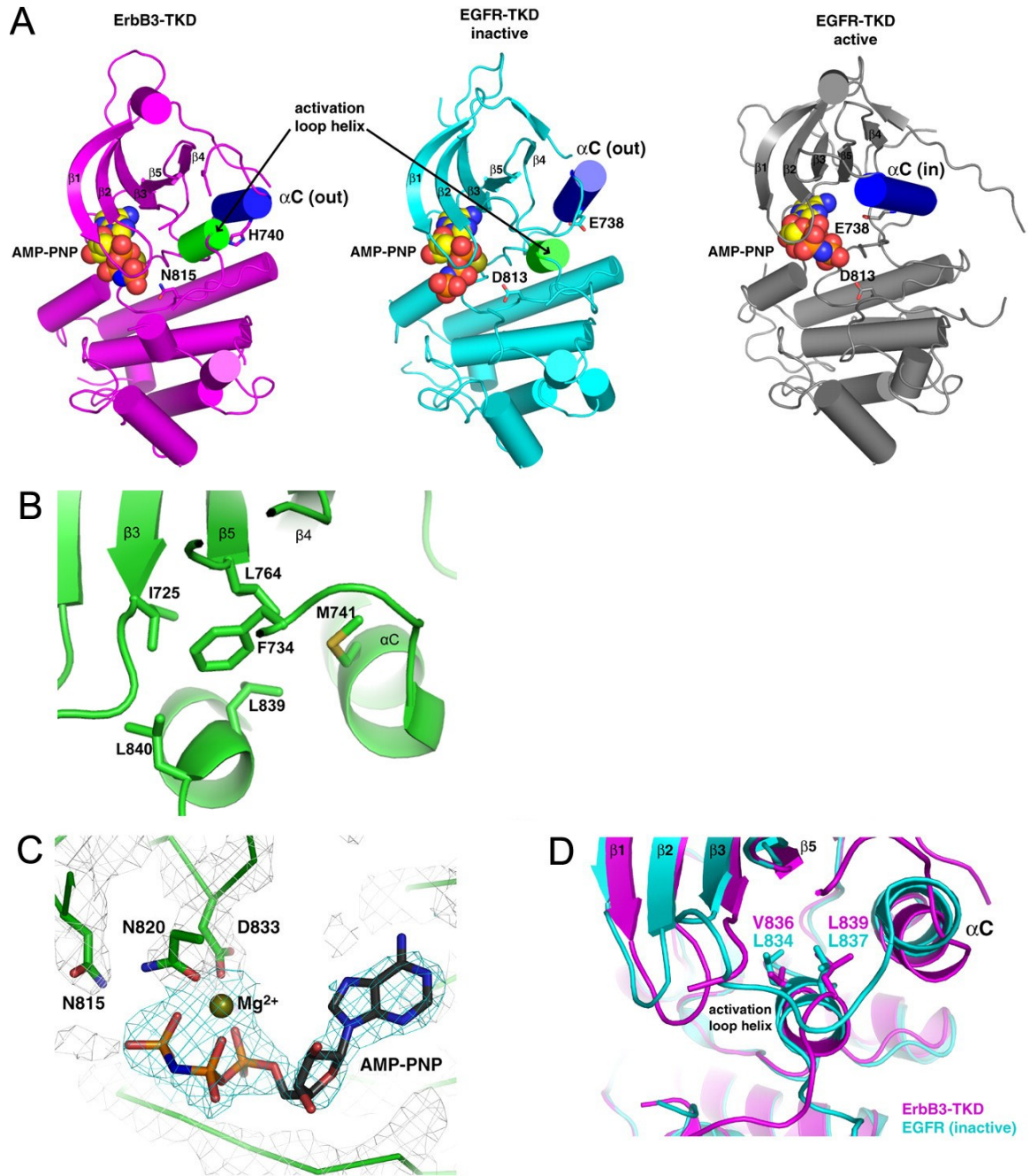


Figure 1.8: Crystal structure of ErbB3-TKD. **(A)** Cartoon representations are shown for ErbB3-TKD⁶⁶⁵⁻¹⁰⁰¹ (left: red) EGFR-TKD in its inactive configuration (Zhang, Gureasko et al. 2006) from PDB code 2GS7 (middle: cyan), and EGFR-TKD in its active configuration with a bound bisubstrate analogue of ATP and peptide (Zhang, Gureasko et al. 2006) from PDB code 2GS6 (right: grey). Bound AMP-PNP and Mg²⁺ ions are shown in spheres and marked, with only the nucleotide portion of the bisubstrate analogue shown for active EGFR. The α C helix is colored blue in each structure, and is denoted as being in the ‘out’ position in ErbB3 and inactive EGFR, and the ‘in’ position in active EGFR. The short α -helix in the activation loop of ErbB3 and inactive EGFR is colored green. H740 in the α C helix of ErbB3 replaces a conserved glutamate (E738 in EGFR), and is shown in stick representation. N815 (which replaces the conserved catalytic base D813) is also marked and shown in stick representation. β -strands in the N-lobe are also labeled. **(B)** Close-up view of the unraveling of α C in ErbB3 TKD structure. The protein sequence (residues 732-739) equivalent to the amino-terminal half of the EGFR α C forms a well-defined loop in ErbB3-TKD that appears to be anchored by backbone-mediated interactions with the β 4/ β 5 loop and the projection of the F734 side-chain into a hydrophobic pocket formed largely by side-chains from β 3 (I725), β 5 (L764), α C (M741), and the activation loop (L839 and L840). **(C)** Close-up view of Mg²⁺-AMP-PNP in the ErbB3-TKD⁶⁶⁵⁻¹⁰⁰¹ active site, with electron density shown as a $2F_o - F_c$ map calculated at 1.8σ with phases from a model into which nucleotide had not been placed. Coordination of the bound Mg²⁺ ion by the side-chains of N820 and D833 (from the DFG motif), plus the α - and β -phosphates of AMP-PNP is depicted. The position of N815 (close to the γ -phosphate) is also shown. The side-chain of K723 (in strand β 3), which interacts with the α -phosphate of AMP-PNP and the D833 side-chain is occluded by the Mg²⁺ ion in this view, and cannot be seen. **(D)** Close-up view of the short α -helix seen in the activation loop of ErbB3-TKD (red) and inactive EGFR-TKD (cyan), with the two kinase superimposed. Mutations at L834 or L837 in EGFR activate the receptor in NSCLC. The side-chains of these residues overlay very well with V836 and L839 in the inactive-like ErbB3-TKD structure, and interact with the hydrophobic pocket that contributes to stabilization of the α C helix in the ‘out’ position.

The activation loop configuration seen in ErbB3-TKD closely resembles that of the inactive EGFR and ErbB4 kinase domains (Zhang, Gureasko et al. 2006; Qiu, Tarrant et al. 2008), and is quite distinct from that seen for active kinases (Huse and Kuriyan 2002). The short α -helix in the activation loops of EGFR and ErbB4 contains several aliphatic side-chains (L834, L837 and L838 in EGFR) that participate in interactions with a hydrophobic pocket formed by side-chains from the β -sheet in the N-lobe and the α C helix. Mutations at L834 and L837 (L834R and L837Q) are known to activate EGFR in some NSCLC cases (Sharma, Bell et al. 2007) by disrupting these interactions, and appear to be oncogenic driver mutations in this cancer. ErbB4 can be activated similarly (Qiu, Tarrant et al. 2008). Moreover, mutating residues that contribute to the hydrophobic pocket into which these aliphatic side-chains project can activate EGFR *in vitro* (Choi, Mendrola et al. 2007). In ErbB3, a conserved VLL motif (V836, L839, L840) in the short activation loop helix makes a very similar set of interactions, apparently stabilizing the ‘inactive-like’ position of the α C helix. As shown in Figure 1.8D, residues V836 and L839 in ErbB3 overlay almost exactly with L834 and L837 in EGFR (key sites of activating NSCLC mutations). To investigate whether similar mutations in ErbB3 can potentially disrupting this inactive-like conformation – we made V836R and L839Q mutations in ErbB3 (parallel to the NSCLS mutations in EGFR), and their effects on cellular signaling will be examined in the next section. Unfortunately, recombinant ErbB3 TKD protein containing either of the mutations does not remain monomeric in solution but form aggregates during purification, therefore its effect on kinase activity cannot be measured directly by *in vitro* kinase assay. However, properties of a similar

V836A mutant of ErbB3 TKD suggest that mutating this hydrophobic VLL motif may likely disrupt this conformation, as it displays compromised ATP binding ability (Figure 1.5D) and kinase activity (Figure 1.3D).

In addition to replacement of the proposed catalytic base with an asparagine in ErbB3 (N815), one of the notable sequence alterations that led to the assignment of ErbB3 as a pseudokinase is replacement of the conserved glutamate in the α C helix with a histidine (H740). Interestingly, this histidine forms a predicted hydrogen bond with the carbonyl oxygen of G835 in the ErbB3 DFG motif. Recent indications of the importance of the conformational dynamics of the DFG motif (Jura, Shan et al. 2009) suggest that this interaction could be relevant for controlling ErbB3 kinase activity. In the inactive EGFR TKD, E738 does not make an equivalent predicted hydrogen bond, but may interact with the side-chain of K836 that follows the DFG motif in EGFR.

The crystal structure of ErbB3 has revealed important structural features of ErbB3 TKD and its binding mode to ATP. However, it is unclear whether the catalytic activity observed in our *in vitro* assays is mediated by this conformation, since it closely resembles the inactive conformation of EGFR kinase. On the other hand, since ErbB3's enzymatic activity is much lower than EGFR, it is possible that this limited catalysis of the phosphoryl transfer reaction could be mediated through this unusual conformation. Indeed, QM/MM simulations by the Radhakrishnan lab at U. of Penn. have depicted a possible reaction pathway for ErbB3 to catalyze tyrosine phosphorylation in such a conformation (Figure 1.9) (Shi, Telesco et al.). The estimated activation energy (E_a) for phosphoryl transfer is 23 kcal/mol for ErbB3 kinase in this conformation, higher than the

16 kcal/mol activation energy for EGFR kinase in the active conformation, consistent with the fact that ErbB3 is a relatively weaker kinase. At this point, we do not have evidence to support or disregard the possibility that alternative conformation(s) of ErbB3 TKD contribute to its catalytic activity.

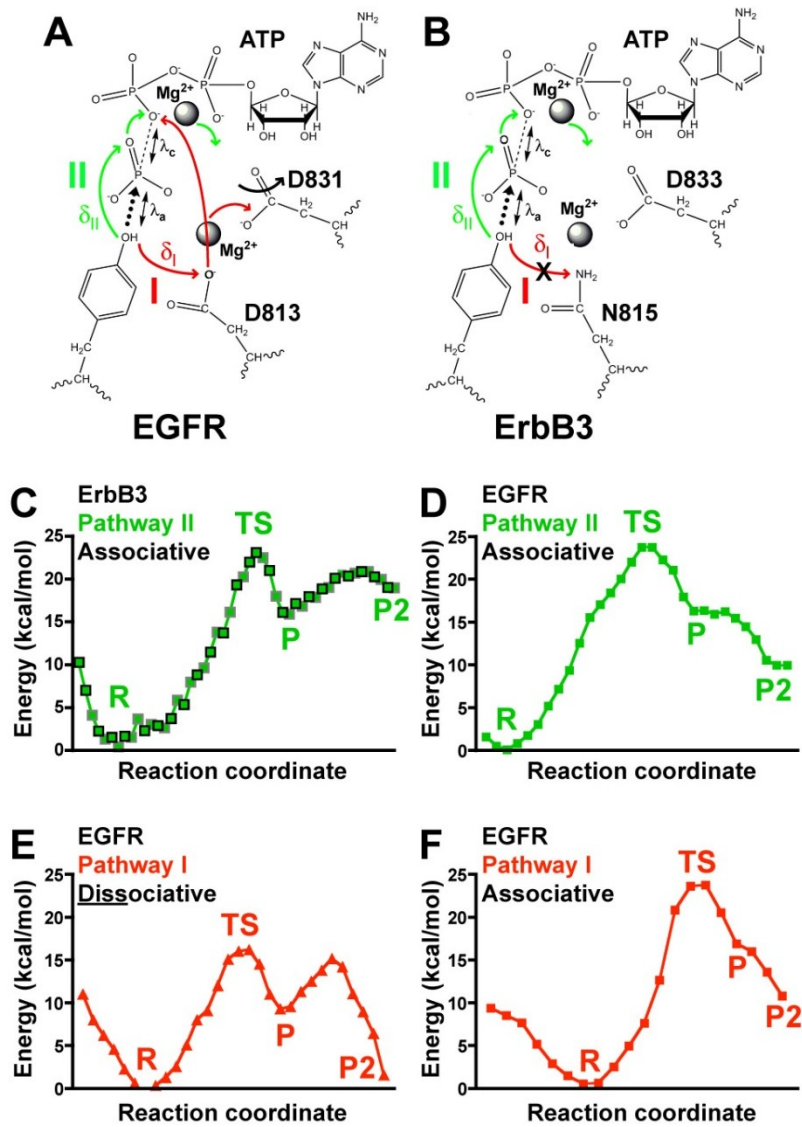


Figure 1.9: QM/MM simulations of phosphoryl transfer of ErbB3 and EGFR kinases (Shi, Telesco et al. 2010). Schematic of the phosphoryl-transfer pathway in (A) EGFR-TKD and (B) ErbB3-TKD, as captured in QM/MM simulations. Mg^{2+} ions are marked, as are the catalytic aspartates (D831 in EGFR, D833 in ErbB3), the proposed catalytic base in EGFR (D813), and its replacement in ErbB3 (N815). Two potential pathways for proton migration (concomitant with phosphoryl transfer) are marked as described in the text: pathway I (*Red*) and pathway II (*Green*). The distance from the substrate -OH proton to the O δ 2 oxygen of D813 in EGFR is labeled δ_I , and its distance to the O1 γ oxygen of ATP is δ_{II} . (C–F) Energy changes along the reaction pathway in QM/MM simulations for the noted mechanisms involving pathway II (*Green*) or pathway I (*Red*). States correspond to “R” (reactant); “TS” (transition state with trigonal-bipyramidal geometry around P γ); “P” (product after phosphoryl transfer with proton bound to ATP O1 γ); and “P2” (product with proton transferred to ATP O2 β) (C) Energy changes along the simulated ErbB3 reaction pathway. Symbols bounded by black squares represent the forward scan, and those bounded by gray squares represent the reverse scan. Only pathway II is utilized, and estimated E_a for phosphoryl transfer is 23 kcal/mol. (D) Energy changes along the EGFR reaction pathway (active configuration) utilizing pathway II and the associative mechanism: Estimated E_a is 24 kcal/mol. (E) Phosphoryl transfer catalyzed by EGFR via the dissociative mechanism (utilizing pathway I for proton migration—via D813) has the lowest E_a value, at 16 kcal/mol. (F) Associative phosphoryl transfer concomitant with pathway I for EGFR has an estimated E_a of 24 kcal/mol. See supplementary materials of (Shi, Telesco et al. 2010) for details.

1.4 Cellular Studies to Investigate the Role of ErbB3 Kinase Domain in ErbB Signaling

It is unclear from the *in vitro* assays described above whether the weak catalytic activity of ErbB3 plays a physiologically relevant role in cellular ErbB signaling. Since the kinase activity of ErbB3 TKD is about 1000 fold weaker than that of EGFR kinase (and other

ErbB kinases), and upon ligand binding ErbB3 forms heterodimers with other ErbB family proteins (rather than homodimer), it seems plausible that ligand-induced ErbB autophosphorylation in cells is carried out predominantly by the other ErbB kinase in the heterodimer. On the other hand, even with weaker kinase activity, ErbB3 may still function as a kinase in cells, especially during abnormal cancer development. Indeed, a weak kinase activity may be sufficient for *trans*-phosphorylation of heterodimerization partners, with the higher activity levels seen for EGFR and ErbB2 only being necessary for the phosphorylation of downstream signaling molecules such as PLC γ , Shc, and other examples.

In efforts to investigate the cellular role of ErbB3's kinase activity, we introduced exogenous full length ErbB3 into BaF3 and CHO cells, which lack significant endogenous ErbB3 expression, and investigated whether amino acid substitutions in the ErbB3 kinase domain affect ErbB3-dependent signaling. Among the mutations that have been introduced, K723M, K723R and V836A mutants show significantly compromised kinase activity in *in vitro* kinase assays (Figure 1.3D). Whereas ATP binding to the K723R mutant is retained (Figure 1.5D), ATP binding to the V836A and K723M variants is greatly reduced (Figure 1.5C&D) – consistent with their loss of kinase activity. Two other mutants (V836R and L839Q) are tested here since the equivalent mutations in EGFR kinase disrupt the packing of the conserved hydrophobic patch in the beginning of activation loop (in the inactive conformation) and play oncogenic roles in NSCLC cells. I919R is located on the C-lobe of ErbB3, and would be predicted to impair the ability of ErbB3 to function as an “activator” in asymmetric ErbB TKD dimers – thus disrupting

the ability of ErbB3 TKD to activate its dimerization partner's kinase domain in an ErbB heterodimer.

1.4.1 Effect of ErbB3 mutations on Autophosphorylation of ErbB2/ErbB3

Heterodimers in BaF3 Cells

We first investigated whether ErbB3's kinase activity is required for ErbB autophosphorylation in ErbB2/ErbB3 heterodimers induced by neuregulin binding. We used BaF3 cells as a 'null' background for these studies, since these murine pro-B cells contain no detectable EGFR, ErbB2, or ErbB4 – although a low level of ErbB3 expression can be detected at the mRNA level. BaF3 cells are commonly used as a cellular background in studies of ErbB receptor properties for these reasons (Riese, van Raaij et al. 1995). Co-expression of full length ErbB3 protein (wildtype or mutated) and wildtype ErbB2 protein in BaF3 cells was achieved through transfection of pIRES plasmids that allow dual expression of both cDNAs. After selecting for stable cell lines co-expressing the desired combination of receptor variants, cells were stimulated with the ErbB3 ligand neuregulin1 β (Nrg1 β), and ligand-induced ErbB autophosphorylation was examined by Western blotting (Figure 1.10A&B). Tyrosine phosphorylation levels of ErbB2 and ErbB3 was detected using 3 different phosphotyrosine antibodies (ErbB2 pTyr877-specific, ErbB3 pTyr1289-specific, and pan pTyr antibodies). Although the expression levels of ErbB2 and ErbB3 variants were clearly different in each cell line (bottom two blots in each panel) despite significant efforts to normalize them using FACS, the data strongly suggest that mutations in the ErbB3 kinase domain did not affect its ability to induce neuregulin-induced ErbB2 (or ErbB3) phosphorylation, clearly

arguing against our initial hypothesis. In fact, none of the following ErbB3 mutations seemed to have a substantial influence on ErbB2 (or ErbB3) phosphorylation when compared with wild-type ErbB3: K723M, K723R, T768G, V836A, V836R, L839Q, V836R/L839Q (Figure 1.10A&B), despite that the K723M, K723R and V836A mutations substantially impair ErbB3 kinase activity *in vitro* (Figure 1.3C&D) (aggregation of purified recombinant TKD protein prevented us from drawing reliable conclusions on this for the other mutants). Taken together, these data argue that ErbB3 is not (at least directly) the kinase responsible for ErbB autophosphorylation in the ligand-induced ErbB2/ErbB3 heterodimers in these BaF3 cell studies. The ErbB3 I919R mutation is distant from the ATP binding pocket and disrupts the presumed ability of the C-lobe of ErbB3 to interact ErbB2's N-lobe to form asymmetric dimers as depicted in Figure 1.2C. Therefore, I919R-mutated ErbB3 will be defective in its ability to allosterically transactivate ErbB2 kinase in ErbB3/ErbB2 heterodimers. The lack of ligand-induced ErbB autophosphorylation in this cell line (Figure 1.10A) suggests that ErbB2's kinase activity is responsible for the autophosphorylation observed in the other cell lines carrying ErbB3 (wildtype or mutant).

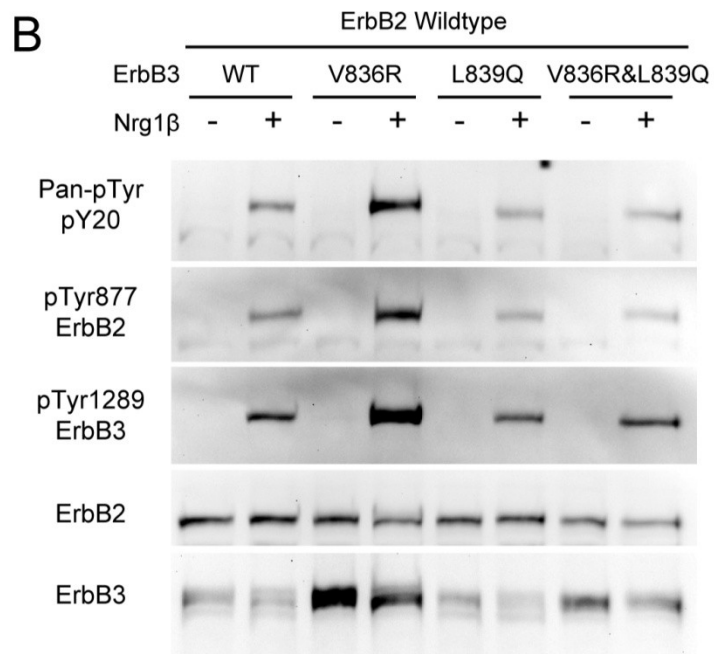
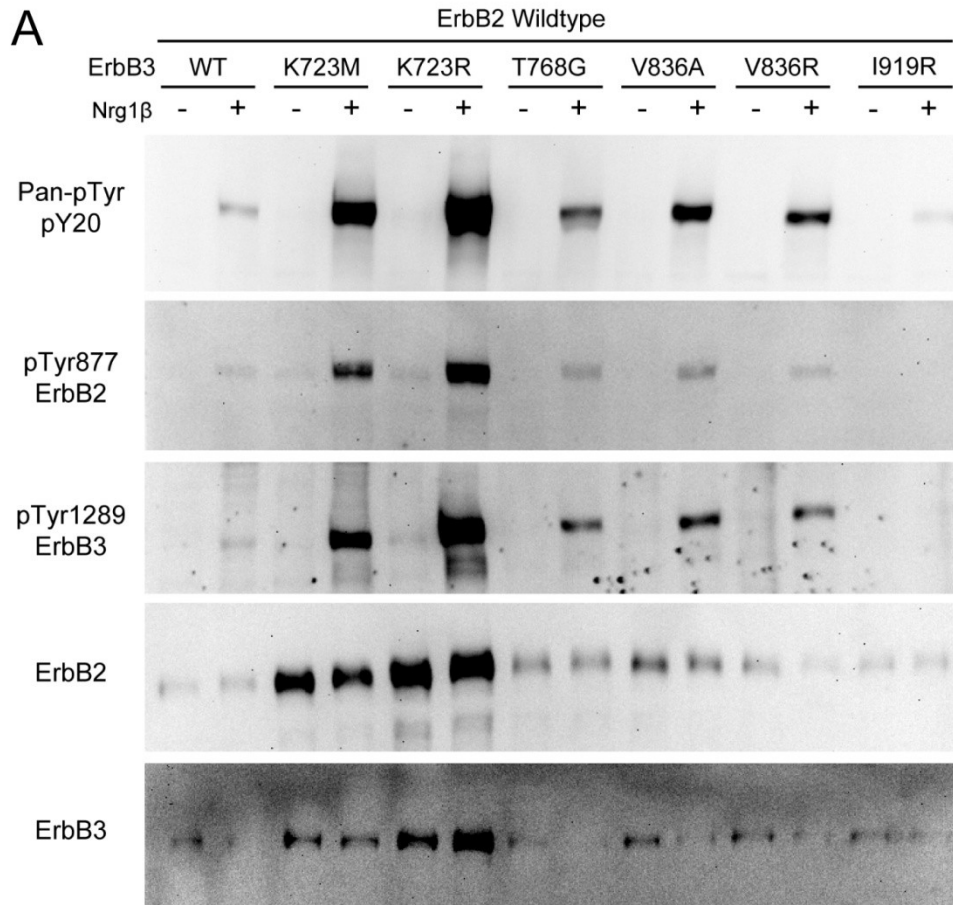


Figure 1.10: Autophosphorylation of ErbB2 and ErbB3 in ligand-induced ErbB2/ErbB3 heterodimers in BaF3 cells. **(A-B)** BaF3 cells were stably transfected with pIRES plasmids containing both wildtype ErbB2 and (wildtype or mutated) ErbB3 mutants, which allows constitutive co-expression of both full length ErbB2 and ErbB3 in the cells. Cells were selected for high ErbB expression using FACS cell sorting. For detection of autophosphorylation, BaF3 cells were serum starved for 6 hours, then washed and resuspended in cold PBS at a density of 1×10^7 cells/ml, and stimulated with neuregulin1 β (50 ng/ml) for 10 min at 4 °C. Cells were then lysed in RIPA buffer, and all glycoproteins were pulled down with Concanavalin A beads (40ul beads for 10^7 cells) in a final volume of 100ul, and samples were prepared for Western blotting with indicated antibodies to assess ErbB2 and ErbB3 phosphorylation.

1.4.2 Mutations within the ErbB3 Kinase Domain Affect its Ability to Activate Akt Signaling in CHO Cells

We next investigated the effects of ErbB3 kinase domain mutations on the ability of this receptor to activate Akt signaling in response to neuregulin. Indeed, ErbB3 has been shown to be mainly responsible for Akt activation in the ErbB2/ErbB3 heterodimer (Hellyer, Kim et al. 2001). We switched to CHO cells for this part of study, since the Akt response could not easily be observed in BaF3 cells. CHO cells are well known not to express endogenous EGFR (Xu, Nagarajan et al. 2011). And other ErbBs are expressed at very low levels (if at all) in CHO cells (Azios, Romero et al. 2001). Accordingly, parental CHO cells show no Akt activation response following addition of the ErbB3 ligand (Nrg1 β) (right-most two lanes in Figure 1.11). In contrast, when transfected with wildtype full length ErbB3, CHO cells show robust activation of the Akt pathway in response to ligand stimulation (left-most two lanes in Figure 1.11), as detected with

antibodies specific for phosphorylated S473 of Akt (a diagnostic of Akt activation). Similar levels of neuregulin-dependent Akt activation were observed in CHO cells expressing the K723M-mutated variant of ErbB3, which we showed has dramatically reduced autophosphorylation activity (in Figure 1.3C&D), and a greatly reduced affinity for ATP (Figure 1.5C). Similarly, T768G and V836R-mutated ErbB3 variants were able to support neuregulin-dependent Akt activation, consistent with the results from studies of ErbB2 *trans*-phosphorylation in BaF3 cells. We also included the I919R ErbB3 variant as a control since this mutation is in the C-lobe of the ErbB3 kinase domain and is predicted to prevent it to *trans*-activate the other ErbB kinase in the heterodimer as shown in Figure 1.2C. The lack of ligand induced Akt activation in I919R mutated ErbB3 variant suggested that Akt activation in these studies does involve formation of asymmetric TKD dimers, most likely in heterodimers of ErbB3 with low levels of endogenous ErbB2 or ErbB4 in CHO cells. Again, overall our data suggest that suppressing the kinase activity of ErbB3 does not significantly affect its ability to signal (via PI3K) to Akt in CHO cells.

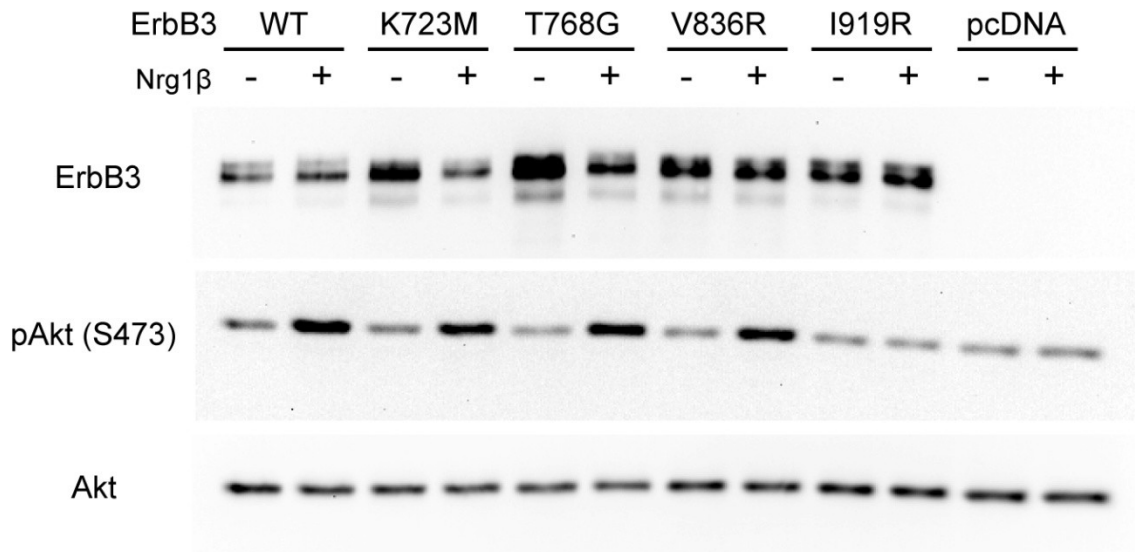
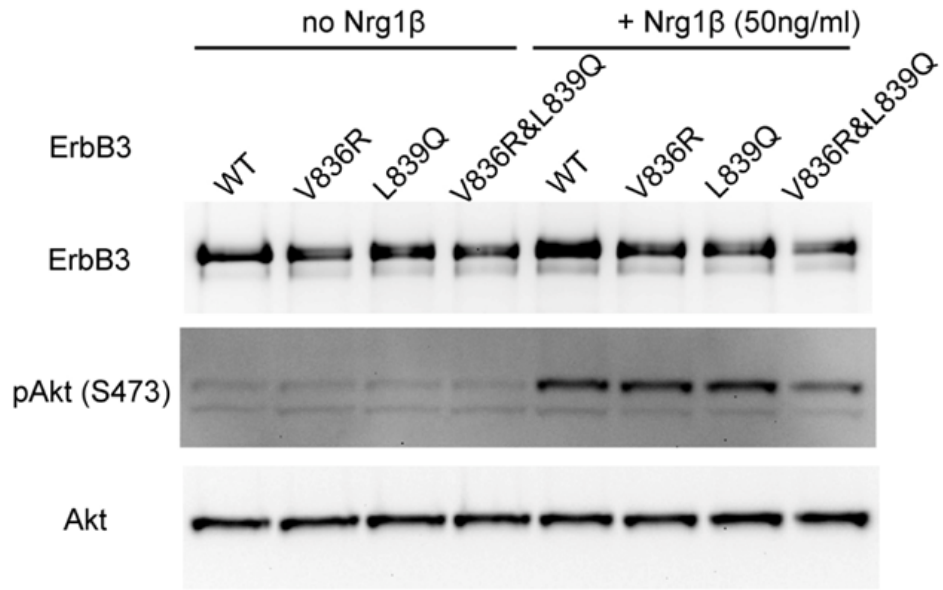


Figure 1.11: ErbB3 mediates neuregulin induced Akt activation in CHO cells. CHO cells were transiently transfected with pcDNA3.1 plasmids containing full length ErbB3 (wildtype or mutant) or parental pcDNA3.1 plasmid as indicated. 24 hours after transfection, CHO cells were serum starved overnight, and then stimulated with neuregulin1 β (40ng/ml) (or PBS as negative control) for 30 min. Then cells were lysed in RIPA buffer and subjected to Western blotting with the indicated antibodies. For the total Akt blot, the pAkt(S473) blot was incubated with stripping buffer after exposure to remove antibodies and was then re-probed with Akt antibodies.

Surprisingly, disrupting the hydrophobic patch that links the small α -helix in the ErbB3 activation loop with the α C helix does appear to compromise ErbB3's ability to activate Akt to some extent, as shown for ErbB3 harboring both the V836R and L839Q mutations (Figure 1.12 A&B). These mutations are interesting because they correspond structurally to the L834R and L837Q mutations in EGFR that activate EGFR's kinase and are now well known to be oncogenic driver mutations in non-small cell lung cancer

(Sharma, Bell et al. 2007). Here, in ErbB3, the equivalent mutations appear to have a negative (rather than activating) influence on activation of Akt signaling. As shown in Figure 1.12, the normalized level of neuregulin-dependent Akt activation was reduced by ~30% in cells expressing V836R/L839Q doubly-mutated ErbB3 compared with cells expressing wildtype or singly mutated ErbB3 in an average over four experiments. To further assess this effect, we performed equivalent experiments using chimeric proteins in which the EGFR extracellular region is fused to the (wildtype or mutated) ErbB3 intracellular region – again in CHO cells (which lack EGFR). As with the ErbB3 experiments, the EGFR/ErbB3 chimera was transiently transfected into CHO cells and its effect on ligand-induced (in this case by EGF) Akt activation was analyzed. The basic observation was reproduced in this context (Figure 1.13): whereas single V836R or L839Q mutations did not significantly affect the ability of the EGFR/ErbB3 chimera to activate Akt signaling, the combined V836R/ L839Q mutations caused a significant decrease of Akt activation upon ligand stimulation – to approximately 40% of levels induced by wildtype ErbB3.

A



B

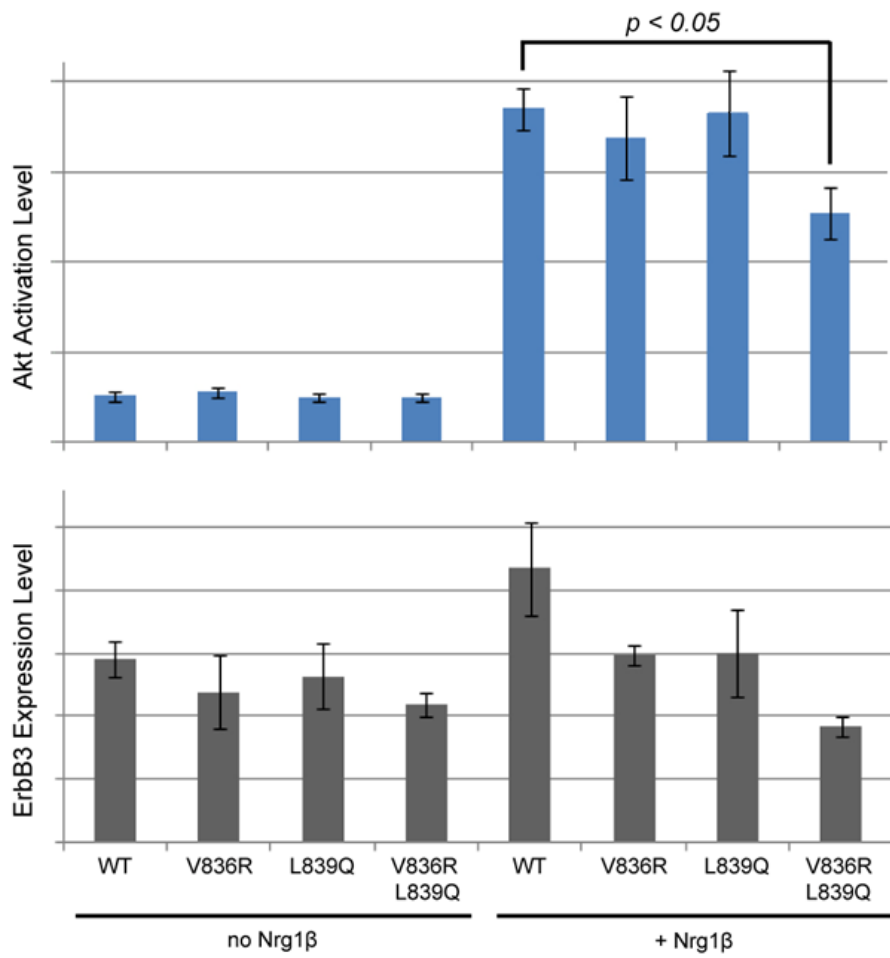


Figure 1.12: V836R and L839Q double mutation in ErbB3-TKD impairs its ability to activate Akt pathway in CHO cell. **(A)** Western blots of neuregulin induced Akt activation in CHO cells transfected with full length ErbB3 (wildtype or mutant). Transfected CHO cells were serum-starved overnight, and neuregulin 1 β (50 ng/ml final concentration) was added for 20 minutes. Cells were then lysed in RIPA buffer and subjected to Western blotting with the indicated antibodies. For each Akt blot, the corresponding pAkt(S473) blot was incubated with stripping buffer after exposure to remove antibodies and was then re-probed with anti-Akt antibodies. Blots are representative of 4 independent experiments. **(B)** Quantitative analysis of Akt activation level (blue) and ErbB3 expression level (grey), calculated from all 4 independent experiments. Band intensities (ErbB3, pAkt, Akt) were determined from Western blots using ImageJ software. In each independent experiment, normalized Akt activation levels were calculated as the ratio of the pAkt(S473) and Akt band intensities. ErbB3 expression levels were also normalized by total (endogenous) Akt levels. Values from all 4 experiments were combined to calculate the final means and standard deviations. Error bars represent one standard deviation. Significance is shown as the difference of ligand induced Akt activation levels between CHO cells transfected with wildtype or V836R&L839Q double mutated ErbB3 ($p < 0.05$).

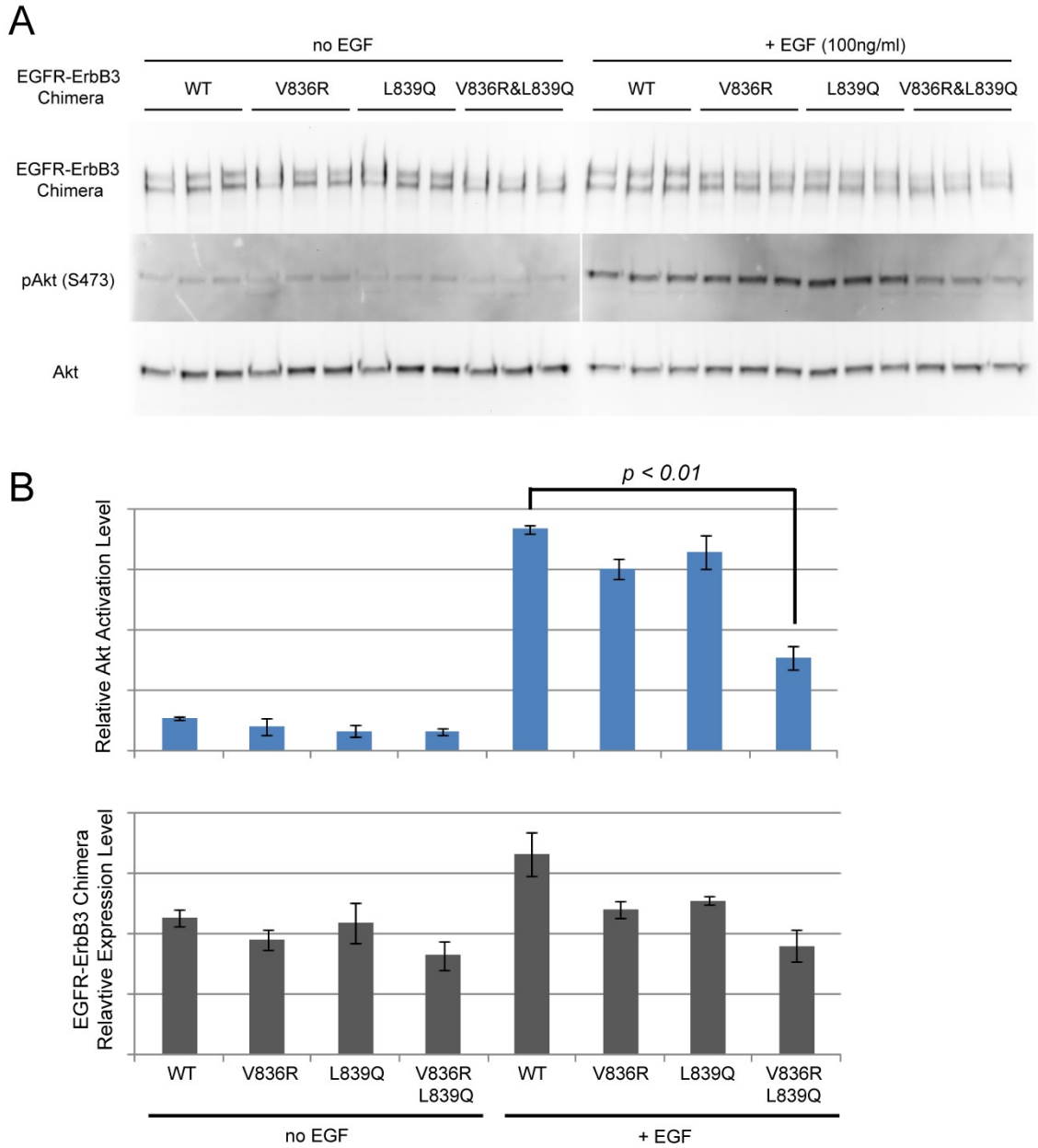


Figure 1.13: V836R and L839Q double mutation impairs the ability of an EGFR/ErbB3 chimeric protein to activate the Akt pathway in CHO cells. (A) Western blots of EGF-induced Akt activation in CHO cells transfected with an EGFR/ErbB3 chimera (wildtype or mutated). Transfected CHO cells were serum-starved overnight, and EGF (100 ng/ml final concentration) was added for 20 minutes on ice. Cells were then lysed in RIPA buffer and subjected to Western blotting with the indicated antibodies. For each Akt blot, the corresponding pAkt(S473) blot was incubated with stripping buffer after exposure to remove

antibodies, and was then re-probed with anti-Akt. Each condition is represented with samples from 3 independent experiments. **(B)** Quantitative analysis of Akt activation level (blue) and EGFR/ErbB3 chimera expression level (grey), calculated from all 3 independent experiments. Band intensities (EGFR/ErbB3, pAkt, Akt) were determined from Western blots using ImageJ software. In each independent experiment, Akt activation levels were calculated as the ratio of the pAkt(S473) and Akt band intensities. EGFR/ErbB3 expression levels were also normalized by total (endogenous) Akt levels. Values from all 3 experiments were combined to calculate the final means and standard deviations. Error bars represent one standard deviation. Significance is shown as the difference of ligand induced Akt activation levels between CHO cells transfected with wildtype or V836R/L839Q doubly mutated EGFR/ErbB3 chimera ($p < 0.01$).

For reasons that are not clear, the V836R/L839Q double mutant also consistently expresses at lower levels than either full length wildtype ErbB3 or the EGFR/ErbB3 chimera. However, the effect is smaller than a factor of two, so this is unlikely to explain the reduced Akt activation that we observe – which does not appear to correlate with receptor expression level in this range in our studies in Figures 1.11-1.13. The lack of dependence of Akt activation on receptor expression levels in Figure 1.11, for example, suggests that the amount of ErbB3 in our CHO cell studies is over-saturating in all cases. Indeed, the V836R or L839Q single mutants maintain normal Akt signaling ability despite also displaying reduced expression levels. We therefore suggest that the ErbB3 V836R/L839Q double mutant has an intrinsic signaling defect. Importantly, this defect is seen in both full length ErbB3 and the EGFR/ErbB3 chimera, despite the fact that the extracellular domains of ErbB3 and EGFR have disparate dimerization properties (EGFR

ectodomain prefers homodimer whereas ErbB3's only forms heterodimers), and therefore the composition of ligand induced ErbB dimers should be very different in these two cases. In the CHO cell experiments, even upon ligand stimulation the autophosphorylation of ErbB3 could not be detected by Western blotting (data not shown), again suggesting a lack of dimerization partners (eg. ErbB2) in these cells – as anticipated from the literature. This contrasts with the BaF3 stable cell lines described in Figure 1.10, which express high levels of both ErbB2 and ErbB3 and show robust ErbB2 and ErbB3 phosphorylation upon ligand stimulation in Western blots.

The fact that the V836R/L839Q double mutation compromises the downstream signaling ability of ErbB3 TKD is surprising. This observation seems unlikely to reflect a simple loss of ErbB3 kinase activity, since known kinase-defective variants (K723M, K723R and V836A) retain the ability to activate Akt. (However, we cannot completely rule out the possibility that the V836R/L839Q double mutation is required to reduce ErbB3's kinase activity to a sufficiently low level to compromise its signaling in CHO cells. Unfortunately, we have not been able to assess the kinase activity of V836R/L839Q-mutated ErbB3 *in vitro*, since the recombinant kinase domain harboring this pair of mutations aggregates during purification.) Also, the reduced Akt signaling activity is unlikely to result from a failure of the mutated ErbB3 to *trans*-activate another ErbB receptor present at low levels in CHO cells, since this effect shall only involve the C-lobe of ErbB3 TKD, which should be unaffected by these mutations. Moreover, the V836R/L839Q double mutation in ErbB3 did not change the ligand-induced ErbB2 or ErbB3 autophosphorylation levels in BaF3 cells (Figure 1.10B). We therefore suggest

that the V836R/L839Q double mutation influences downstream Akt signaling through some other mechanism. If both mutations are required to disrupt the association between the activation loop helix and helix α C in Figure 1.8A&D, they may alter the TKD conformation, which in turn might affect its interaction properties with downstream signaling proteins.

1.5 Summary and Discussion of ErbB3 Studies

ErbB3 has been historically considered to have an inactive kinase domain, due to amino acid changes at key positions when compared with ‘canonical’ protein kinase domains. We have shown that the kinase domain of ErbB3 does retain significant phosphoryl transferase activity despite these sequence alterations, as evidenced by *trans*-autophosphorylation of the purified ErbB3 intracellular region *in vitro*. The observed kinase activity appears to be about 1000-fold weaker than that seen for EGFR. The ErbB3 kinase domain binds ATP with a K_D of approximately 1.1 μ M, similar to (and even stronger than) that reported for many other known active kinases. Using commercially available kinase inhibitor libraries, we have shown that ErbB3 kinase is poorly targeted by current inhibitors. We also describe a crystal structure of ErbB3 kinase bound to an ATP analogue, which resembles the inactive EGFR and ErbB4 kinase domains (but with a shortened α C-helix). A conserved hydrophobic patch at the beginning of the ErbB3 activation loop, involving side-chains from a small α helix in this loop, appears to be responsible for holding the protein in an inactive-like conformation. Mutations that disrupt this hydrophobic patch in EGFR are known to destabilize such inactive conformation, causing hyper-activation of the kinase – and are oncogenic drive

mutations in NSCLC. By contrast, equivalent mutations in ErbB3 appear to compromise ErbB3's ability to activate downstream Akt signaling in cellular studies. Thus, the ErbB3 TKD has novel properties – beyond simply *trans*-activating neighboring ErbB kinases in ligand induced heterodimer as proposed (Jura, Shan et al. 2009).

A key question is whether or not the kinase activity observed *in vitro* is sufficient to mediate meaningful tyrosine phosphorylation in cells. The rate of ErbB3-ICD autophosphorylation when clustered on vesicles containing DOGS-NTA-Ni was about 1000 fold slower than that seen for EGFR-ICD under similar conditions, and exogenous peptide phosphorylation was negligible. Since the ErbB3 TKD is predicted not to form the same asymmetric homodimers as seen for EGFR (Zhang, Gureasko et al. 2006), this difference might simply reflect our failure to activate ErbB3 completely using this *in vitro* approach. Alternatively, the maximum kinase activity of ErbB3 might indeed be ~1000 fold weaker (or more) than EGFR and other ErbB kinases. If so, might this nonetheless be relevant for receptor signaling? There are several reasons to suspect so.

Activation of most RTKs involves initial 'activating' *trans*-autophosphorylation events that follow ligand-induced dimerization (Schlessinger 2000), which typically increase the catalytic efficiency of the kinase by 150-1000 fold overall (Cobb, Sang et al. 1989; Favelyukis, Till et al. 2001; Till, Becerra et al. 2002; Furdui, Lew et al. 2006). The resulting 'full' kinase activation is required for the receptor to phosphorylate exogenous substrates such as insulin receptor substrate-1 (IRS-1) and phospholipase-C γ (PLC γ) (Furdui, Lew et al. 2006), but is clearly not necessary for the initial activating *trans*-autophosphorylation steps (which are mediated by the much weaker unactivated kinase).

Indeed, literature estimates suggest that the initial *trans*-phosphorylation events responsible for activation of the insulin receptor and FGF receptor – mediated by a kinase domain that has not been autophosphorylated – involve kinases that are no more active than ErbB3 in our assays, which are strong arguments as to why the weak kinase activity of ErbB3 might be sufficient to promote (maybe transiently) receptor *trans*-autophosphorylation within RTK dimers (such as ErbB2/ErbB3 heterodimers), which can be crucial for signaling in certain cellular contexts.

The weak kinase activity of ErbB3 could be clinically relevant in cases where this receptor is implicated in mechanisms of resistance to agents that target other ErbB family members (Baselga and Swain 2009). ErbB3 signaling has been found to be important in resistance to gefitinib in NSCLC that arises from MET amplification (Engelman, Zejnullahu et al. 2007), and escape of ErbB2-overexpressing cell lines from growth inhibition or suppression by ErbB kinase inhibitors (Sergina, Rausch et al. 2007). Efforts to inhibit ErbB3 in these (and other) settings have focused on the use of therapeutic antibodies to date (Baselga and Swain 2009). However, if the kinase activity of ErbB3 plays a role in the mechanism by which cancer cells bypass current ErbB-targeted cancer treatments, it will be an attractive target for clinical intervention. The development of small molecules that bind specifically to ErbB3's ATP-binding site would thereby provide useful therapeutic leads. Even if the kinase activity of ErbB3 is not signaling-relevant, certain compounds of this class may be capable of stabilizing ErbB3 TKD conformations that do not support signaling (*eg.* mimic the effects of the V836R/L839Q double mutation described above), and therefore have therapeutic applications.

Further testing of the importance of ErbB3's weak kinase activity will require approaches that have not been described here. In the field of pseudokinases, the key question is that of whether the (pseudo) kinase domain communicates with other aspects of the signaling pathway using kinase activity *per se* or through protein-protein interactions that may be regulated by extracellular ligand binding. Distinguishing between these two possibilities is a difficult challenge. Using the mutation-based approach employed here, it is impossible to determine whether a kinase-inactivating mutation also alters the conformation. Thus, a mutation that aims to impair kinase activity might actually exert its negative effects on signaling by altering pseudokinase conformation. To circumvent this problem, we have exerted significant effort in developing approaches to inhibit ErbB3's kinase activity pharmacologically. We chose to use an approach employing analog-sensitive alleles that was pioneered by the laboratory of Kevan Shokat (Bishop, Kung et al. 1999; Alaimo, Shogren-Knaak et al. 2001; Elphick, Lee et al. 2007). The basic idea is that one mutates the gatekeeper residue in the kinase of interest in order to render it sensitive to 'bumped inhibitors' developed by the Shokat group. If signaling is reconstituted using such an analog-sensitive allele (T768G in ErbB3), the available bumped inhibitors can be used as specific inhibitors to investigate the importance of its kinase activity. Our experiences with this approach are summarized in Appendix 2, in order to document the technical problems experienced. In brief, we were able to apply the allele-sensitive analog approach in pilot studies with EGFR – as has also been achieved by Shokat and colleagues. However, signaling by the variant of ErbB3 expected to be analog sensitive (T768G) did not appear to be effectively inhibited by any available bumped inhibitors. (We were able to detect some effects of the

bumped inhibitors in cells, but the concentrations required to do so were sufficiently high that off-target effects are highly likely.) However, the lack of signaling response of analog sensitive ErbB3 to bumped inhibitors may be a consequence of the fact that ErbB3's kinase is relatively insensitive to broad-specificity kinase inhibitors (as mentioned in discussion of Figure 1.6), and therefore the affinities of the bumped inhibitors are not strong enough for ErbB3 kinase. In collaboration with the Shokat laboratory, we are now working to develop inhibitors that will specifically block the ErbB3 ATP-binding site with high affinity. These studies are still at an early stage, and further work to assess the role of ErbB3's kinase activity in cell signaling awaits progress with these compound development efforts.

Although kinase-impaired ErbB3 mutants showed no apparent signaling defect in our cellular studies, our data do not necessarily rule out the possibility that ErbB3 can function as a kinase in cells. Indeed, the readout of our assay is limited to essentially a few specific tyrosine phosphorylation sites within the complex ErbB signaling network. A more general, proteomic approach such as SILAC might be required in order to study specific effects of disrupting ErbB3 kinase activity. Due to limited time and mass spectrometry resources, I have not been able to explore this approach. Another useful approach – for which my initial efforts are outlined in Appendix 2 – would be to use an analog-sensitive ErbB3 allele and bumped ATP in order to identify ErbB3 substrates as described by the Shokat group (Alaimo, Shogren-Knaak et al. 2001; Elphick, Lee et al. 2007). Even at the absence of such data, we can formulate some reasonable hypotheses regarding ErbB3 kinase activation in cells:

1) ErbB3 might need other cellular factors to become fully activated in the cell, and this would not be captured in our simplified heterodimer system in BaF3/CHO cells or in our *in vitro* system. For example, a phenomenon of this sort might be relevant for MET/ErbB3 cross-talk, with MET signaling providing such activating factors.

2) ErbB3 kinase may have a (uncharacterized) specific substrate preference, which is overlooked in my cellular studies. For example, it may be subject to a substrate-assisted activation mechanism, which is not uncommon in other enzymes (Dall'Acqua and Carter 2000). Such a mechanism could be particularly interesting in the case of ErbB3 kinase. Based on the structure, the only “canonical” catalytic element missing in the ErbB3 kinase active site is a carboxylate group that is typically found on the conserved Asp (substituted by an Asn in ErbB3) proposed to function as a catalytic general base. A kinase substrate that provides such a carboxylate group at the right position might conceivably complement such a deficiency, and thus become an optimal substrate for ErbB3 kinase.

Zhang et al. (Zhang, Gureasko et al. 2006) previously argued based on sequence comparisons that the ErbB3 TKD should be able to participate as an ‘activator’ in allosteric activation of the EGFR kinase domain within the context of an asymmetric dimer, due to the similarity of its C-lobe to that of EGFR-TKD, but not as the ‘receiver’ that becomes activated (because of substantial change in the ErbB3 N-lobe comparing to that of other ErbBs). Jura *et al.* (Jura, Shan et al. 2009) reported an ErbB3-TKD⁶⁷⁴⁻¹⁰⁰¹ structure (PDB ID 3KEX) that is essentially identical to the structure described here, and have confirmed the ability of ErbB3-TKD to function as an allosteric activator of the

EGFR kinase domain *in vitro*. The structural differences in the N-lobe – including the shortened α C helix described above – reinforce the argument that ErbB3-TKD cannot be activated by the same types of asymmetric dimer interactions thought to activate EGFR, ErbB4 and ErbB2 in heterodimeric complexes. If the ErbB3 TKD can function as a ‘receiver’ kinase in ErbB receptor dimers, it must do so through mechanisms that are quite different from those described for EGFR (Zhang, Gureasko et al. 2006) and ErbB4 (Qiu, Tarrant et al. 2008).

A common argument for ErbB3 not being a physiologically relevant active kinase is that the N-lobe of ErbB3 TKD is different from that of other ErbBs, suggesting that it cannot function as a receiver kinase in the asymmetric dimer (and thus become activated). However, this argument implies that ErbB2 kinase is sufficiently active to carry out all the tyrosine phosphorylation of both C-tails in the heterodimer – of ErbB3 (in *trans*) and ErbB2 (in *cis*). Given also that ErbB2 is an orphan receptor (and only forms heterodimers with other ErbBs), ErbB2 has no need to function as an activator kinase in the asymmetric dimer if it can mediate all phosphorylation by itself when activated by the other kinase in the heterodimer – which in turn suggests that the C-lobe interface of ErbB2 kinase does not have to be evolutionarily conserved. In fact, the ErbB2 C-lobe interface is highly conserved for asymmetric dimer formation, suggesting that, in the heterodimer with ErbB2, the other ErbB kinase also needs to be activated by ErbB2. Therefore, in the case of ErbB heterodimer involving ErbB3, ErbB3 kinase activity may be required for optimal signaling, although it may function through a different mechanism due to an altered N-lobe of ErbB3 TKD.

So far we have been discussing the possibility that ErbB3 functions as a kinase in the cell. Our cellular studies have also shown that, even though kinase-inactivating mutations within ErbB3 TKD have no effect on its autophosphorylation or activation of Akt pathway, the V836R/L839Q double mutation compromises its ability to mediate neuregulin-induced Akt activation (but not levels of ligand-induced ErbB autophosphorylation). The finding that disrupting the hydrophobic patch between the activation loop helix and α C helix within the ErbB3 kinase domain reduces downstream signaling activation provides supporting evidence for the hypothesis that ErbB3 TKD plays additional signaling roles beyond simply *trans*-activating neighboring ErbB kinases in ErbB3-containing heterodimers. Since the Akt pathway is directly involved in the development of cancers and their drug resistance via ErbB3 (Engelman, Janne et al. 2005; Sergina, Rausch et al. 2007; Castaneda, Cortes-Funes et al.), understanding how the ErbB3 kinase domain affects these signaling pathways should provide useful clues for developing therapeutic approaches in cancer. Unfortunately, my studies do not provide a clear view of the degree to which these changes affect ErbB3 kinase activity or ATP binding ability, since introducing these mutations – together or individually – into recombinant ErbB3 ICD protein (over-expressed in Sf9 insect cells) impairs protein stability, resulting in protein aggregation during protein purification and an inability to perform *in vitro* assays. Additional cellular studies are needed to uncover the molecular mechanism underlying ErbB3 TKD's regulation of downstream Akt signaling activation.

Based on our CHO cell study it seems likely that ErbB3 kinase domain acts as a scaffolding protein that may allosterically regulate downstream signaling. Such function

is not usual, even for highly active kinases. For example, recent studies of Akt protein itself have revealed that, in addition to catalysis, its kinase domain can function as a protector for phosphorylated residues upon binding to ATP or ATP-competitive inhibitors (Chan, Zhang et al.; Lin, Lin et al.) – *i.e.* a scaffolding function. Binding of ATP (or inhibitor) stabilizes Akt kinase domain in a restricted conformation, which brings its phosphorylated T308 and S473 residues close to the kinase domain surface and shields them from phosphatases, whereas binding of ADP has the opposite effect (facilitating dephosphorylation) (Lin, Lin et al.). A similar function may exist in ErbB3 kinase domain (the ‘inactive’ conformation with ATP bound protects the phosphorylated tyrosine from being hydrolyzed), which could explain the observed cellular effect of V836R&L839Q double mutation.

Several earlier studies have suggested a non-canonical role for the ErbB3 kinase domain, reminiscent of proposed ‘scaffold-like’ functions for its pseudokinase domain:

- 1) Using a yeast two-hybrid approach, Yoo et al. measured the interaction between ErbB3 ICD and the p85 unit of PI3K using a β -galactosidase reporter assay (Yoo and Hamburger 1998). Intriguingly, wildtype rat ErbB3 (which retains its catalytic base aspartate at D815 - unlike human ErbB3) generates low output signal, suggesting a lack of ErbB3 tyrosine phosphorylation. However, a D815N rat ErbB3 mutant facilitates the interaction and increase the assay output by 26 fold. Curiously, further mutating the conserved key lysine in the ATP binding site (*i.e.* rat ErbB3 K723A/D815N double mutant) abolishes this output increase. Although it is unclear whether the increase of signal is caused by ErbB3 kinase activity or change of conformation, this result implies a

functional role of Asn815 (instead of Asp) in ErbB3 TKD to modulate PI3K interaction – perhaps through a scaffolding function.

2) In a study by Engelman et al. (Engelman, Janne et al. 2005), CHO cells transfected with wildtype EGFR showed sustained Akt activation even after 4 hours of EGF stimulation, whereas the long term phosphoAkt signal was abolished in CHO cells transfected with EGFR L858R (equivalent to ErbB3 V836R) activating mutant. This result is reminiscent of our CHO cell studies, in which the ErbB3 V836R/L839Q double mutant shows compromised ability to activate Akt pathway compared to wildtype ErbB3. In both cases, a specific conformation change accompanied with the mutations may disrupt the ability of ErbB protein (EGFR and ErbB3) to relay ligand stimulation to downstream signaling.

In addition to the ErbB3 kinase described here, the signaling scaffold function has been proposed in many other pseudokinases, such as STRAD proteins to the kinase domain of LKB1, KSR for MAP kinase signaling, CASK in the synaptic protein complex, and the autonomous regulation of JAK2's pseudokinase domain to its upstream tyrosine kinase domain (summarized in (Boudeau, Miranda-Saavedra et al. 2006)). Intriguingly, all these pseudokinases have been reported to possess either ATP binding ability (for STRAD (Boudeau, Scott et al. 2004)) or kinase activity (for KSR1 (Hu, Yu et al. 2011; Shi and Lemmon 2011), CASK (Mukherjee, Sharma et al. 2008) and JAK2 (Bandaranayake, Ungureanu et al. 2012)), although the exact roles of such functions are often unclear. Further in-depth analysis is required to provide us with a better picture of the role of pseudokinases such as ErbB3's.

1.6 Experimental Procedures for Chapter 1

Materials and Reagents. Mant-ATP (2'-(3')-O-(N-methylanthraniloyl)adenosine 5'-triphosphate) was purchased from Invitrogen (Cat.# M-12417). 1, 2-dioleoyl-*sn*-glycero-3-([N(5-amino-1-carboxypentyl)iminodi-acetic acid]succinyl} nickel salt (DOGS-NTA-Ni) was purchased from Avanti Polar Lipids. Primary antibodies mentioned here include: pY20 antibody (BIOMOL), anti-His5 antibody (QIAGEN), anti-ErbB2 pTyr877, anti-ErbB3 pTyr1289, anti-Akt and anti-pAkt(Ser473) antibodies (Cell Signaling), anti-ErbB2 Ab8 and anti-ErbB3 Ab7 antibodies (NeoMarker/LabVision). Neuregulin 1 β was purchased from R&D Systems Inc.

Protein Expression and Purification. DNA fragments encoding the relevant regions of the human ErbB3 intracellular domain (ErbB3-ICD⁶⁶⁵⁻¹³²³) or tyrosine kinase domain (ErbB3-TKD⁶⁶⁵⁻¹⁰⁰¹ and ErbB3-TKD⁶⁴⁸⁻¹⁰⁰¹) with an amino-terminal hexahistidine tag were subcloned into the pFastBac1 vector (Invitrogen) to generate corresponding baculoviruses using the Bac-to-Bac expression system (Invitrogen). *Spodoptera frugiperda* Sf9 cells were infected with the respective baculoviruses for 3 days, and cells were collected and resuspended in buffer containing 20 mM HEPES pH 8.0, 300 mM NaCl, 5% glycerol, 5 mM 2-mercaptoethanol and a protease inhibitor cocktail (Roche). ErbB3 proteins were affinity purified using Ni-NTA beads (Qiagen), followed by anion exchange chromatography with a UnoQ1 column (Bio-Rad) in 20 mM Tris pH8.0, 5% glycerol and 1 mM DTT (eluting with a linear gradient from 120 mM to 1 M NaCl). ErbB3-containing fractions were concentrated and subjected to size exclusion

chromatography using a Superdex 200 column (GE Healthcare) equilibrated with 20 mM Tris pH 8.0, 200 mM NaCl, 5% glycerol and 1 mM DTT.

Analysis of Autophosphorylation by Western Blotting. Vesicles containing DOGS-NTA-Ni at 5-10 % (mole/mole) in a background of dioleoylphosphatidylcholine (Sigma) were prepared as described (Zhang, Gureasko et al. 2006). Vesicles (50-150 μ M total lipid) were incubated with ErbB3 proteins at the concentrations noted in the legend to Figure 1.3 in 100 mM MOPS pH 7.4, containing 200 mM NaCl, 5 % glycerol, 1 mM ATP, 5 mM $MgCl_2$, 2 mM $MnCl_2$, and 0.1 mM DTT for 30 min at 25°C, and the reactions were stopped by adding 50 mM EDTA and SDS-PAGE gel-loading buffer. Proteins were subjected to electrophoresis and transferred to nitrocellulose for Western blotting. Blots were probed with the indicated primary antibodies, and detection was accomplished using an HRP-conjugated anti-mouse (or rabbit) antibody (Amersham) and enhanced chemiluminescence.

Mant-ATP Binding Assay. Binding assays were carried out in 20 mM Tris pH 8.0, containing 200 mM NaCl, 5 % glycerol, 1 mM DTT, 5 mM $MgCl_2$ and 0.6 μ M Mant-ATP, with varying amount of ErbB3⁶⁴⁸⁻¹⁰⁰¹ protein. Fluorescence measurements were taken in triplicate using a Tecan SAFIRE II plate reader, with excitation wavelength of 280 nm and emission wavelength of 450 nm (5 nm bandwidth for both) to monitor FRET between protein and bound mant-ATP.

Crystallization and Structure Determination. Purified ErbB3-TKD⁶⁶⁵⁻¹⁰⁰¹ was concentrated to 6 mg/ml and incubated with 5 mM $MgCl_2$ and 1 mM AMP-PNP (Sigma).

Crystals were obtained using the hanging-drop method at 21°C by mixing the protein with an equal volume of reservoir solution (50 mM MOPS pH 7.4, 27 % (w/v) PEG8000, 0.17 M (NH₄)₂SO₄ and 15% glycerol). Needle-like crystals appeared within 2 days and were frozen in liquid nitrogen directly from the mother liquor. Diffraction data were collected at the Argonne Advanced Photon Source (beamline GM/CA CAT) and processed with the program HKL2000 (Otwinowski and Minor 1997). The structure was solved using molecular replacement (MR) using the program Phaser (CCP4 (Collaborative Computational Project Number 4) 1994) with the inactive EGFR (V924R) TKD structure (PDB code 2GS7) (Zhang, Gureasko et al. 2006) as the search model. The program Coot (Emsley and Cowtan 2004) was used for model building, and refinement employed the programs REFMAC (CCP4 (Collaborative Computational Project Number 4) 1994) and CNS (Brünger, Adams et al. 1998). TLS refinement (Winn, Isupov et al. 2001) was employed in the later stages of refinement, using REFMAC (CCP4 (Collaborative Computational Project Number 4) 1994), with anisotropic motion tensors refined for each lobe of the kinase domain. Structure figures were generated using PyMol (DeLano 2002).

Cellular Studies. For studies with BaF3 cells, BaF3 cells were maintained in RPMI 1640 medium containing 10% FBS, 10mM HEPES, 2mM sodium pyruvate and 1ng/ml IL3. To generate each stable BaF3 cell line co-expressing ErbB2 and ErbB3, a pIRES plasmid with the relevant full length ErbB3 at site A and full length ErbB2 at site B (after IRES) was introduced into BaF3 cells using electroporation with a BTX 600 instrument. Briefly, 4x10⁶ cells were incubated with 40 µg DNA and electroporated at

1500 μ F capacitance, 240 voltage and R10 resistance. 48 hours post-electroporation, G418 was added to a final concentration of 1mg/ml in the medium to select (over 10 days) for cells harboring the plasmid. Cells were then sorted for high ErbB2 expression using FACS and PE-labeled anti-HER2 antibody (Becton Dickinson). For autophosphorylation experiments, BaF3 cells were serum starved for 6 hours, then washed and resuspended in cold PBS at a density of 1×10^7 cells/ml. Cells were then stimulated with neuregulin1 β (50ng/ml) for 10 min on ice. Cells were lysed in RIPA buffer (25 mM Tris-HCl pH 7.5, 150 mM NaCl, 1% Triton X-100, 1% Sodium deoxycholate, 0.1% SDS) containing 1 mM PMSF, 1 μ g/ml leupeptin, 1 μ g/ml aprotinin, 25 mM NaF, 5 mM Na₂MoO₄, and 0.2 mM Na₃VO₄, and debris was pelleted by centrifugation. All glycoproteins in the lysate were then collected by incubating the lysate with concanavalin A beads (GE Healthcare, 40ul beads for 10^7 cells) for 2 hours at 4 °C. Beads were then washed, resuspended in RIPA buffer (final volume of 100ul), and added 3x RSB with 5% BME and EDTA to a final concentration of 50mM. Samples were then boiled for Western blotting with indicated antibodies.

For Akt activation experiments, CHO cells were maintained in Hank's F12 media containing 10% FBS, 2 mM L-glutamine and 1.5 g/L sodium bicarbonate. For transient transfection, parental CHO cells were seeded at 4×10^5 cells/well in 6-well plates. 24 hours after seeding, cells were transfected with indicated pcDNA3.1-ErbB3 full-length or pRc/CMV-EGFR-ErbB3 chimera constructs using FuGENE transfection reagent (1.5 μ g DNA and 6 μ l reagent per well). 24 hours after transfection, medium was removed and replaced with serum-free medium overnight. Cells were then stimulated with

neuregulin1 β (or PBS as negative control) for 10-30 minutes, then lysed in RIPA buffer containing 1 mM PMSF, 1 μ g/ml leupeptin, 1 μ g/ml aprotinin, 25 mM NaF, 5 mM Na₂MoO₄, and 0.2 mM Na₃VO₄. Lysates were then subjected to Western blotting with indicated antibodies. For blots of total Akt, the corresponding pAkt(S473) blot was incubated with stripping buffer after HRP signal development to remove pAkt antibodies, and was then re-probed with anti-Akt antibodies.

Chapter 2

Characterization of Derailed-Wnt Interactions

Ryk/Derailed family receptor tyrosine kinases (RTKs) are membrane signal transducers thought to mediate signaling induced by extracellular Wnt proteins. While developmental studies have characterized the indispensable roles of Ryk/Derailed family RTKs in cell patterning and differentiation, especially during neuronal development, few studies have attempted to uncover the molecular mechanisms of their signaling and ligand recognition. Utilizing biophysical methods, my study aims to understand the molecular interactions between Ryk/Derailed family RTKs and Wnt ligands, using *Drosophila* Derailed – DWnt5 as a model system.

2.1 Overview of Ryk/Derailed – Wnt Signaling Pathway

2.1.1 Introduction to Wnt proteins and Wnt Pathway

Wnts, named after Wg (wingless) and Int (Integration 1), are a family of highly conserved, secreted proteins containing a characteristic Wnt domain that is comprised of ~330 amino acids with a characteristic distribution of 24 cysteine residues. A total of nineteen Wnt family proteins have been identified in the deduced mammalian proteome. They play diverse roles in embryonic development and adult homeostasis, including segment polarity (Baker 1987) and neural tube development (Ikeya and Takada 1998) during embryogenesis and adult limb formation during metamorphosis (Yokoyama, Maruoka et al.). Wnt proteins are typically lipid modified, rendering the proteins hydrophobic (Willert, Brown et al. 2003; Takada, Satomi et al. 2006; Kurayoshi, Yamamoto et al. 2007).

In canonical Wnt signaling, the Wnt – β -catenin – TCF axis plays a central role. In the absence of Wnt signaling, β -catenin is constantly phosphorylated in a protein complex formed by Axin/APC/casein kinase 1 (CK1)/glycogen synthase kinase 3 (GSK3). Phosphorylated β -catenin is then ubiquitinated and degraded by proteasome. The binding of Wnt proteins to the cysteine-rich domain (CRD) of Frizzled receptors (their best known cell surface receptors) and LRP 5/6 co-receptors leads to recruitment of Dishevelled (Dvl) protein through its PDZ domain to the intracellular tail of the Frizzled receptor and subsequent phosphorylation of LRP6. Phosphorylated LRP protein on the membrane then recruits the Axin complex, thus freeing β -catenin protein from degradation in the cytosol. Accumulated β -catenin then translocates into the nucleus and binds to DNA-bound TCF transcription factors, which in turn initiates transcription of genes that are controlled by TCF promoter (Figure 1A, left) (Logan and Nusse 2004; MacDonald, Tamai et al. 2009; Clevers and Nusse 2012).

Very recently, a crystal structure of *Xenopus* Wnt8 (XWnt8) in complex with the CRD of mouse Frizzled-8 (mFz-8) was reported (Figure 2.1B) (Janda, Waghray et al.). The CRD of mouse Frizzled-8 displays a mostly α -helical structure as described before (Dann, Hsieh et al. 2001). XWnt8 comprises a large N-terminal region that is mostly α -helical (with four short β strands formed as a sheet on one side) and a smaller C-terminal region that contains two long β strands in a hairpin-like configuration. The crystal structure also revealed Ser207 of XWnt8 (equivalent to Ser868 of DWnt5) as a lipidation site. XWnt8 binds to mFz-8 CRD through two separate loop regions. The first binding region, located on the N-terminal side of XWnt8, mainly uses the palmitoyl lipid moiety

(PAM in Figure 2.1B) to engage a hydrophobic groove on the CRD. The second binding region, which is located in between the two long β strands on the C-terminal side of XWnt8, consists of a long loop and is thought to contribute to selectivity of Wnt binding to CRDs from different Frizzled receptors. However, it is yet unclear from this structure how binding of Wnt ligand leads to signaling through Frizzled receptors.

In addition to the canonical Wnt signaling, Wnt proteins also participate in the orientation of planar cell polarity (PCP) through signaling to c-Jun N-terminal kinase (JNK) (Wang 2009), and control of cell migration through the activation of heterotrimeric G proteins that leads to increased level of intracellular Ca^{2+} and signaling by calcium dependent kinases (De 2011) (Figure 1A, right).

Increasing evidence has shown unequivocally that the canonical, PCP, and Wnt/ Ca^{2+} pathways are only some of the many signaling events initiated by Wnt binding, and the specific cellular response for any Wnt ligand reflects the combined actions of a diverse set of Wnt receptors present on the cell surface (van Amerongen, Mikels et al. 2008). In addition to the ten Frizzled receptors in mammals, the RTKs Ryk and Rors have been shown to act as Wnt receptors on the cell surface that mediate Wnt signaling (Figure 1A). Ror1 and Ror2 contain CRD domains that are related to those in Frizzleds. On the other hand, Ryk/Drl lack a CRD-related domain for Wnt binding. Instead, they are thought to bind Wnts through their extracellular WIF domains, which are homologous to human Wnt Inhibitory Factor-1 (hWIF-1) protein.

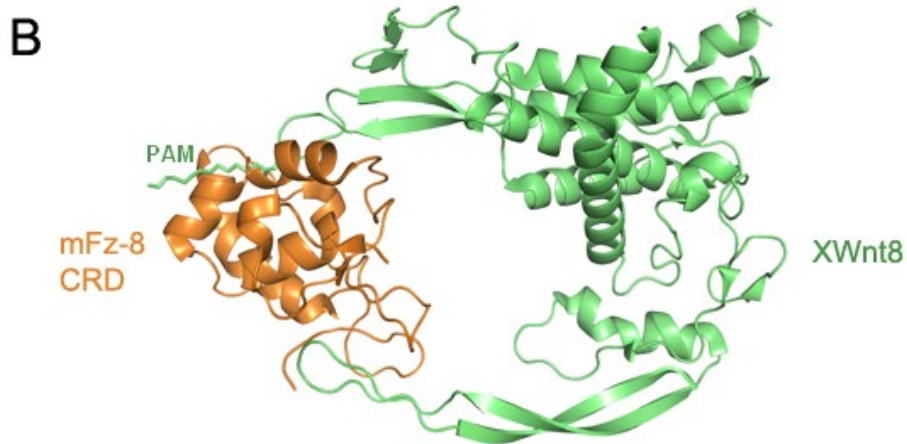
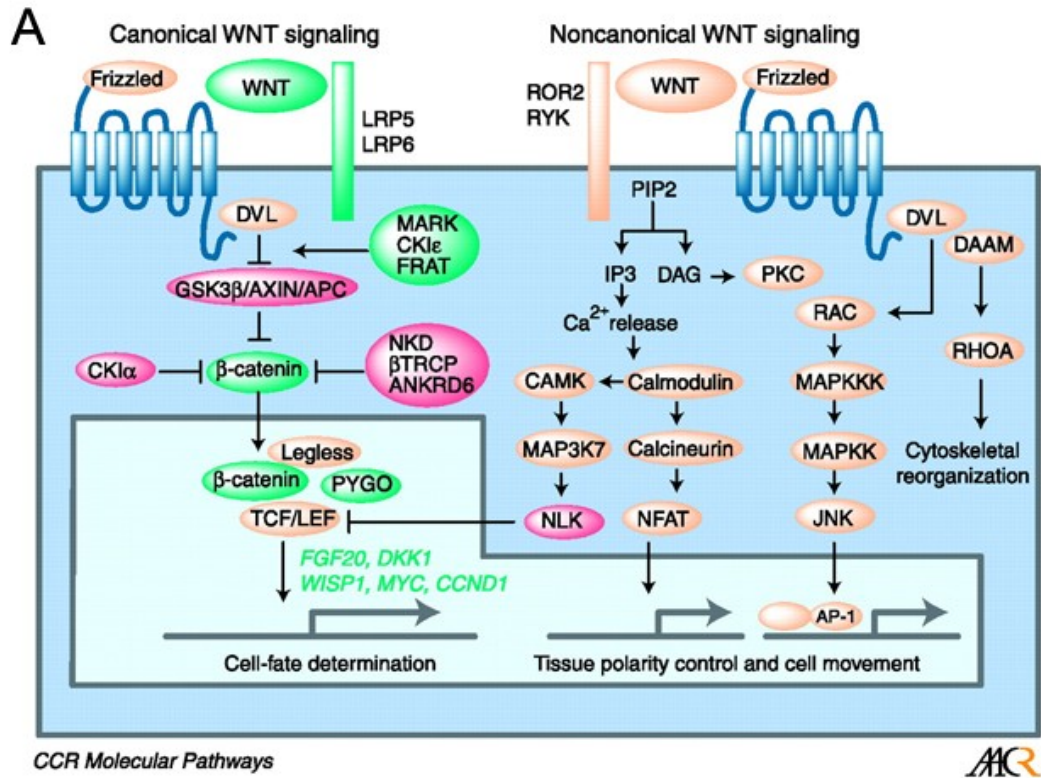


Figure 2.1: Overview of Wnt signaling. (A) Illustration of canonical and non-canonical Wnt signaling (adapted from (Katoh and Katoh 2007)). (B) Crystal structure of *Xenopus* Wnt8 (XWnt8) in complex with the cysteine rich domain (CRD) of mouse Frizzled-8 (mFz-8) (PDB: 4F0A) (Janda, Waghray et al. 2012). The lipid moiety of XWnt8 is labeled PAM.

2.1.2 Introduction to Ryk/Derailed Family Receptor Tyrosine Kinases

Ryk (Related to tYrosine Kinases) is a protein with a single transmembrane domain that belongs to the vertebrate RTK family, first isolated in the early 1990s using PCR with degenerate primers (Hovens, Stacker et al. 1992; Yee, Bishop et al. 1993). Ryk orthologs are also present in invertebrate, such as Derailed in *Drosophila melanogaster* and LIN-18 in *C. elegans*. Ryk and its invertebrate orthologs are characterized by an extracellular WIF (Wnt Inhibitory Factor) domain (see below) and an intracellular pseudokinase domain (Figure 2.2).

Ryk is expressed in various mammalian tissues during both embryogenesis and adulthood (Halford, Oates et al. 1999). Homozygous Ryk-null mice display distinctive development defects, including a shortened craniofacial region and diminished limbs (Halford, Armes et al. 2000). These morphological features are similar to the symptoms observed in mice lacking members of the EphB family of RTKs (Bush and Soriano 2010), implying signaling crosstalk or collaboration between the Ryk and EphB classes of RTKs. Accordingly, Ryk has been shown to co-immunoprecipitate with both EphB2 and EphB3 (Halford, Armes et al. 2000; Trivier and Ganesan 2002; Kamitori, Tanaka et al. 2005). In addition, overexpression of Ryk has been reported to cause transformation of NIH3T3 cells, leading to their tumorigenicity when injected into nude mice (Katso, Manek et al. 1999).

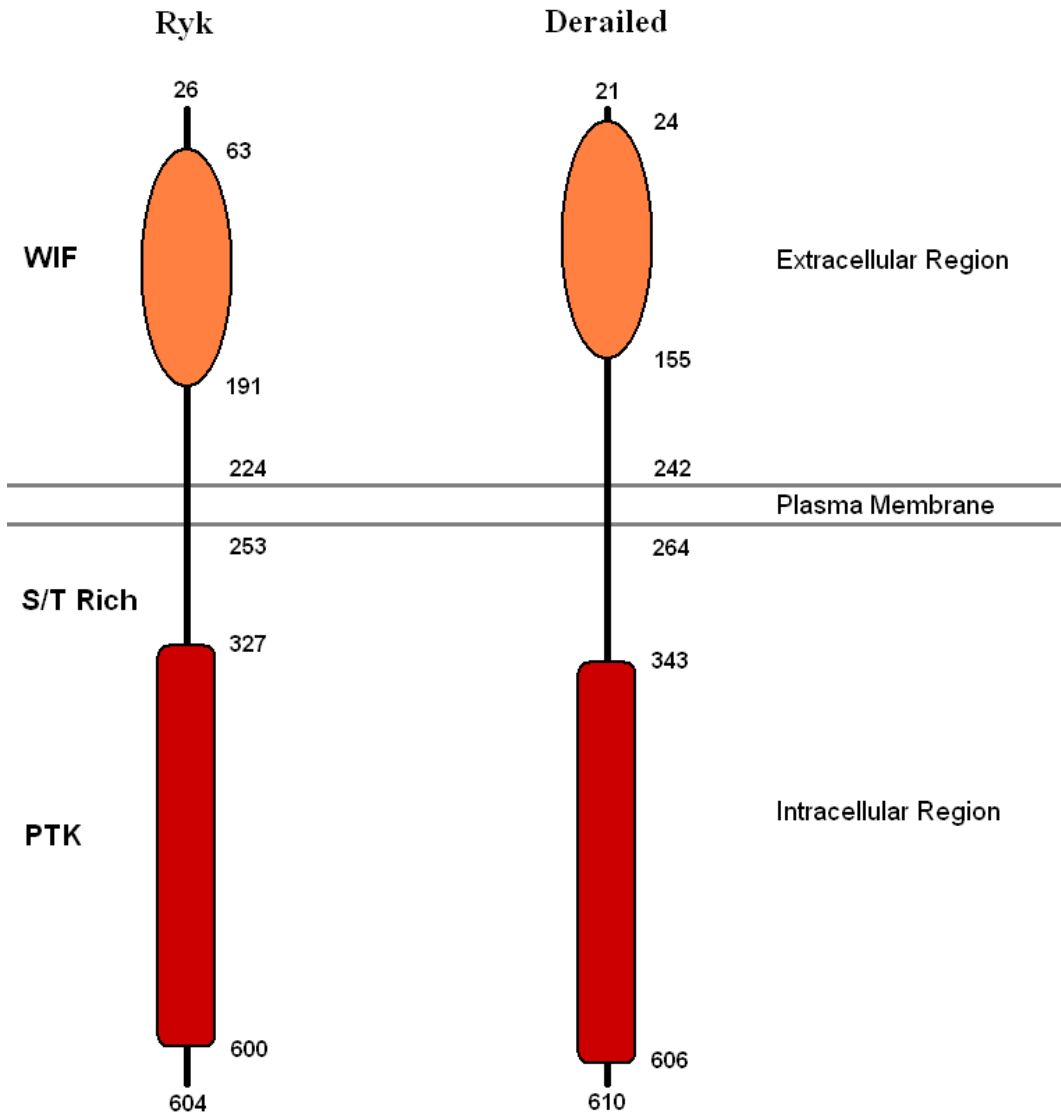


Figure 2.2: Domain organization of Ryk and Derailed (mature protein with signal peptide cleaved). WIF: Wnt Inhibitory Factor domain; S/T Rich: Serine/Threonine rich segment; PTK: Protein Tyrosine Kinase domain.

The best characterized Ryk ortholog in invertebrate is Derailed (Drl) in *D. melanogaster*. Drl protein has the same domain organization as human Ryk (Figure 2.2), with 34% sequence identity between their WIF domains and 48% sequence identity between their pseudokinase domains. Drl was first isolated based upon its function in neuronal axon pathfinding (Callahan, Muralidhar et al. 1995). Abnormal muscle attachment to epidermis was also observed in *drl* knockout flies (Callahan, Bonkovsky et al. 1996). At the same time, another research group independently identified *Drl* as the gene responsible for the learning and memory deficits displayed in fly *linotte* mutants (Dura, Taillebourg et al. 1995).

Signaling by receptor tyrosine kinases is known to be initiated through their stimulation by extracellular ligands (Lemmon and Schlessinger 2010). Ryk and Derailed are no exceptions to this rule. Owing to the presence of a WIF-homologous domain in their extracellular regions, Ryk and Derailed have been characterized as potential receptors for Wnt ligands (to which human WIF-1 protein is known to bind), and a variety of studies have shown that they contribute to the complex regulation of tissue development by Wnt signaling.

2.1.3 Introduction to Human Wnt Inhibitory Factor-1 (hWIF-1)

Human WIF-1 is a secreted protein known to bind various Wnt proteins, and is thought to inhibit their signaling by preventing Wnts from binding to their cell-surface receptors. hWIF-1 is composed of an N-terminal signal sequence and a WIF domain followed by

five EGF repeats and a short C-tail. When overexpressed in *Xenopus laevis* embryos, hWIF-1 causes their dorsalization or anteriorization, mimicking phenotypes observed when *Xenopus* Wnt8 (XWnt8) signaling is blocked (Hsieh, Kodjabachian et al. 1999). hWIF-1 was also found to block the ability of overexpressed XWnt8 to induce axis induction in a dose-dependent manner, and the WIF domain alone is as effective in inhibiting this process as full-length hWIF-1 (Hsieh, Kodjabachian et al. 1999). A total of six mammalian Wnt proteins have been reported to associate with hWIF-1 (Malinauskas, Aricescu et al. 2011). *In vitro* binding studies have been carried out to map the regions of WIF-1 responsible for Wnt binding (Malinauskas, Aricescu et al. 2011). Full-length WIF-1 binds tightly to Wnt3a with K_D of 60 nM. Both WIF domain and EGF repeats appear to contribute to Wnt-association: the WIF domain alone binds Wnt3a with a K_D of 3.4 μ M, whereas a fragment containing the EGF repeats alone binds Wnt3a with a K_D of 0.9 μ M (Malinauskas, Aricescu et al. 2011).

NMR and X-ray crystallographic studies have provided structural insights into the WIF domain (Liepinsh, Banyai et al. 2006; Malinauskas, Aricescu et al. 2011): the WIF domain adopts an overall immunoglobulin-like fold, with nine beta strands and two short alpha helices (Figure 2.3 A&B). Interestingly, both studies have reported WIF binding to hydrophobic detergent or lipid. The NMR-based study reported tight binding of the detergent Brij-35 between the second beta-strand and second alpha helix of the WIF domain (Liepinsh, Banyai et al. 2006; Malinauskas, Aricescu et al.). In the crystal structure, the alkyl-chains of a phospholipid were found to penetrate into the core of WIF domain from the opening between the two alpha helices (Malinauskas, Aricescu et al.

2011). Given the fact that Wnts are typically lipid-modified, these observations raised the intriguing possibility that the WIF domain binds to Wnts by recognizing their lipid moiety as well as regions of the Wnt protein itself. However, the region(s) on the WIF domain that are directly responsible for Wnt binding have not yet been identified experimentally.

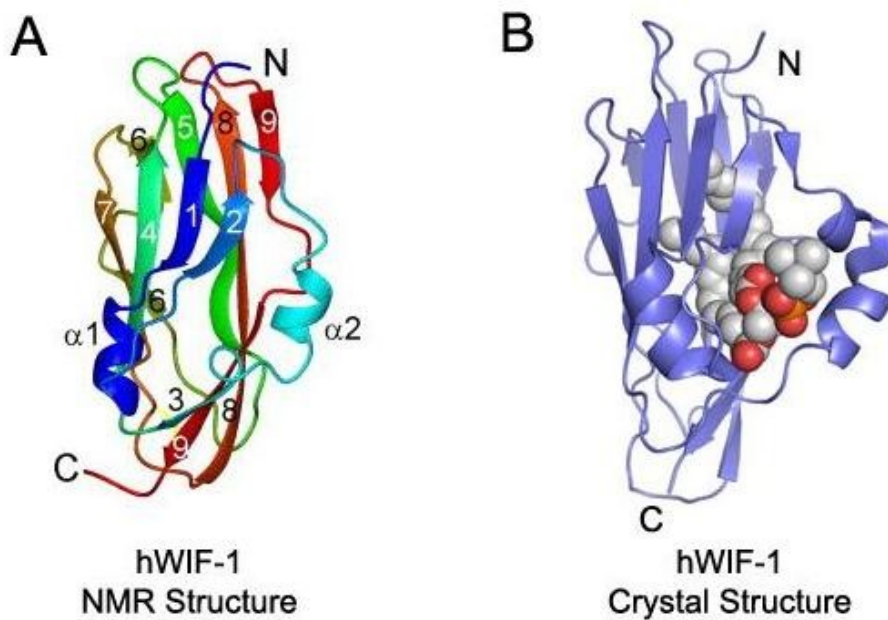


Figure 2.3: Reported structures of human Wnt Inhibitory Factor -1 (hWIF-1). (A) NMR structure of WIF domain of hWIF-1 with no lipid (PDB: 2D3J) (Liepinsh et al. JMB 2006). (B) Crystal structure of WIF domain of hWIF-1 with DOPC bound (PDB: 2YGN) (Malinauskas, Aricescu et al. 2011).

2.1.4 Ryk/Drl Interact with Wnts and Mediate Wnt Signaling

The WIF domain of human Ryk contains about 130 amino acids and shares 23% sequence identity to hWIF-1 (Figure 2.4A). Lu *et al.* (Lu, Yamamoto et al. 2004) have demonstrated that the Ryk WIF domain co-immunoprecipitates with Wnts (Wnt-1 or Wnt-3a), and that overexpression of Ryk increases Wnt-induced TCF-driven transcription in 293T cells. Conversely, RNAi knockdown of Ryk expression abolishes TCF pathway activation by Wnts. Ryk siRNA also causes a reduced level of Wnt3a-induced neurite outgrowth in dorsal root ganglion (DRG) explants (Lu, Yamamoto et al. 2004). Later studies of Ryk-Wnt signaling have focused mainly on its effects in neuronal development. Schmitt *et al.* examined the effect of Ryk-mediate Wnt3 signaling on retinal ganglion cells (RGCs) of chick (Schmitt, Shi et al. 2006), and showed that Ryk mediates a Wnt3-induced axonal repulsion (inhibitory) response in neuron explants, which could be inhibited by a specific anti-Ryk serum. By contrast, Frizzleds mediate an axonal attraction response – which is thought to collaborate with repulsive Ryk signaling in retinotectal topographic mapping (Schmitt, Shi et al. 2006). Similar Wnt-repulsive effects of Ryk have also been reported by other studies in Ryk knockout mice (Keeble, Halford et al. 2006) and in cultured neurons treated with anti-Ryk antibodies (Liu, Shi et al. 2005). Since Wnts are typically distributed in a local concentration gradient in developing organisms, the differential responses of Ryk-expressing and Frizzled-expressing neurons presumably contribute to the formation of intricate neuron topographic patterning. Recently, Ryk has also been implicated in cell fate determination of neural progenitor cells (NPCs); knocking out Ryk from NPCs switches neural differentiation towards

oligodendrocyte neurons, whereas re-introducing Ryk reverses this preference and instead promotes differentiation towards GABAergic neuron (Li, Hutchins et al. 2009).

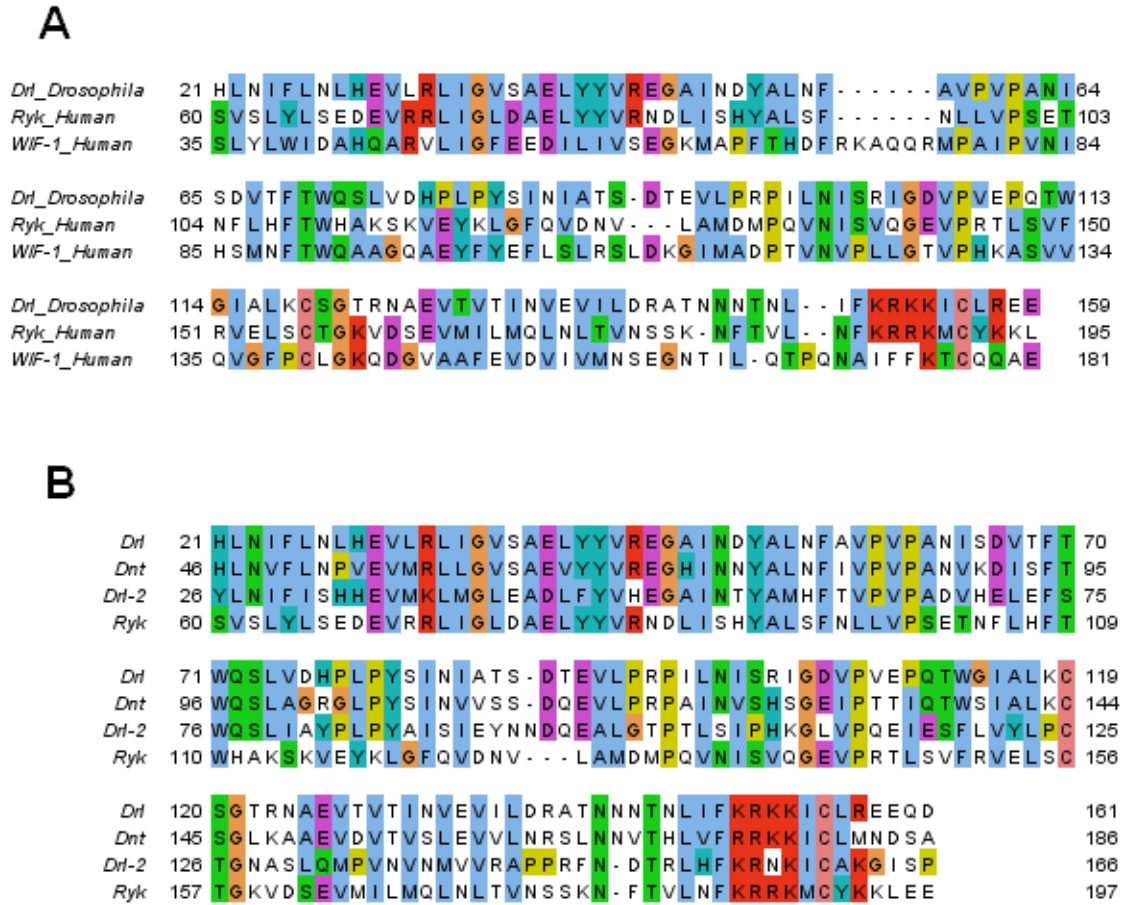


Figure 2.4: Sequence alignments of WIF domains. (A) Alignment of WIF domains in *Drosophila* Derailed, human Ryk and human Wnt Inhibitory Factor -1. (B) Alignment of WIF domains in *Drosophila* Derailed, *Drosophila* Doughnut, *Drosophila* Derailed-2 and human Ryk. Alignments are generated using ClustalW and colored using JalView (Clustalx color scheme).

The *Drosophila melanogaster* Ryk ortholog, Drl, has been shown to mediate signaling by *Drosophila* Wnt5 (DWnt5), an ortholog of human Wnt5s (hWnt5). Extensive studies have characterized Drl-DWnt5 mediated axon pathfinding in the *Drosophila* embryonic central nervous system (CNS). In the *Drosophila* ventral nerve cord, many neurons need to project axons across the midline to the opposite side of the CNS via either the anterior commissure (AC) or posterior commissure (PC). Autonomous expression of the Drl receptor guides a subset of axons to project through the anterior commissure (rather than the posterior commissure) of each segment, and embryonic neurons in flies lacking Drl showed defects in choosing the correct crossing path (hence the name of the gene: *derailed*) (Callahan, Muralidhar et al. 1995; Bonkowsky, Yoshikawa et al. 1999). Drl guides commissure choice through its interaction with DWnt5, which is expressed predominantly on posterior commissural neurons and induces repulsive signals in the Drl-expressing subset of neurons to promote their projection into the anterior commissure (Fradkin, van Schie et al. 2004). Abolishing DWnt5 expression undermines this guidance function of Drl, and causes a lack of separation between AC and PC neurons when crossing the midline (Yoshikawa, McKinnon et al. 2003; Fradkin, van Schie et al. 2004). Yoshikawa *et al.* also showed that a Drl ectodomain-Fc fusion protein is able to accurately label the DWnt5 expression region in *Drosophila* embryos as well as immunoprecipitate DWnt5, suggesting physical interaction between DWnt5 and Drl (Yoshikawa, McKinnon et al. 2003). Drl-mediated DWnt5 signaling has also been implicated in the patterning of olfactory receptor neurons (ORNs) in the *Drosophila* antennal lobe (Yao, Wu et al. 2007; Sakurai, Aoki et al. 2009), in the development of

mushroom bodies (Moreau-Fauvarque, Taillebourg et al. 1998; Grillenzoni, Flandre et al. 2007), and in salivary gland migration (Harris and Beckendorf 2007).

In addition to Drl, two other Ryk homologs, Derailed-2 (Drl-2) and Doughnut (Dnt), are also found in *Drosophila* (Figure 2.4B). The Drl and Drl-2 WIF domains share 44% sequence identity. Drl-2 was shown to be predominantly expressed in ORN axons and to participate in development of the olfactory system – with functional complementarity to Drl-DWnt5 signaling (Sakurai, Aoki et al. 2009). The Drl and Dnt WIF domains share 64% sequence identity. Although Dnt has a distinct expression pattern from that of Drl during embryogenesis, targeted overexpression of Dnt can partially rescue embryonic muscle attachment defects in Drl null mutants. (Oates, Bonkovsky et al. 1998)

2.1.5 The Pseudokinase Domains of Ryk/Drl Lack Kinase Activity but are Capable of Signal Transduction

The signaling cascades triggered after Wnt binding to Ryk/Drl – which mediate the repulsive signals outlined above – are unclear. The typical RTK activation scheme – where ligand-induced receptor dimerization induces kinase activation and autophosphorylation – is unlikely in this case. Despite having a highly conserved intracellular kinase domain, Ryk/Drl are considered to have kinase-inactive ‘pseudokinase’ domains, due to sequence alterations at several conserved residues that are important for the activity of ‘canonical’ kinases (summarized in (Halford and Stacker 2001)). Specifically,

1. The first glycine in the GxGxxG ‘P-loop’ motif is altered (mostly replaced by glutamine).
2. The DFG motif, thought to be a nexus of kinase regulation, is replaced by the sequences DNA (in Ryk) or DSA (in Drl).
3. In the ATP binding pocket, a conserved alanine is replaced by a bulky phenylalanine (in Ryk) or leucine (in Drl) in the VAIK motif, which may prevent the accommodation of ATP substrate.

Several studies have attempted to address the question of whether Ryk/Drl can function as kinases, and if not, how they might mediate signal transduction. Yoshikawa *et al.* showed that a Drl mutant with the “invariant” lysine in its kinase domain substituted by alanine (K371A) – a mutation that greatly impairs activity of most kinases – is indistinguishable from wildtype Drl in phenotypic rescue or gain-of-function assays studying fly axon guidance and muscle attachment, suggesting that kinase activity is not required for Drl-mediated signaling (Yoshikawa, Bonkowsky *et al.* 2001). In another study (Taillebourg, Moreau-Fauvarque *et al.* 2005), the same presumed Drl kinase-dead mutant was also shown to phenocopy wildtype Drl in inducing a gain-of-function phenotype involving mushroom body defects in flies, despite a lower level of mRNA expression. Similar to Drl, no kinase activity has been observed for Ryk kinase domain (Trivier and Ganesan 2002). A TrkA extracellular – Ryk intracellular chimeric protein also displayed lack of autophosphorylation upon NGF stimulation (Katso, Russell *et al.* 1999).

In summary, so far no role in phosphotransfer catalysis has been observed for the kinase domain of Ryk/Drl family RTKs. Yet the highly conserved cytoplasmic region seems to be capable of signaling (Yoshikawa, Bonkowsky et al. 2001). In neuronal cells, the Ryk intracellular domain (ICD) is thought to possess a Notch receptor like function. After stimulation by Wnt binding, the Ryk ICD is cleaved off and translocates into the nucleus, where it functions to promote neuronal differentiation (Lyu, Yamamoto et al. 2008; Lyu, Wesselschmidt et al. 2009). Indeed, Ryk ICD fused to a nuclear localization signal (NLS) can functionally replace full-length Ryk in cell fate determination of neural progenitor cells (Zhong, Kim et al. 2011). In studies with TrkA ECD/Ryk ICD chimeras, the chimeric protein with the wildtype Ryk kinase domain is able to induce Erk phosphorylation and activate MAPK pathway. Interestingly, mutating the invariant lysine K334 to alanine in this case abolishes Erk phosphorylation (Katso, Russell et al. 1999). Wouda *et al.* also showed that Src family kinases bind to and phosphorylate Drl, and participate its downstream signaling (Wouda, Bansraj et al. 2008). Although these studies have demonstrated a clear signaling capability of Ryk ICD, the mechanism of signal transduction from Wnt binding to intracellular signaling activation remains unclear.

2.1.6 Biophysical Characterization of Drl-DWnt5 Interactions as a Model System for Ryk/Drl Signaling

As summarized above, extensive studies have documented important roles of Ryk/Drl RTKs in Wnt signaling and embryonic development, especially in axon pathfinding. In sharp contrast, little is known regarding the molecular mechanisms of Wnt-Ryk/Drl interactions or the resulting cellular signal transduction. Even the very first step of this

signaling pathway – binding of Wnts to the WIF domain of Ryk/Drl – is poorly understood, and many questions remain regarding this process. For example, current evidence for binding of Wnts to Ryk/Drl is based mainly on co-immunoprecipitation or the use of anti-Ryk/Drl postimmune sera. These studies do not preclude the possibility that, rather than interacting directly with Wnt proteins, Ryk/Drl communicate indirectly with Wnts through an intermediate factor. Even if the binding is direct, other proteins may be necessary to form a functional signaling unit. Indeed, Ryk can be co-immunoprecipitated with both Wnt and Frizzled (Lu, Yamamoto et al. 2004), and sFRP2 (Secreted Frizzled-related Protein 2) blocks only Wnt3-Frizzled5 interactions but not Wnt3-Ryk interactions (Schmitt, Shi et al. 2006), suggesting the possibility of a Ryk-Wnt-Frizzled ternary complex.

To begin addressing these questions, it is essential first to characterize the interaction between Ryk/Drl and Wnt at a molecular level using tools from biophysical and structural biology. In my efforts to understand the mammalian Ryk-Wnt system, I encountered major experimental difficulties with obtaining well-behaved recombinant Ryk and Wnt proteins. On the other hand, the *Drosophila* system has proven far more tractable, since both Drl and DWnt5 could be readily obtained using insect cell expression systems. Owing to the high sequence homology and functional similarity between Drl and Ryk, understanding Drl-DWnt5 signaling should also shed light on the molecular mechanism of their mammalian counterparts.

Using Drl-DWnt5 as a model system, my goals were to address the following questions:

1. Does Ryk/Drl interact directly with Wnt proteins? If so, what is the binding affinity?
2. Which protein region(s) is(are) responsible for the formation of Ryk/Drl-Wnt complexes? Does the region of Wnt that binds Ryk/Drl overlap with the region that binds Frizzleds – so that binding to the two classes of receptor would be mutually exclusive – or do different regions of the Wnt surface bind to the different receptors?

In describing my studies, I start by describing the expression and purification of individual proteins, followed by characterization of their binding using ‘pull-down’ and surface plasmon resonance (SPR) studies. I will then discuss structural insights into the properties of the WIF domain from a Drl homolog that I have obtained using X-ray crystallography. Based on this structure, I have generated and characterized a set of mutations in the Drl WIF domain in order to locate the primary site for DWnt5 binding. My studies serve as a good starting point for understand recognition of Wnt proteins by the Ryk/Drl extracellular regions, and for interrogating Ryk/Drl signaling at a molecular level.

2.2 Biophysical Characterization of Derailed-DWnt5 Interactions

2.2.1 Expression, Purification and Characterization of *Drosophila* Derailed and DWnt5 Proteins

I was able to express the Drl extracellular region (residues 1 - 242) with a C-terminally appended 6xHis tag in Sf9 cells at high levels. Purification of the secreted protein was achieved as described in Experimental Procedures. Pure, glycosylated Drl full extracellular region (sDrl) runs as a 35 kDa protein on SDS-PAGE gels (Figure 2.5A).

Protein constructs with serial truncation from the C-terminus (up to residue 180) could be expressed with similar yields and purified in the same way. Three N-linked glycosylation sites (N63, N99 and N143) were identified within the Drl WIF domain. Mutating each of these Asn residues independently to Gln causes disappearance of the upper (slower mobility) band of sDrl in SDS-PAGE (Figure 2.5B), suggesting the presence of sugar moieties at all three N-glycosylation sites.

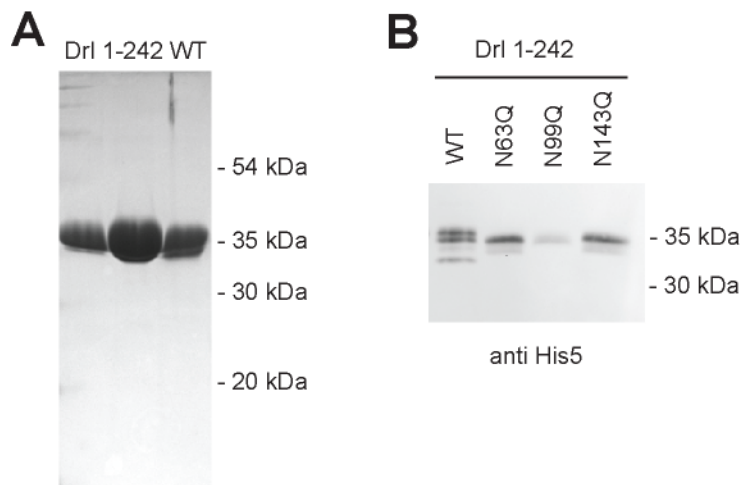


Figure 2.5: Characterization of recombinant Derailed extracellular region. (A) SDS-PAGE of purified, wildtype Drl full extracellular region (sDrl) with a C-terminally appended 6xHis tag. This gel was stained with Coomassie Blue. (B) Western blot showing that point mutations at any of the predicted N-linked glycosylation sites in the Drl extracellular region (N63, N99, or N143) resulted in faster protein migration during SDS-PAGE, suggesting removal of glycan. sDrl proteins were detected using a pentahistidine antibody that recognizes the 6xHis tag.

DWnt5 contains an unusually long (~500 amino acids), non-conserved N-terminal region (yellow in Figure 2.6A) as well as a ~150aa insert in the Wnt domain (blue in Figure 2.6A) when compared with other Wnt proteins that consist primarily only of the Wnt-homologous region (green in Figure 2.6A). In a *Drosophila* imaginal disc cell line, DWnt5 protein is secreted in two forms – a full length, 140 kDa glycoprotein and a proteolytic 80 kDa fragment (Fradkin, Noordermeer et al. 1995).

When full length DWnt5 is expressed in *Drosophila* Schneider 2 (S2) cells, it is secreted mainly as a ~70 kDa glycoprotein (Figure 2.6B), similar in size to the reported 80 kDa proteolytic DWnt5 fragment (Fradkin, Noordermeer et al. 1995). The identity of the DWnt5 protein was confirmed by Western blotting using two polyclonal antibodies (kindly provided by Dr. Lee Fradkin (Fradkin, Noordermeer et al. 1995)). The epitope for antibody A is located just N-terminal of the Wnt domain, whereas the epitope for antibody B is located within the Wnt domain insert (Figure 2.6A).

Secreted, mature DWnt5 protein was extracted from the medium and purified as described in the Experimental Procedures (Figure 2.6C). Surprisingly, the DWnt5 protein is stable in solution without detergents, a property that contrasts with that described for other known Wnt proteins. The mature, ~70 kDa DWnt5 protein is the result of proteolytic cleavage close to the C-terminus of the N-terminal region, as suggested by the fact that it is recognized by antibody A (Figure 2.6B). N-terminal protein sequencing at the Keck Facility (Yale University) showed that the major N-terminal starting sequence of mature DWnt5 protein is SQPSIS (residue 455 - 460). ESI mass spectrometry of the purified protein (conducted by the CHOP Proteomics Core) also

showed an absence of peptide coverage at N-terminal domain. Taken together, the mass spectrometry and Western blotting results suggest that purified, mature DWnt5 protein consists primarily of the Wnt domain, extending from residue 455 of DWnt5 to residue 1004 (although the C-terminus has not been confirmed).

To identify N-glycosylation sites within the mature DWnt5 protein, purified DWnt5 protein was treated with PNGaseF in H₂O¹⁸ and subjected to ESI mass spectrometry (conducted by the CHOP Proteomics Core). Three N-glycosylation sites were identified: N484-485 (KVSME**N**NTSVTD), N724 (NVDAK**N**DTSLV) and N952 (RVCHK**N**SSGLE). Indeed, PNGaseF-treated DWnt5 showed increased mobility in SDS-PAGE, confirming the presence of surface-accessible N-linked glycosylation (Figure 2.6D). Surprisingly, mass spectrometry data readily identified peptide fragments containing unmodified S868, the putative lipid modification site of DWnt5. This is an unexpected result, which suggests that our recombinant DWnt5 protein is not lipid modified at this site. The lack of lipid modification is consistent with the fact that our DWnt5 protein has much better solubility characteristics than those seen for other Wnts. The fact that we can generate quantities of purified DWnt5 useful for biochemical and biophysical studies may open up unique opportunities for quantitative study of Wnt signaling.

In order to examine whether the unique Wnt domain insert of DWnt5 (residue 681 to 838) is involved in Drl binding, a construct was generated in which the insert region of DWnt5 was replaced with a short sequence (RERSFKRGSREQG) found in the equivalent region of Wnt5 from the jumping ant *Harpegnathos saltator*, which has no such insert.

The new, shortened construct is named DWnt5 Δ B due to its lack of epitope for antibody B. The mature form of purified DWnt5 Δ B migrates more slowly in SDS-PAGE compared to wildtype DWnt5 (Figure 2.6B left blot), possibly due to an alternative N-terminal cleavage site being used – or a different glycosylation pattern. Western blotting of DWnt5 Δ B confirmed the identity of the protein construct; it can be detected readily using antibody against epitope A, but not with antibody against epitope B (Figure 2.6B right blot), since this epitope has been removed.

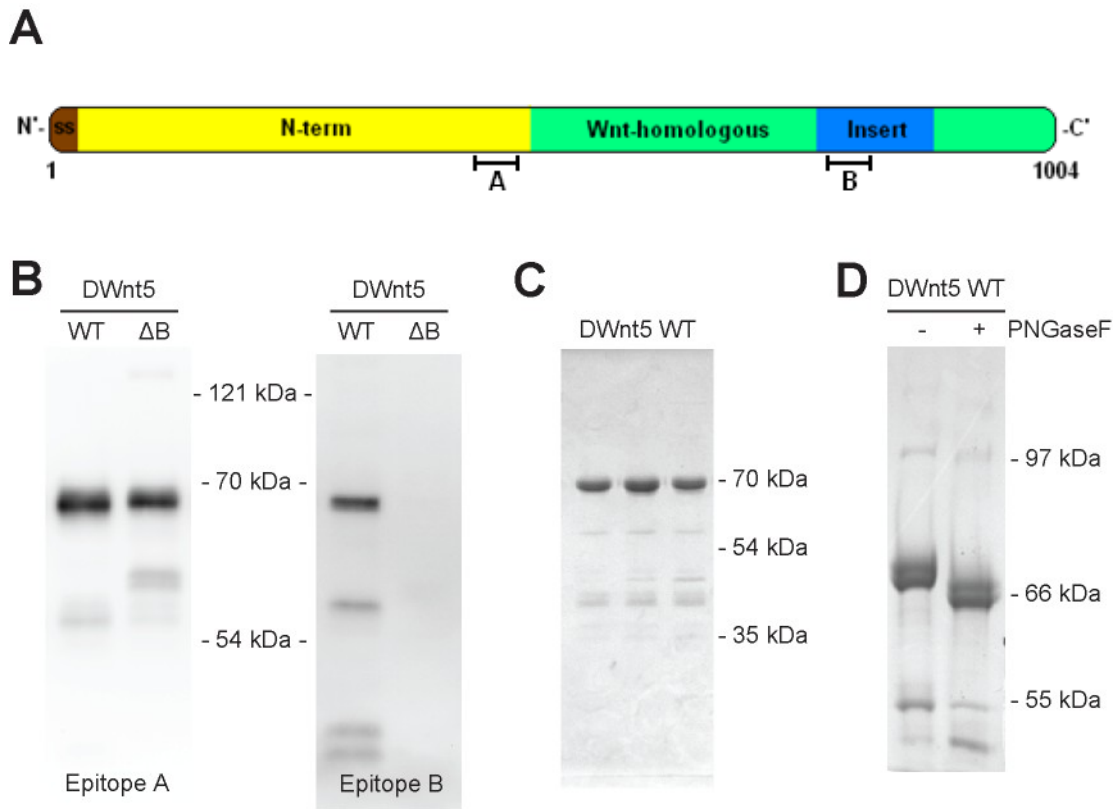


Figure 2.6: Characterization of DWnt5 protein. **(A)** Domain organization of DWnt5. Starting from the N-terminus: signal-peptide sequence (ss), N-terminal region (yellow), Wnt-homologous domain (green) and Wnt domain insert (blue). The locations of two epitopes for DWnt5-specific rabbit polyclonal antibodies are labeled A and B. **(B)** Western blots showing DWnt5 proteins secreted from S2 cells. DWnt5 was detected by two different DWnt5 antibodies as indicated in **(A)**. **(C)** SDS-PAGE gel of purified, mature DWnt5 wildtype protein. **(D)** PNGaseF treatment of DWnt5 protein leads to increased mobility in SDS-PAGE.

2.2.2 Analysis of Derailed-DWnt5 Interactions by *in vitro* Pull-down and SPR

For an initial view of Derailed-DWnt5 interactions, we used a simple pull-down assay to ask if the two recombinant proteins interact. Two C-terminally 6xHis tagged constructs of purified recombinant Drl extracellular region (Drl residues 1-207 and Drl residues 1-219) were used. Each sDrl protein was mixed with conditioned S2 medium containing secreted DWnt5 protein. NiNTA beads were then added to the protein mixture to extract sDrl proteins from the solution. The ability of sDrl proteins to pull down DWnt5 protein from the medium was then examined by Western blotting with DWnt5 specific antibodies. As shown in Figure 2.7, both sDrl proteins were able to extract DWnt5 from the solution, as evidenced both by the loss of DWnt5 in the supernatant fraction and enrichment of DWnt5 in the pull-down fraction. On the contrary, NiNTA beads did not effectively pull down DWnt5 when the 6xHis-tagged sDrl protein was not included in the assay. These results suggest that purified recombinant sDrl proteins interact with DWnt5 *in vitro*.

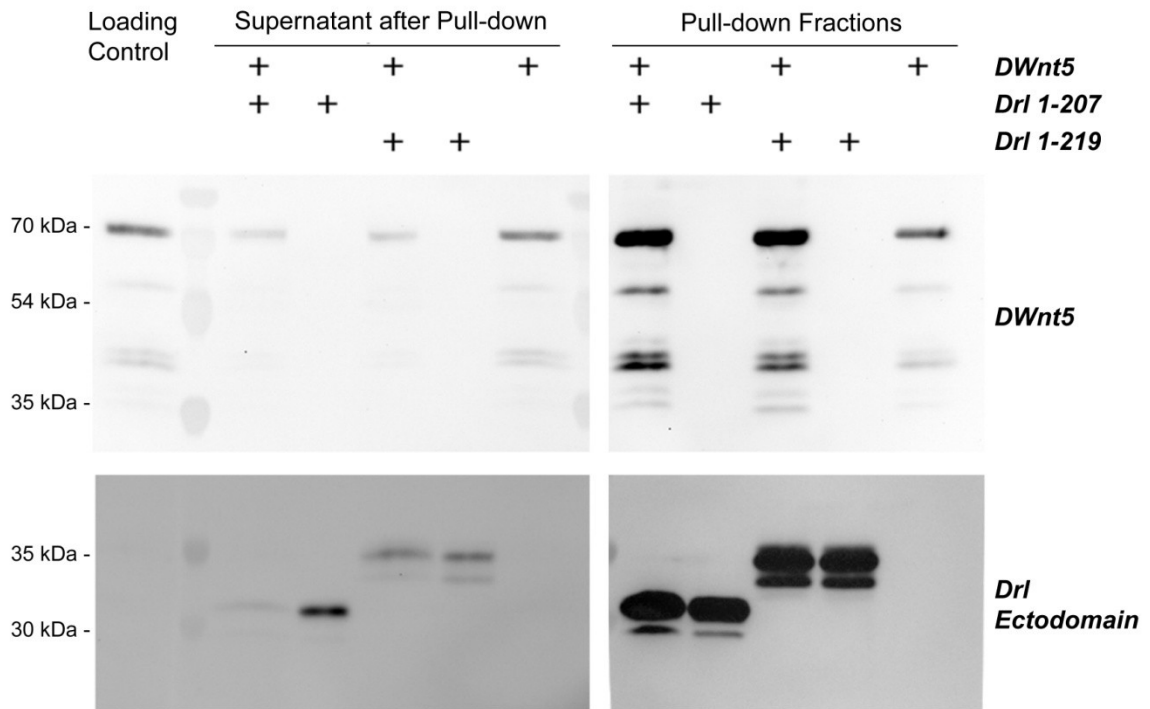
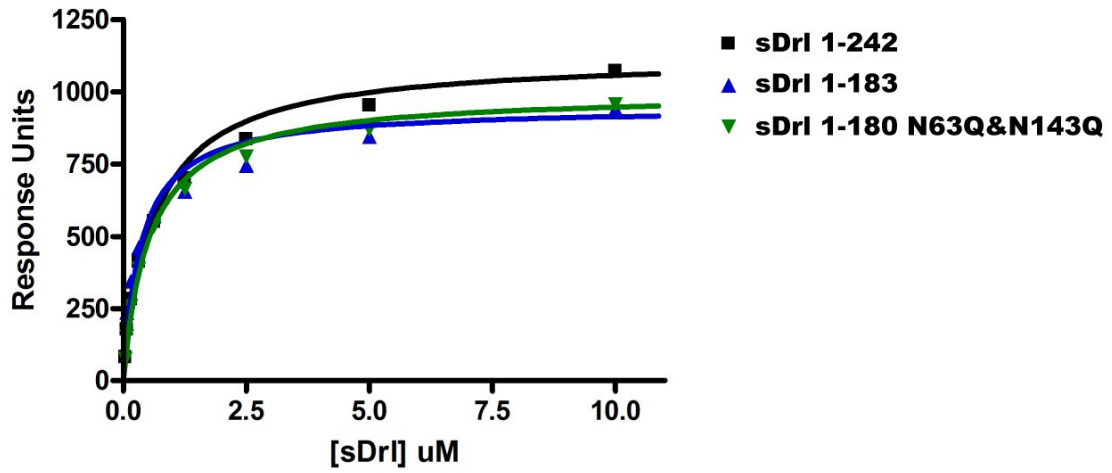


Figure 2.7: Drl ectodomains are capable of pulling down DWnt5 from conditioned medium. S2 media containing secreted DWnt5 protein (pre-concentrated by 10 fold) was mixed with NiNTA beads in the presence (or absence) of purified Drl extracellular domains with an appended 6xHis tag. Two sDrl constructs were used. One encompasses Drl residues 1-207 and the other encompasses Drl residues 1-219. As controls, DWnt5-containing medium or the individual sDrl proteins were also mixed with NiNTA beads on their own. Both sDrl proteins bound strongly to NiNTA beads whether DWnt5 was also present or not. By contrast, DWnt5 was only enriched in the NiNTA pull-down fraction when added together with one of the His-tagged sDrl proteins. NiNTA pull-down fractions were resuspend in 20% of the original media volume, hence the stronger DWnt5 band intensity in the sDrl-free pull-down fraction compared to loading control. A sample of S2 medium before pull-down experiment was analyzed as loading control.

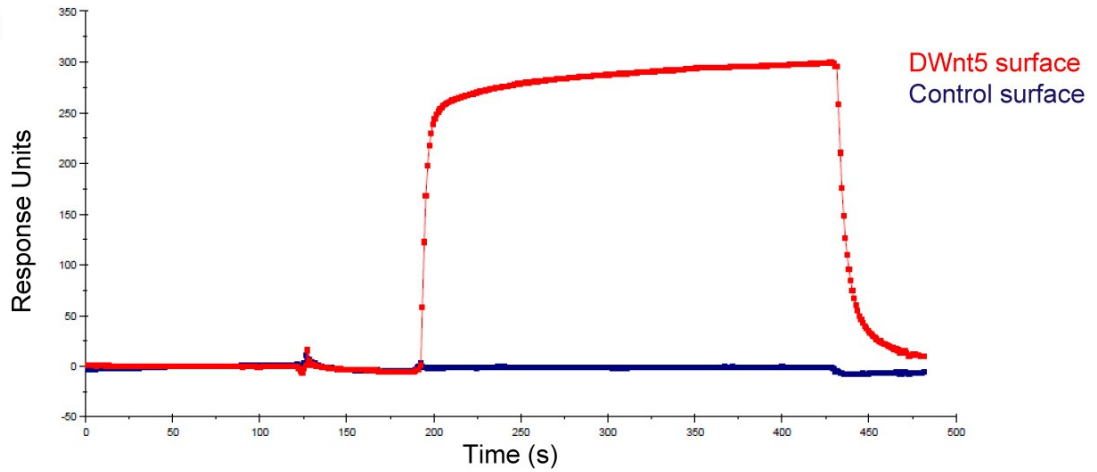
For more quantitative studies of direct interaction between purified sDrl and DWnt5 proteins, we used surface plasmon resonance (SPR) with a Biacore 3000 instrument. Purified DWnt5 was immobilized onto a CM5 sensor chip using amine coupling. Serial dilutions of sDrl proteins were then injected, and steady state binding to the DWnt5-derivatized surface was recorded in SPR response units (RUs), corrected for refractive index effects using a mock-derivatized control sensorchip surface. Steady state RU values measured at different sDrl concentrations were then fit to a single-binding-site hyperbolic curve (Figure 2.8A & B and Table 2.1). Wildtype, full sDrl (1-242) binds directly to DWnt5 with a dissociation constant (K_D) of 0.63 μ M. Elimination of the C-terminal region of sDrl does not significantly affect the binding affinity; sDrl (1-180) bound DWnt5 with a K_D of 0.36 μ M, suggesting that DWnt5 binding is mediated mostly by the WIF domain, which ends at amino acid 161. The presence of sugar moieties at N63 and N143 of sDrl also appears to have minimal influence on DWnt5 binding; sDrl 1-180 with both of these glycosylation sites mutated to glutamine (N63Q/N143Q) also bound DWnt5 with a very similar K_D (0.54 μ M).

To investigate whether the long insert region of DWnt5 contributes to Drl binding, purified DWnt5 Δ B protein was immobilized onto a CM5 sensorchip in the same way as described for wildtype DWnt5, and its binding affinity for sDrl(1-242) was measured by SPR (Figure 2.8C). The results show that DWnt5 wildtype and DWnt5 Δ B proteins have almost identical binding affinities for sDrl (Table 2.1). It is therefore clear that Drl binding does not require the unique insert region of DWnt5.

A sDrl constructs binding to immobilized DWnt5



B



C sDrl 1-242 binding to immobilized DWnt5 (wildtype or ΔB)

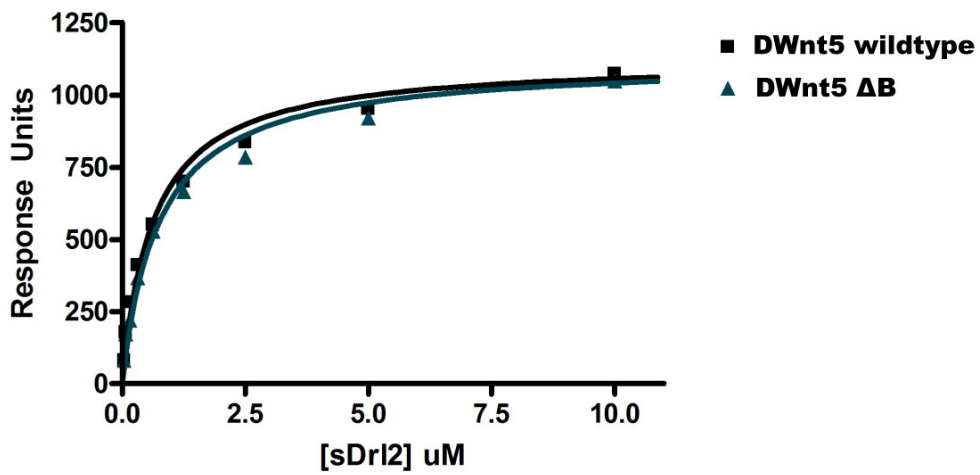


Figure 2.8: SPR studies of sDrl proteins binding to DWnt5 variants. (A) SPR studies with a series of injections of the noted sDrl proteins onto a CM5 chip with immobilized wildtype DWnt5 protein. (B) A representative SPR sensorgram of immobilized DWnt5 binding to sDrl(1-242) (at 320 nM concentration). Colored squares represent actual data points. Sensorgram for DWnt5 immobilized CM5 chip surface is colored red, and sensorgram for mock-derivatized control sensorchip surface is colored blue. Injection of sDrl(1-242) protein solution starts at ~190 s and ends at ~430 s. (C) SPR studies in which a series of injections of sDrl(1-242) at the indicated concentrations were applied to sensorchip surfaces containing immobilized wildtype DWnt5 or DWnt5ΔB.

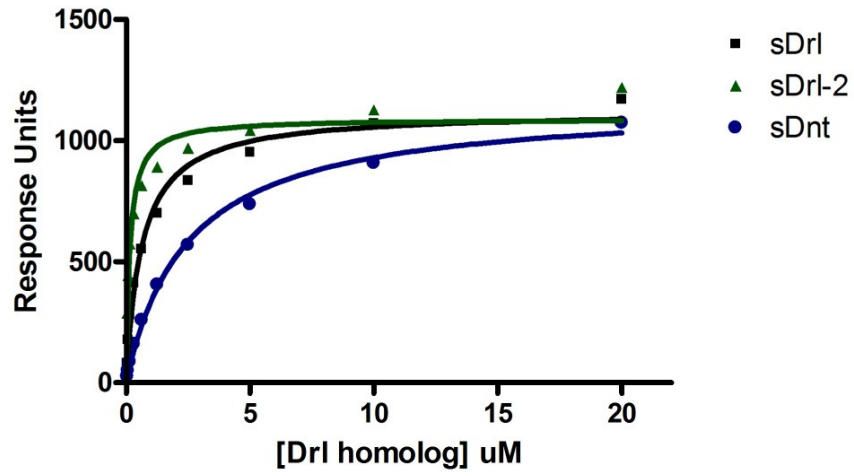
Table 2.1: SPR studies of different sDrl variants binding to DWnt5. Upper: sDrl constructs binding to immobilized wildtype DWnt5. Lower: sDrl 1-242 binding to immobilized DWnt5ΔB.

Analyte	Binding K_D (μ M) to immobilized wildtype DWnt5
sDrl 1-242	0.63 ± 0.08
sDrl 1-183	0.36 ± 0.08
sDrl 1-180 N63Q&N143Q	0.54 ± 0.05
Analyte	Binding K_D (μ M) to immobilized DWnt5ΔB
sDrl 1-242	0.75 ± 0.11

To investigate whether the two additional Drl homologues in *D. melanogaster*, Drl-2 and Dnt, also bind DWnt5, SPR was used to assess the interactions of their extracellular regions with purified DWnt5 (Figure 2.9A and Table 2.2). The full extracellular region of Drl-2 (sDrl-2) displayed a very similar DWnt5-binding affinity to that of sDrl ($K_D = 0.15 \mu\text{M}$). The Dnt extracellular region was also found to bind DWnt5, but with a reduced affinity ($K_D = 2.5 \mu\text{M}$), approximately four-fold lower than that for sDrl.

To demonstrate that immobilization of DWnt5 onto CM5 chip surface does not significantly alter its binding properties in these studies, the reverse SPR experiments were also performed, in which Drl homologs were immobilized onto the CM5 sensorchip and purified free DWnt5 was injected (Figure 2.9B&C and Table 2.2). These studies gave very similar results, with DWnt5 binding strongly to all three Drl homologs. K_D values for DWnt5 binding to immobilized sDrl, sDrl-2 and sDnt were $0.10 \mu\text{M}$, $0.18 \mu\text{M}$ and $0.50 \mu\text{M}$, respectively. Compared to the experiments performed with immobilized DWnt5, these K_D values are relatively lower (suggesting tighter binding), which can likely be attributed to the fact that DWnt5 also weakly interacts with the negatively charged dextran surface of the CM5 sensorchip (we have observed DWnt5 binding to blank CM5 flow cell with high RUs at low micromolar concentrations).

A Drl homologs binding to immobilized DWnt5



B DWnt5 binding to immobilized Drl homologs

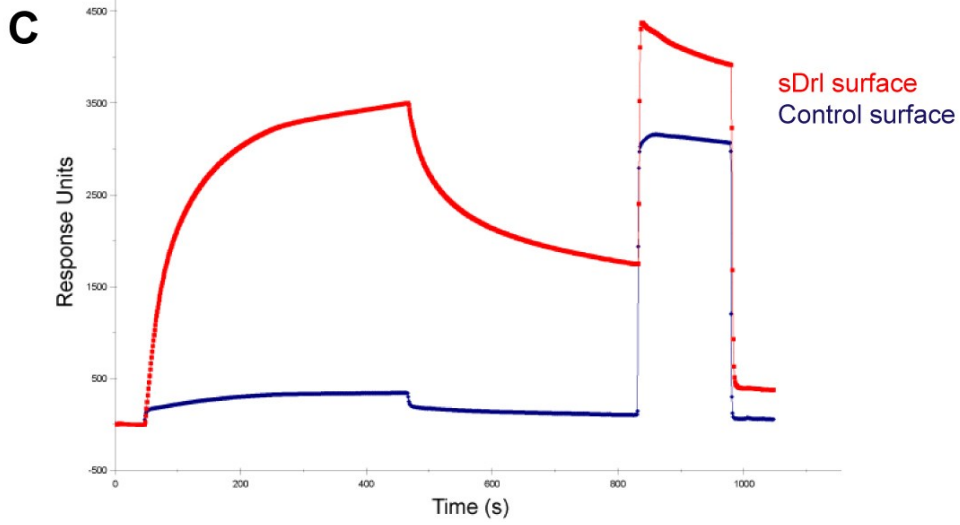
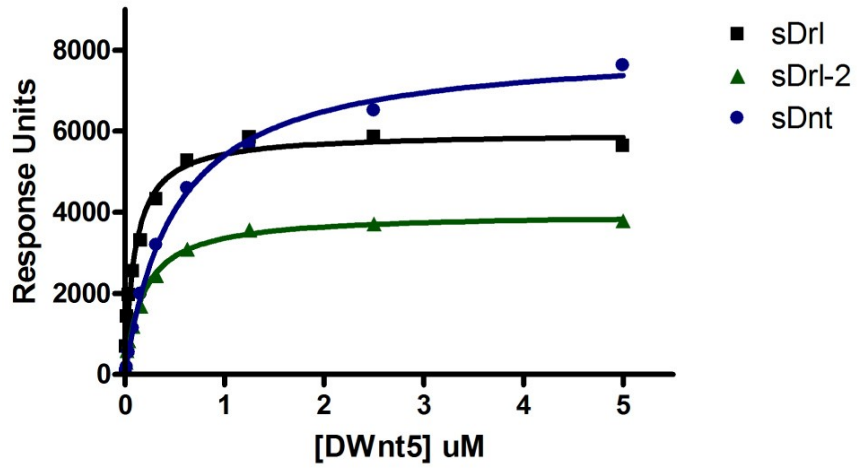


Figure 2.9: SPR studies of DWnt5 binding to *D. melanogaster* Drl homologs. (A) SPR studies used a CM5 sensorchip on which wildtype DWnt5 protein had been immobilized, and injections of the purified extracellular domains of Drl homologs sDrl-2 and sDnt (at the indicated concentrations) were performed in comparison to sDrl(1-242). (B) In a complementary experiment, SPR studies were performed with the extracellular regions of the Drl homologs immobilized on the CM5 chip, and a series of injections of wildtype DWnt5 protein at the indicated concentrations. (C) A representative SPR sensorgram of immobilized sDrl binding to DWnt5 (at 160 nM concentration). Colored squares represent actual data points. Sensorgram for sDrl immobilized CM5 chip surface is colored red, and sensorgram for mock-derivatized control sensorchip surface is colored blue. Injection of DWnt5 protein solution starts at ~50 s and ends at ~470 s. Injection of regeneration buffer starts at ~830 s and ends at ~980 s.

Table 2.2: SPR studies of Drl homologs binding to DWnt5. Upper table: Drl homologs binding to immobilized DWnt5. Lower table: DWnt5 binding to immobilized Drl homologs.

Analyte	Binding K_D (μM) to immobilized DWnt5
sDrl	0.63 ± 0.08
sDrl-2	0.15 ± 0.03
sDnt	2.4 ± 0.2

Immobilized Drl homolog	Binding K_D (μM) of wildtype DWnt5
sDrl	0.10 ± 0.01
sDrl-2	0.18 ± 0.02
sDnt	0.50 ± 0.03

2.3 Structure Determination of the Derailed-2 Extracellular Region

In an effort to gain a structural view of a Ryk/Drl family receptor extracellular region, a great deal of time and effort was spent trying to crystallize sDrl, but without success. However, crystals were obtained for the Drl-2 extracellular region, which has 44% sequence identity to sDrl in the WIF domain region, and binds to DWnt5 with similar affinity. The sDrl-2 crystals diffracted to 2.2 Å resolution on our home source X-ray (Rigaku 007HF with Saturn CCD), and the structure was solved by molecular replacement using a truncated poly-alanine model of the NMR structure of human WIF-1 as search model (Table 2.3).

Table 2.3: Derailed-2 extracellular domain crystallographic statistics (molecular replacement)

Drl-2 ectodomain	
Data collection	Rigaku 007HF
Space group	C222 ₁
Cell dimensions	
<i>a, b, c</i> (Å)	56.954 91.615 76.379
Resolution (Å)	50.00 - 2.25 (2.29-2.25) *
<i>R</i> _{sym} or <i>R</i> _{merge}	0.054 (0.327)
<i>I</i> / σI	42.5 (4.4)
Completeness (%)	99.3 (94.3)
Redundancy	6.5 (3.5)
Refinement	
Resolution (Å)	50.00 – 2.25
No. reflections	8664
<i>R</i> _{work} / <i>R</i> _{free}	22.0/26.4
Model	
Protein amino acids	aa 26-178
No. atoms	1292
Protein	1209
Sugar	42
Water	41
R.m.s. deviations	
Bond lengths (Å)	0.016
Bond angles (°)	2.148

*Values in parentheses are for highest-resolution shell.

Similar to hWIF-1, the Drl-2 WIF domain consists of two α helices and nine β strands (Figure 2.10A), with overall C α root mean squared deviation (RMSD) of 2.0 Å between these two WIF domains using SSM superimposition (Krissinel and Henrick 2004). The N-terminal residue Y26 (immediately after the predicted cleavage site for the signal peptide) forms the start of strand β 1, and the C-terminal tail is located on the opposite side of the domain. Two cysteines, C125 and C160, form a conserved disulfide bond near the C-terminus that links strands β 7 and β 9. Clear electron density was observed for sugar moieties at two N-linked glycosylation sites (N128 and N148), and one O-linked glycosylation site (S171).

Figure 2.10B shows an overlay of the sDrl-2 WIF domain (cyan) with the hWIF-1 NMR structure (no lipid bound, red) (Liepinsh, Banyai et al. 2006) and hWIF-1 domain crystal structure (lipid bound, yellow) (Malinauskas, Aricescu et al. 2011) using PyMOL to minimize RMSD of all matched atoms. The most significant structural difference lies in the conformations and positions of the two helices, α 1 and α 2. For hWIF-1, a comparison between the lipid-free NMR structure and the lipid-bound crystal structure suggests that binding of phospholipid causes an inward shift of helix α 1 relative to that in the solution NMR structure, whereas the helix α 2 region appear to stretch outwardly to accommodate the phospholipid. Unlike hWIF-1, there is no electron density – or space – for an embedded phospholipid in our crystal structure of the sDrl-2 WIF domain. Nevertheless, the position of helix α 1 resembles that seen in the phospholipid-bound hWIF-1 structure rather than in the lipid-free NMR structure. On the other hand, the helix

$\alpha 2$ region of the sDrl-2 WIF domain most closely matches that seen in the lipid-free hWIF-1 NMR structure, despite the fact that this region of sDrl-2 (as well as Ryk/Drl/Dnt) is six residues shorter than that in hWIF-1. It is also worth noting that the region encompassing $\alpha 2$ and $\beta 3$ of hWIF-1 appears to be the most flexible part of the NMR structure (Liepinsh, Banyai et al. 2006), suggesting that this flexibility is required for allowing access of the bound phospholipid. Interestingly, preliminary molecular dynamics (MD) simulations of Drl-2 WIF domain suggest similar flexibility in this region.

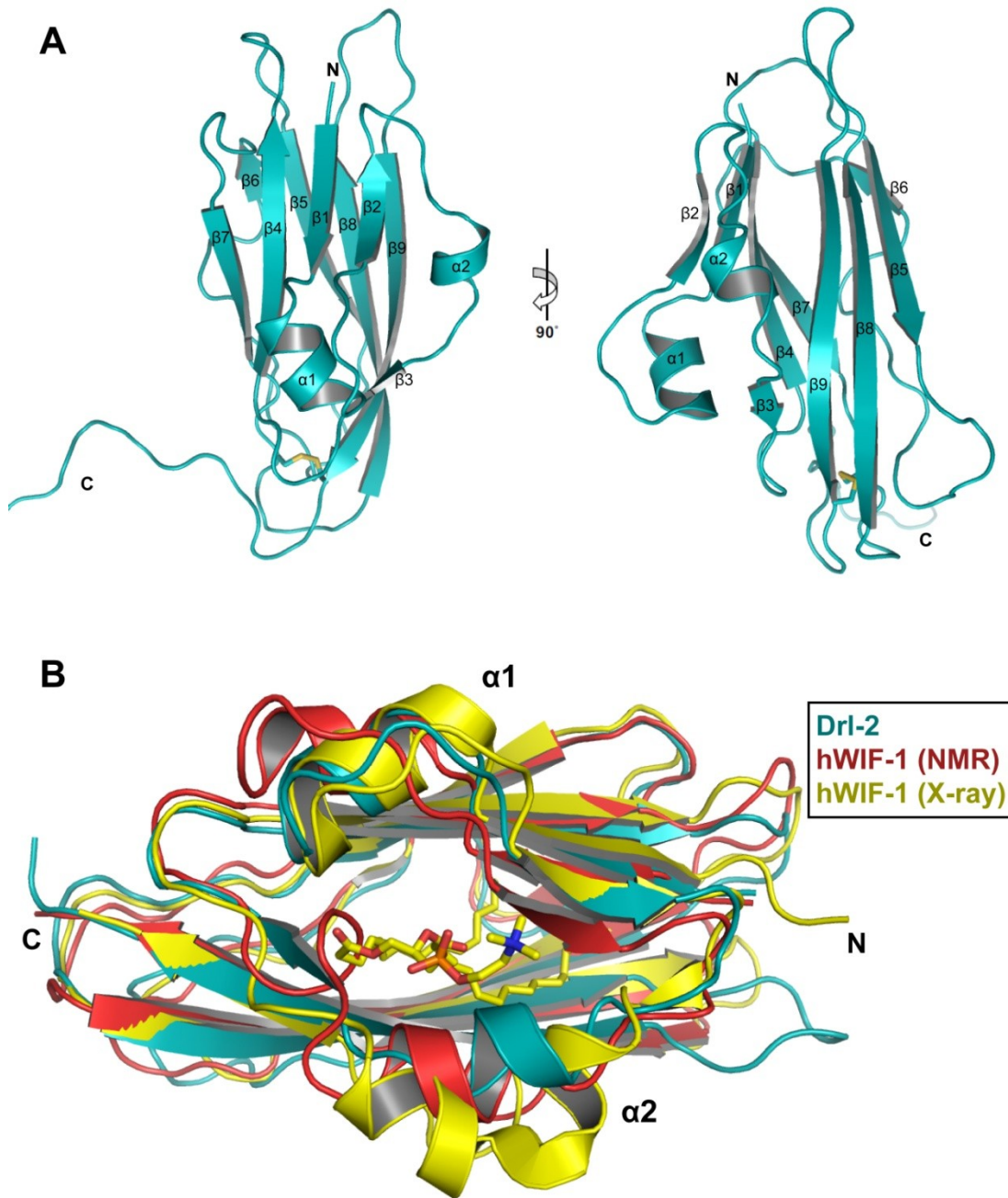


Figure 2.10: Crystal structure of sDrl-2 extracellular domain. (A) Overall crystal structure of sDrl-2. (B) Overlay of sDrl-2 WIF domain with hWIF-1 structures. Cyan: crystal structure of sDrl-2 WIF domain, with two helices labeled. Red: NMR structure of hWIF-1 (no lipid bound, PDB 2D3J). Yellow: crystal structure of hWIF-1 (phospholipid bound, PDB 2YGN). Phospholipid is shown in yellow sticks.

In the sDrl-2 crystal structure, a crystallographic dimer is formed that involves intimate symmetrical interactions between the surface encompassing helices $\alpha 1$ and $\alpha 2$ of one molecule and the same region on its symmetry mate (Figure 2.11A). The binding interface is highly hydrophobic, formed by V36, M37, M40, G41, L42, A44 and L46 around helix $\alpha 1$, together with Y57, A58, F61, T62, P64 and P66 from $\alpha 2$ - $\beta 3$ region, with additional polar interactions involving the Q132 and N157 at the periphery of the interface. The buried surface area is $\sim 300 \text{ \AA}^2$ on each molecule, with a shape complementarity of 0.76. Given the high shape complementarity and the fact that most of these residues are conserved across Ryk family RTKs (Figure 2.4B), it is possible that this interface drives homodimer formation during Ryk/Drl signaling. On the other hand, since the same region on the surface of hWIF-1 is postulated to bind the acyl chain of Wnt proteins, another intriguing possibility is that this conserved region on Ryk/Drl is responsible for Wnt ligand binding – which will be mutually exclusive with this mode of dimerization.

In the crystal, the Ala/Pro-rich C-terminal tail of sDrl-2 lies across the ‘back’ surface of another symmetry mate (Figure 2.11B). It is unclear whether this interaction has any physiological relevance for sDrl-2 to carry out its function, or is simply caused by crystal packing. A similar sequence is not present in other members of the Ryk/Drl family. The seven-residue linker region between the WIF domain and Ala/Pro-rich C-tail (residue 164-170) of sDrl-2 is too short to allow the tail to fold back onto its own WIF domain.

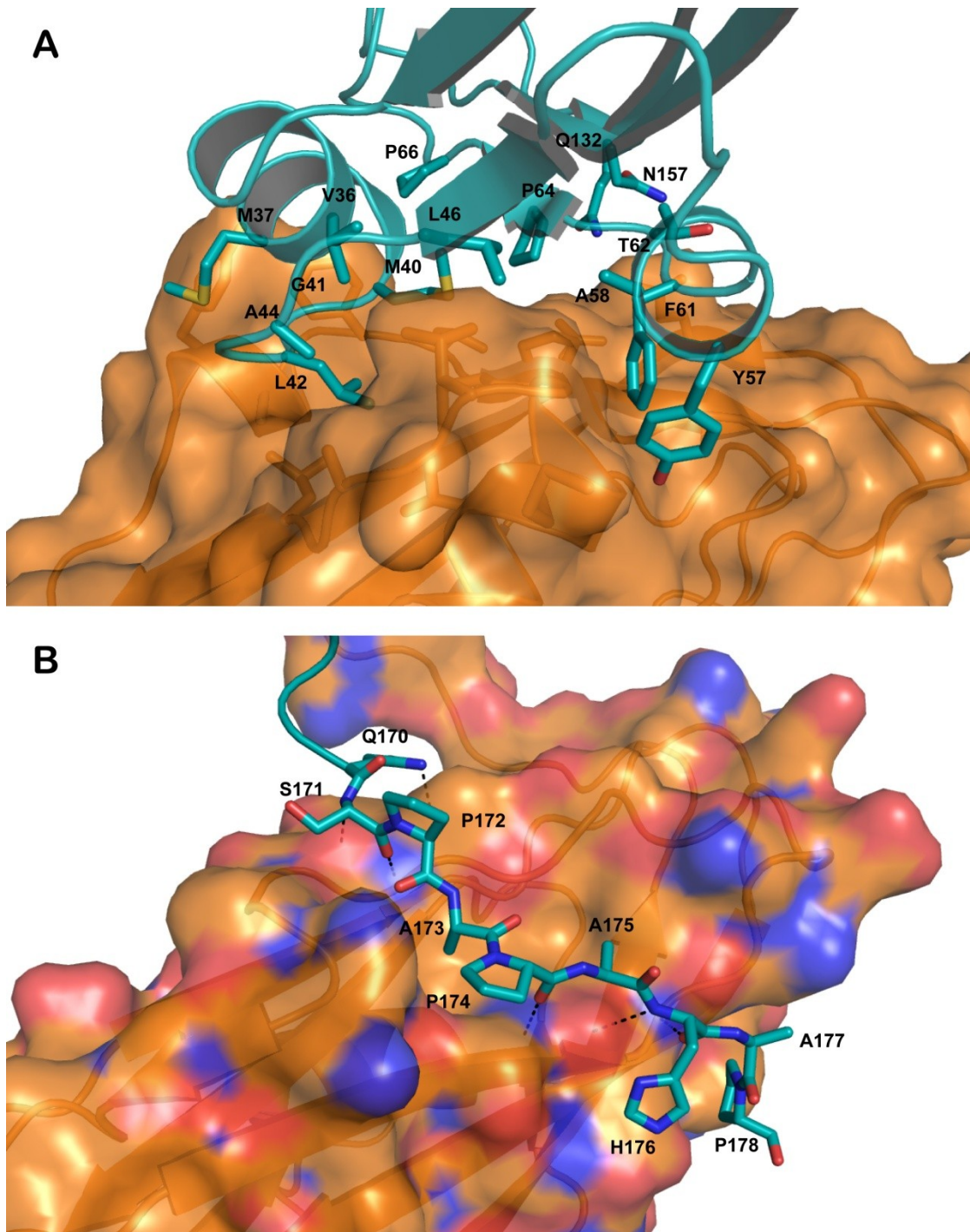


Figure 2.11: Crystal packing of sDr1-2. **(A)** Packing at the symmetrical interface of the crystallographic dimer involving the $\alpha 1/\alpha 2$ region. **(B)** Packing of the sDr1-2 C-terminal tail against the WIF domain of another symmetry mate.

2.4 Structure-Guided Point Mutations in the Derailed Extracellular Region Disrupt its Binding to DWnt5

Due to the high sequence similarity between the sDrl and sDrl-2 WIF domains (44% identical), most of the features observed in the sDrl-2 crystal structure are very likely also to be present in sDrl. Using the sDrl-2 structure as a template, I built a homology model of the sDrl WIF domain using the SWISS-MODEL server (Figure 2.12) (Arnold, Bordoli et al. 2006). The model has a QMEAN4 global score of 0.661 and a Z-score of -1.45, indicating a high level of confidence in model reconstruction (Benkert, Biasini et al.). A surface conservation analysis was then conducted on the structural model of the sDrl WIF domain, using ClustalW sequence alignment of Drl sequences from eight invertebrate species as template (Figure 2.12A, see Experimental Procedures for details). Surface residues in the structural model are colored based upon their conservation in the alignment: red colored regions indicate high conservation, whereas white colored regions indicate low conservation. The three N-glycosylation sites are colored green. Among all surface exposed areas, the surface shown in the lower right part of Figure 2.12A stands out as the most conserved area within the Drl WIF domain (and it is not blocked by N-linked glycosylation sites). A closer look (Figure 2.12B) at this surface area identifies the conserved residues involved, which can be divided into three regions: E40, L41, Y42, K45 and E46 around strand β 2 (region 1, colored green); I49, N50, Y52, A53, N55, F56, V58, P59 and P61 on the helix α 2/strand β 3 segment (region 2, colored orange); E126, K152 and I154 form the third region (region 3, colored yellow). These residues are also

among the most conserved residues between WIF domains of Drl homologs (Figure 2.4B).

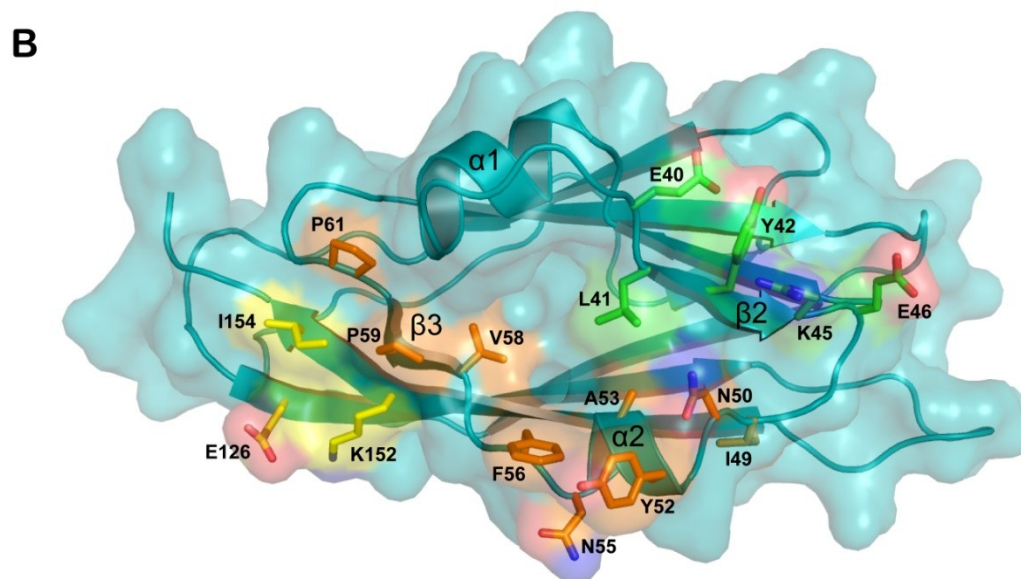
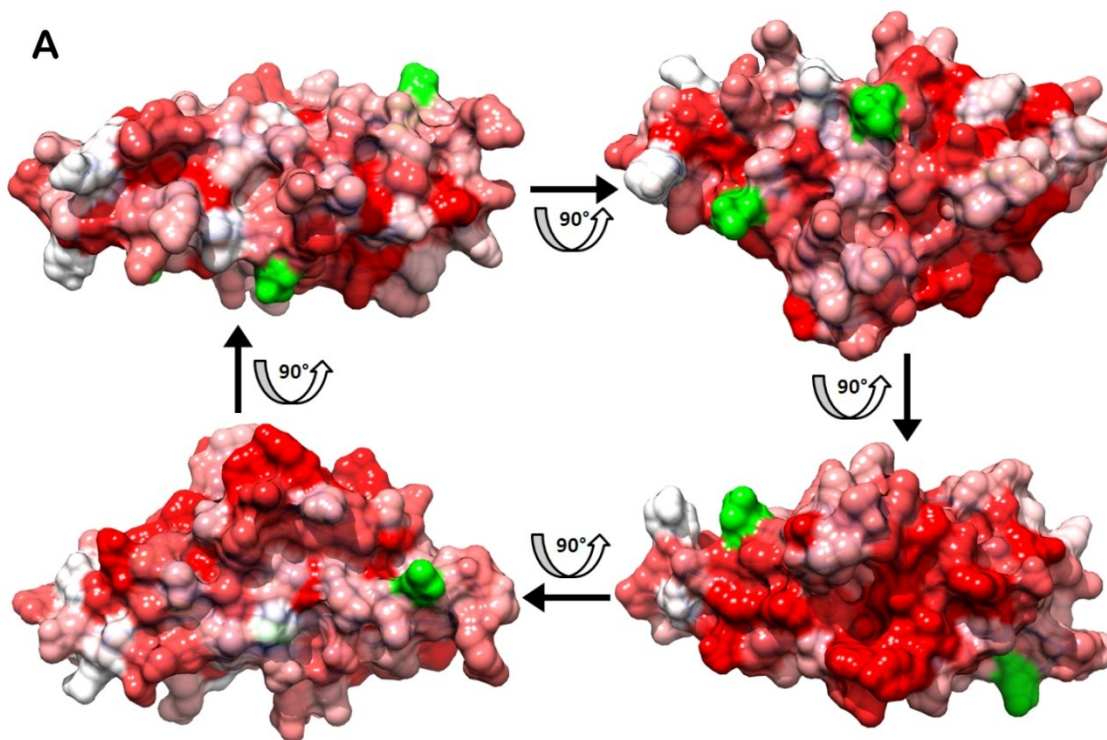


Figure 2.12: Surface conservation of Drl WIF domain homology model. **(A)** Illustration of surface conservation of the Drl WIF domain. The most conserved residues are colored red and the least conserved residues are colored white. The three N-glycosylation sites are colored green. **(B)** Stick and ribbon representation of the conserved residues in the structural model of Drl WIF domain. The model orientation is the same as the lower right figure in **(A)**.

As mentioned in the previous section, the rather hydrophobic region around helices $\alpha 1$ and $\alpha 2$ forms the interface of a crystallographic homodimer in our crystal structure of sDrl-2. High evolutionary conservation also suggests that it may be responsible for binding to Wnt proteins. To test the latter possibility, point mutations were introduced into each area of sDrl, and the resulting variants were tested for their ability to bind DWnt5 using SPR assays (Figure 2.13 and Table 2.4). Any mutation in region 2 (Y52E, F56E and V58E: orange) – in the $\alpha 2/\beta 3$ segment – abolished binding of sDrl to DWnt5. An E40K mutation in region 1 (green) also decreased binding affinity to DWnt5 by ~ 10 fold. The other two mutations in region 1, L41E and Y42E, caused aggregation of sDrl during gel filtration, so their effects on DWnt5 binding could not be characterized. By contrast with these examples, mutations in region 3 of sDrl (E126K and I154E: yellow) had no effect on DWnt5 binding affinity. Therefore, the segment encompassing helices $\alpha 2$ and strand $\beta 3$ (region 2) on sDrl appears to be responsible for DWnt5 binding, with hydrophobic residues in the segment (Y52, F56, V58) being implicated. E40 in Region 1 (at the beginning of strand $\beta 2$) may also contribute to DWnt5 binding.

sDrI variants binding to immobilized DWnt5

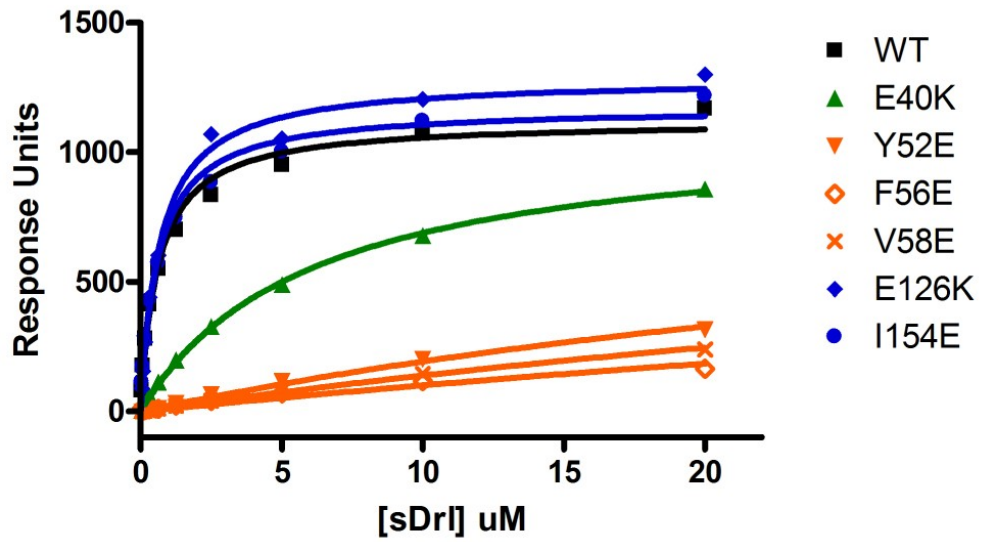


Figure 2.13: SPR studies to characterize the effect of point mutations in sDrI (1-242) on binding to immobilized DWnt5 wildtype protein.

Table 2.4: SPR studies of DWnt5 binding property of Drl ectodomain proteins (residue 1-242) with single point mutation.

Analyte	Binding K_D (μ M) to immobilized DWnt5
sDrl wildtype	0.63 ± 0.09
sDrl E40K	6.1 ± 0.3
sDrl L41E	Aggregation in solution
sDrl Y42E	Aggregation in solution
sDrl Y52E	47 ± 13
sDrl F56E	99 ± 142
sDrl V58E	69 ± 19
sDrl E126K	0.67 ± 0.07
sDrl I154E	0.62 ± 0.08

2.5 Summary and Discussion of Derailed-DWnt5 Studies

In this study, I have characterized the interaction between Derailed family receptor tyrosine kinases and its ligand, DWnt5, *in vitro* using purified proteins. I have shown, for the first time, that Ryk/Drl family proteins' extracellular region binds *directly* to a Wnt ligand. The DWnt5 binding affinities (K_D) of Drl homologs lie in the range of 100 nM to low micromolar as determined by SPR. A crystal structure of sDrl-2 has revealed important features of the WIF domains of Drl family proteins. Based on the structure, the region on the Drl WIF domain that is responsible for DWnt5 binding has been mapped using site-directed mutagenesis and SPR assays. The residues implicated form a ring around a depression that lies between the two α -helical regions, suggesting that this is the key ligand-binding site.

Given the high sequence homology within the mammalian and *Drosophila* Ryk/Drl family and Wnt family, the interaction mode and binding interface of Drl-DWnt5 characterized here are likely to be conserved in the case of human Ryk-Wnt interactions. Unfortunately, due to experimental difficulties in generating useful quantities of the soluble Ryk extracellular region and human Wnt proteins in detergent-free conditions, similar biophysical studies have not proven possible using this strategy.

Previous studies in the literature have attempted to measure the interaction affinities between Wnt proteins and their cell surface receptors such as Frizzled, Ror and Ryk using cell-based or ELISA assays. Most of those studies have reported K_D values in the low nanomolar range. For example, Liu *et al.* (Liu, Shi et al. 2005) reported a K_D

value of 8 nM for binding of human Wnt1 to cell surface-expressed Ryk. Using a similar cell-based overlay assay and a Wnt3/alkaline phosphatase fusion protein, Schmitt *et al.* (Schmitt, Shi et al. 2006) also measured Wnt3 – Ryk interaction with an apparent K_D value of 4 nM. These reported values are more than an order of magnitude lower (suggesting tighter binding) than that of the Drl-DWnt5 interaction which I have determined in SPR assays. This is a common observation in studies of cell surface receptors. For example, although cellular studies of EGF binding to its receptor yield K_D values in the low nanomolar (6-12 nM) range (Burgess, Cho et al. 2003), studies of EGF binding to the isolated extracellular region of its receptor typically yield well-validated K_D values in the 100-200 nM range (Dawson, Berger et al. 2005) – revealing a similar difference of an order of magnitude as seen in my DWnt5 studies. These differences can arise for several reasons, and are not likely to reflect any intrinsic difference between the binding properties of Drl and DWnt5 when compared with other receptor/Wnt complexes. If Wnt binding induces receptor dimerization, this dimerization will be favored in the membrane context compared with solution – and the resulting linked equilibria will yield a higher apparent Wnt binding affinity for cellular assays. The differences might also reflect the different assay systems employed. For example, the detection antibodies employed in the cell-based or ELISA-based studies (for measuring the amount of bound protein) frequently cause self-association of both receptor and ligand, which will at the same time increase the avidity (and therefore apparent affinity) of binding. Alternatively, the differences might reflect the presence of other cellular factors that contribute to complex formation. Extracellular ligands such as Wnt proteins commonly display weak interactions with the sugars, proteoglycans, and (since they are acylated) hydrophobic

membranes present on the surface of cells. Interactions of this sort would contribute to the increased binding affinity observed in cellular studies. In addition, the presence of a co-receptor cannot be ruled out.

It is intriguing to postulate what might happen after binding of Wnt to Ryk/Drl on the cell surface. Ryk/Drl contain an intracellular pseudokinase domain that has no observable kinase activity, even when they are clustered (and oligomerized) onto lipid vesicles (my unpublished results). If the intracellular domains of Ryk/Drl have no catalytic function, they must initiate downstream signaling through as-yet-unknown signaling mechanism, which (in the absence of kinase activity) sets them apart from other RTKs. Unlike seven transmembrane domain proteins such as like GPCRs, the cytoplasmic region of Ryk/Drl is linked to extracellular Wnt binding through a single transmembrane domain, making it unlikely that a ligand-induced conformational change could be propagated across the membrane without either ligand-induced dimerization or association (heterodimerization) with some other cell-surface molecules – which could be other Wnt receptors, for example.

Several studies have already suggested that Wnt ligands can bind simultaneously to Ryk and other cell surface receptors. For example, a Ryk/Wnt/Frizzled complex can be co-immunoprecipitated (Lu, Yamamoto et al. 2004), indicating the formation of ternary complex. In addition, the soluble Ryk extracellular region blocks Wnt binding to cell-surface Ryk, but not to Frizzleds – whereas secreted Frizzled-like proteins block Wnt binding to cell-surface Frizzled but not to Ryk (Schmitt, Shi et al. 2006). Thus, the basis for Wnt binding to these classes of receptor appears to be different, suggesting different

Wnt recognition properties for the WIF and CRD domains. Ryk has also been shown to co-immunoprecipitate with receptors EphB2 and EphB3 (Halford, Armes et al. 2000; Trivier and Ganesan 2002; Kamitori, Tanaka et al. 2005). Taken together, these data suggest that Wnt binding may bring Ryk/Drl into close proximity with other cell receptors, with which it collaborates in promoting intracellular signaling.

Many important questions remain to be addressed concerning the Ryk/Drl-Wnt signaling system. For the next steps of this study, key goals will include the following:

1. Structural characterization of Wnt proteins using X-ray crystallography and hydrogen/deuterium (H/D) exchange, and identification of the region(s) responsible for binding to Ryk/Drl.
2. Addressing the cellular signaling effects of Ryk/Drl-Wnt when binding-defective mutations are introduced.
3. Determining the stoichiometry of the Ryk/Drl-Wnt complex, and assessing whether DWnt5 binding induces dimerization of Ryk/Drl extracellular regions.
4. Understanding the signaling mechanisms of Wnt-bound Drl/Ryk.

At present, the only structural information of Wnt family protein comes from the crystal structure of XWnt8 in complex with a mouse Frizzled-8 CRD domain with which it was co-expressed; this co-expression was required for production of soluble XWnt8. Unlike other Wnts, DWnt5 can be purified in large quantities and is well-behaved in solution without detergents – making it a promising candidate for crystallographic studies to provide further structural information of Wnt proteins. In particular, since the only

Wnt structure known is bound to a Frizzled CRD, it will be important to determine a structure of a free Wnt protein. Additionally, a co-crystal structure of DWnt5 with sDrl (or other sDrl homologs) will greatly help our understanding of their binding mode.

Alternatively, in the absence of a DWnt5 crystal structure, H/D exchange method coupled with mass spectrometry can offer important structural insights regarding the structural dynamics of Wnt domain and also likely identify DWnt5 segments that are responsible for Drl binding when it is performed with DWnt5-Drl complex.

Albeit soluble, mature wildtype DWnt5 protein has heterogeneous N-terminal start sites as well as a long, 150 amino acids insert in the Wnt domain. These properties introduce potential structural heterogeneity and instability for further biophysical characterization, especially protein crystallography. Several strategies are being employed in order to improve current DWnt5 protein construct for crystallography purposes:

1. Replacing the long Wnt domain insert with a short 6xHis tag, which serves two purposes: (a) removing the loop to improve protein homogeneity and stability, and (b) allowing an additional purification step using NiNTA resin. Removal of this region should have minimal effect on Wnt domain integrity since (a) most of Wnt5 homologs found in other species do not have such an insert and (b) the DWnt5 Δ B construct fully retains sDrl binding affinity and has better expression.
2. Introducing a TEV protease cleavage site in between residue 470-540 to remove the extra N-terminal non-conserved residues and to improve protein homogeneity.

This region is in between the poly-serine segment (and N-terminal start of mature DWnt5) 455-SQPSISSSSSS-465 and the Wnt domain.

With completion of the goals summarized above, the insights I have gained into Wnt signaling through Drl proteins will be further developed towards a mechanistic understanding of this important signaling axis.

2.6 Experimental Procedures for Chapter 2

Expression and Purification of sDrl and DWnt5 Proteins

For sDrl expression, DNA encoding 6xHis tagged Drl full extracellular region (1-242) was cloned into pFastBac1 using 5'-GAATGGATCCAACATGGCCCCCAACTTGCTAACAA TCGGATTAC-3' as forward primer and 5'-GAATCTCGAGTTAGTGATGGTGATGGTGATG GCCACTGGCCGGTGGCACCAG-3' as reverse primer. Recombinant baculoviruses were generated using the Bac-to-Bac system (Invitrogen). For protein expression, Sf9 medium was harvested three days post infection and subjected to extensive dialysis at 4 °C. Proteins were then extracted from medium using self-packed NiNTA resin. NiNTA resin was washed twice with low imidazole buffer (20 mM HEPES pH 7.5, 150 mM NaCl and 15 mM imidazole) and sDrl protein was then eluted from NiNTA resin with buffer containing 20 mM HEPES pH 7.5, 150 mM NaCl and 100 mM imidazole. sDrl protein was further purified using an UnoQ anion exchange column (BioRad) (loading buffer was 20 mM HEPES pH7.5 and 70 mM NaCl, with an elution gradient of 70 mM -1 M NaCl) and a Superose 12 sizing column (GE Healthcare) (running buffer: 10mM HEPES pH 7.5 and 150mM NaCl), with a final yield of ~ 1mg/liter of medium. All purifications

were performed at room temperature. Other sDrl variants are purified in the same way. pFastBac1 plasmids containing either sDrl-2 or sDnt were obtained from Dr. Lee Fradkin. Both constructs contain ORF encoding full extracellular regions of either Drl-2 or Dnt with native signal peptide and a C-terminal RPLESRGGPFEGKPIPNPLLGLDSTR TGHHHHHH sequence.

For expression of DWnt5 protein, S2 cells were stably transfected with a mixture of three plasmids (*i*) pUAST-DWnt5, (*ii*) pAc-Gal4 and (*iii*) pCoHygro (10 μ g:10 μ g:1 μ g) using calcium phosphate method, and were selected in Schneider's medium (Sigma) supplemented with 10% fetal calf serum (Sigma, Cat#F0643) and 300 μ g/ml hygromycin (cellgro) for 3 weeks. Schneider's cell medium was then replaced with EXCELL 420 serum-free medium (SAFC Biosciences) for subsequent cell culture, and constitutive secretion of DWnt5 into the medium was verified using DWnt5 specific antibodies (Fradkin, Noordermeer et al. 1995). Binding of Gal4 protein (constitutively expressed from pAc-Gal4 vector) to the promoter region of pUAST-DWnt5 induces high-level expression of DWnt5 protein in S2 cells. For large scale DWnt5 expression, cells were seeded at 4x10⁶ cells/ml in spinner flasks. After 5 days of growth, medium (~3 litres) was harvested and flowed through 4ml Fractogel SO3 (EMD) resin at 4°C. Then SO3 resin was washed twice with 10ml of wash buffer (20 mM HEPES pH 7.5, 250 mM NaCl). DWnt5 was then eluted from SO3 column with three washes of 4ml elution buffer (20 mM HEPES pH 7.5, 900 mM NaCl). Protein solution was then diluted with 3 volumes of 20 mM HEPES pH7.5 buffer to lower the NaCl concentration to <250 mM. All subsequent purification steps were performed at room temperature. The protein sample

was next loaded onto a self-packed 2ml Fractogel SO3 FPLC column pre-equilibrated with 20 mM HEPES pH7.5 and 150 mM NaCl. A gradient from 150 mM – 1 M NaCl was then used to elute the bound DWnt5 protein from the column (elution peak around 650mM NaCl). Eluted fractions were then diluted again with 3 volumes of 20 mM HEPES pH7.5 buffer, loaded onto CHT2 column (BioRad) equilibrated with buffer containing 20 mM HEPES pH7.5, 150 mM NaCl, 2.5 mM NaH₂PO₄, 2.5 mM K₂HPO₄. A 0-100% gradient of Buffer B (250 mM NaH₂PO₄, 250 mM K₂HPO₄ and 150 mM NaCl) was used to elute the protein. Finally, eluted fractions were pooled together, concentrated, and loaded onto a Superose 6 column (GE Healthcare) with running buffer containing 10 mM HEPES pH 7.5 and 150 mM NaCl. The purified protein could be flash frozen in the presence of 10% glycerol with no significant aggregation or loss of sDrl-binding activity upon thawing.

Pull-down of DWnt5 by Drl Extracellular Regions

EXCELL 420 serum-free S2 medium containing secreted DWnt5 was concentrated by 10-fold in an Amicon concentrator. The purified recombinant Drl extracellular region (sDrl) was added at a 1 μ M final concentration to 1.2 ml of concentrated S2 medium, and incubated for 2 hours at 4 °C. Then, 60 μ l of pre-washed NiNTA bead slurry (enough to bind all the added 6xHis-tagged sDrl) was added to the solution for an additional hour at 4 °C. Supernatant and beads were then separated and NiNTA beads were resuspended in buffers (20 mM HEPES pH7.5, 150 mM NaCl) to make samples for Western blotting using rabbit anti-DWnt5 polyclonal Ab (epitope B, (Fradkin, Noordermeer et al. 1995)) and mouse anti-His5 Ab (QIAGEN).

Surface Plasmon Resonance Studies

SPR experiments were performed using a Biacore3000 instrument (GE). DWnt5 protein was immobilized onto a CM5 sensorchip using the amine coupling method as recommended by the manufacturers. Briefly, purified DWnt5 protein was diluted in HBS-EP buffer (10 mM HEPES pH7.5, 150 mM NaCl, 3 mM EDTA, 0.005% Polysorbate 20) to a final concentration of 1 μ M and allowed to flow across an EDC/NHS-activated CM5 chip surface at 5 μ l/min for a total volume of 100 μ l. The sensorchip surface was then quenched with an injection of 1M ethanolamine pH 8.0. Typically, about 10000 RU of DWnt5 was immobilized onto the surface. DWnt5 sensorchips were relatively stable in a short term (1-2 weeks), as determined by tests of sDrl binding, when stored at 4 °C, but tended to lose sDrl binding affinity and capacity (in terms of both K_D and B_{max}) over time.

For sDrl binding experiments, 10 samples of purified, serially diluted (1:1 in HBS-EP) sDrl proteins (20 μ M - 4 nM) were prepared. Then samples were sequentially injected at room temperature, starting from the lowest concentration. For each injection, steady state binding of protein was achieved, and bound sDrl proteins were then allowed to spontaneously detach from the sensorchip surface after each injection in HBSEP running buffer. An example sensorgram, including the dissociation phase, is shown in Figure 2.8B. In a typical case, the SPR signal fell to within 20 RUs of that measured before ligand injection by the end of the dissociation phase (typically 5 minutes). RUs recorded from steady state binding at each concentration were then used to fit the sDrl binding curve to a simple hyperbola using Prism software.

For the reverse experiment (immobilizing sDrl homologs and flowing DWnt5 protein across the Drl-derivatized surfaces), 25 μ M of purified extracellular regions of Drl homologs (in 8 mM HEPES pH 7.5, 120 mM NaCl, 10% glycerol) were diluted 1:4 in 10mM sodium acetate (pH 4.5) solution and flowed across an activated CM5 sensorchip surface at 10 μ l/min for 9 minutes. About 10000 - 14000 RUs of each Drl homolog were immobilized onto the surface. Purified DWnt5 protein was then injected on to the sensor chip (concentrations from 10 nM to 5 μ M), and was allowed at each injection to reach steady state binding (typically 10 μ l/min for 7 minutes). A typical sensorgram is shown in Figure 2.9C. 25 μ l of regeneration buffer (10 mM sodium acetate pH4.5 and 500 mM NaCl) was then used to wash off bound DWnt5 proteins from the CM5 surface after each injection, bringing the SPR signal after each experiment down to within 10% of the maximal binding RU of that injection. Other aspects of the experimental setup are similar.

Crystallography and Structural Determination of sDrl-2

sDrl-2 full extracellular region (1-183) with a C-terminal Factor Xa (FXa) cleavage site (IEGR), spacer peptide (ASGPFEGKPIPNPLLGLDSTRTG) and 6xHis tag was subcloned into pFastBac1 vector and expressed in *Trichoplusia ni* cells using baculovirus infection and ESF921 medium (ExpressionSystems). Cell-conditioned medium was collected and passed through a NiNTA column. The column was then washed twice with low imidazole buffer (20 mM HEPES pH 7.5, 150 mM NaCl and 15 mM imidazole) and sDrl2 protein was eluted from NiNTA bead with buffer containing 20 mM HEPES pH 7.5, 150 mM NaCl and 100 mM imidazole. After buffer exchange to remove imidazole, FXa protease

was used to cleave the 6xHis tag from the protein (10 µg protease for 1 mg purified sDrl-2 in 1 ml solution for 1 hour at room temperature). Cleaved sDrl-2 protein was then passed through a Superose 12 sizing column (GE Healthcare) equilibrated with gel filtration buffer (10 mM HEPES pH 7.5, 150 mM NaCl) at room temperature. Protein at the major peak was collected, partially deglycosylated with PNGaseF (New England BioLabs) (2,000 Unit/mg of sDrl-2 protein) for 3 hours at room temp and concentrated to > 12 mg/ml for crystallization. Crystals were grown at 21°C using the hanging drop vapor diffusion method by mixing 1 µl protein solution with 1 µl well solution containing 100 mM Tris pH 8.5, 25% PEG 6000, 100 mM Sodium Acetate and 15% glycerol. Crystals formed within 2 days and were frozen directly in liquid nitrogen. Data were collected using a home source X-ray unit (Rigaku), and were processed using HKL2000 software (Otwinowski and Minor 1997). Initial phasing was obtained by molecular replacement using a truncated poly-alanine model of the NMR structure of human WIF-1(PDB: 2D3J) (Liepinsh, Banyai et al. 2006) as the search model in Phaser (CCP4 (Collaborative Computational Project Number 4) 1994). Structural refinement and model building were carried out using Refmac (CCP4 (Collaborative Computational Project Number 4) 1994) and Coot (Emsley and Cowtan 2004). Structure figures were generated using PyMol (DeLano 2002).

Homology Modeling and Surface Conservation Analysis of Drl WIF Domain

Homology model of Drl WIF domain was built using the SWISS-MODEL server (Arnold, Bordoli et al. 2006) based on the crystal structure of sDrl-2 ectodomain. Surface conservation analysis was conducted based on alignment of Drl protein sequences from

eight invertebrate species: GI17137162 (*Drosophila melanogaster*), GI194759318 (*Drosophila ananassae*), GI195049987 (*Drosophila grimshawi*), GI195115220 (*Drosophila mojavensis*), GI157130072 (*Aedes aegypti*), GI91092648 (*Tribolium castaneum*), GI328789866 (*Apis mellifera*) and GI156547777 (*Nasonia vitripennis*). Illustration of surface conservation was generated using UCSF Chimera software (Pettersen, Goddard et al. 2004).

Appendix 1 List of Kinase Inhibitors Used in Chapter 1.2.3

(Calbiochem Cat. # 539744)

ID	Plate Location	Catalog Number	Product Description	CAS Number	PubChem Compound ID#
1	A1	DMSO			
2	A2	121767	AG 1024	65678-07-1	2044
3	A3	121790	AGL 2043	226717-28-8	9817165
4	A4	124011	Akt Inhibitor IV	681281-88-9	5719375
5	A5	124012	Akt Inhibitor V, Triciribine	35943-35-2	290486
6	A6	124018	Akt Inhibitor VIII, Isozyme-Selective, Akti-1/2	612847-09-3	10196499
7	A7	124020	Akt Inhibitor X	925681-41-0	16760284
8	A8	521275	PDK1/Akt/Flt Dual Pathway Inhibitor	331253-86-2 and 329710-24-9	5113385
9	A9	189404	Aurora Kinase Inhibitor II	331770-21-9	6610278
10	A10	197221	Bcr-abl Inhibitor	778270-11-4	5311510
11	A11	203290	Bisindolylmaleimide I	133052-90-1	2396
12	A12	BLANK			
13	B1	DMSO			-
14	B2	203297	Bisindolylmaleimide IV	119139-23-0	2399
15	B3	203696	BPIQ-I	174709-30-9	2427
16	B4	220285	Chelerythrine Chloride	3895-92-9	72311
17	B5	234505	Compound 56	171745-13-4	2857
18	B6	260961	DNA-PK Inhibitor II	154447-35-5	9860529
19	B7	260962	DNA-PK Inhibitor III	404009-40-1	9859309
20	B8	528100	PI-103	371935-74-9	9884685
21	B9	266788	Diacylglycerol Kinase Inhibitor II	120166-69-0	657356
22	B10	317200	DMBI	5812-07-7	5353593
23	B11	324673	EGFR/ErbB-2 Inhibitor	179248-61-4	9843206
24	B12	BLANK			
25	C1	DMSO			
26	C2	324674	EGFR Inhibitor	879127-07-8	9549299
27	C3	324840	EGFR/ErbB-2/ErbB-4 Inhibitor	881001-19-0	11566580
28	C4	343020	Flt-3 Inhibitor	301305-73-7	1048845
29	C5	343021	Flt-3 Inhibitor II	896138-40-2	11601743
30	C6	344036	cFMS Receptor Tyrosine	870483-87-7	11617559

			Kinase Inhibitor		
31	C7	365250	Gö 6976	136194-77-9	3501
32	C8	365251	Gö 6983	133053-19-7	3499
33	C9	371806	GTP-14564	34823-86-4	3385203
34	C10	375670	Herbimycin A, Streptomyces sp.	70563-58-5	16760502
35	C11	343022	Flt-3 Inhibitor III	852045-46-6	11772958
36	C12	BLANK			
37	D1	DMSO			-
38	D2	407248	IGF-1R Inhibitor II	196868-63-0	9549305
39	D3	407601	IRAK-1/4 Inhibitor	509093-47-4	11983295
40	D4	420099	JAK Inhibitor I	457081-03-7	5494425
41	D5	420104	JAK3 Inhibitor II	211555-04-3	3795
42	D6	420121	JAK3 Inhibitor IV	58753-54-1	176406
43	D7	420126	JAK3 Inhibitor VI	856436-16-3	16760524
44	D8	428205	Lck Inhibitor	213743-31-8	6603792
45	D9	440202	LY 294002	154447-36-6	3973
46	D10	440203	LY 303511	154447-38-8	3971
47	D11	448101	Met Kinase Inhibitor	658084-23-2	9549297
48	D12	BLANK			
49	E1	DMSO			-
50	E2	513035	PD 158780	171179-06-9	4707
51	E3	513040	PD 174265	216163-53-0	4709
52	E4	521231	PDGF Receptor Tyrosine Kinase Inhibitor II	249762-74-1	5330548
53	E5	521232	PDGF Receptor Tyrosine Kinase Inhibitor III	205254-94-0	10907042
54	E6	521233	PDGF Receptor Tyrosine Kinase Inhibitor IV	627518-40-5	9797370
55	E7	521234	PDGF RTK Inhibitor	347155-76-4	16760609
56	E8	527450	PKR Inhibitor	608512-97-6	6490494
57	E9	527455	PKR Inhibitor, Negative Control	852547-30-9	16760619
58	E10	528106	PI 3-Kg Inhibitor	648450-29-7	5289247
59	E11	528108	PI 3-KbInhibitor II	648449-76-7	5287855
60	E12	BLANK			
61	F1	DMSO			-
62	F2	529574	PP3	5334-30-5	4879
63	F3	529581	PP1 Analog II, 1NM-PP1	221244-14-0	5154691
64	F4	539652	PKCbII/EGFR Inhibitor	145915-60-2	6711154
65	F5	539654	PKCb Inhibitor	257879-35-9	6419755
66	F6	553210	Rapamycin	53123-88-9	16760631
67	F7	555553	Rho Kinase Inhibitor III, Rockout	7272-84-6	644354

68	F8	555554	Rho Kinase Inhibitor IV	not registered	16760635
69	F9	539648	Staurosporine, N-benzoyl-	120685-11-2	16760627
70	F10	567805	Src Kinase Inhibitor I	179248-59-0	1474853
71	F11	572660	SU11652	326914-10-7	5329103
72	F12	BLANK			
73	G1	DMSO			-
74	G2	574711	Syk Inhibitor	622387-85-3	6419747
75	G3	574712	Syk Inhibitor II	227449-73-2	16760670
76	G4	574713	Syk Inhibitor III	1485-00-3	672296
77	G5	616451	TGF-b RI Kinase Inhibitor	396129-53-6	447966
78	G6	616453	TGF-b RI Inhibitor III	356559-13-2	16079009
79	G7	658390	AG 9	2826-26-8	2063
80	G8	658401	AG 490	133550-30-8	5328779
81	G9	658440	AG 112	144978-82-5	5328804
82	G10	658550	AG 1295	71897-07-9	2048
83	G11	658551	AG 1296	146535-11-7	2049
84	G12	BLANK			-
85	H1	DMSO			-
86	H2	658552	AG 1478	175178-82-2	2051
87	H3	676480	VEGF Receptor 2 Kinase Inhibitor I	15966-93-5	6419834
88	H4	676481	VEGF Receptor Tyrosine Kinase Inhibitor II	269390-69-4	9797919
89	H5	676482	VEGF Receptor Tyrosine Kinase Inhibitor III, KRN633	286370-15-8	9549295
90	H6	676485	VEGF Receptor 2 Kinase Inhibitor II	288144-20-7	5329155
91	H7	676487	VEGF Receptor 2 Kinase Inhibitor III	204005-46-9	5329098
92	H8	676489	VEGF Receptor 2 Kinase Inhibitor IV	216661-57-3	5329468
93	H9	260964	DNA-PK Inhibitor V	404009-46-7	16760391
94	H10	189405	Aurora Kinase Inhibitor III	879127-16-9	9549303
95	H11	569397	Staurosporine, Streptomyces sp.	62996-74-1	451705
96	H12	BLANK			

Appendix 2 A Chemical Genetic Approach to Study ErbB Signaling in Cells

As shown in Chapter 1.4, the kinase inactivating mutations of ErbB3 have shown little effect on ligand induced ErbB autophosphorylation in BaF3 cells or Akt activation in CHO cells, arguing that kinase activity of ErbB3 does not directly contribute to these cellular signaling. However, it is still possible that ErbB3 kinase participate in other signaling events that are not investigated in our cellular studies. One common strategy to study the cellular signaling of kinases is to use specific kinase inhibitors. However, this standard approach is impossible for our study since there is no ErbB3 kinase-specific inhibitor currently available. We have also discussed in Chapter 1 about the possibility that ErbB3 kinase may have distinct substrates other than the phosphorylation sites examined in our study. Therefore, we need to look for potential substrates of ErbB3 kinase in cells. However, historically it has been very difficult to track direct substrate of kinases in a cellular content.

To overcome these problems, the Shokat lab at U.C.S.F has developed a chemical genetic approach using a group of specific ATP analogs, which cannot be effectively accommodated by wildtype kinases, as either inhibitors (bumped inhibitors) or substrate phosphate donors (bumped ATPs) for rationally engineered kinases (Figure 1) (Elphick, Lee et al. 2007). Removing the side chain of a ‘gatekeeper’ residue in the ATP binding site of kinase creates extra space for the engineered kinase to bind these ATP analogs (without disrupting intrinsic kinase activity). The engineered kinase is therefore called analog-sensitive (AS) kinase. There are two classes of ATP analogs: (1) ‘bumped ATPs’, in which a bulky group is attached onto the N6 position of ATP, that can be used as ATP

substrate by AS kinases; and (2) membrane-permeable ‘bumped inhibitors’, in which bulky groups are attached onto adenine scaffold, that serve as specific inhibitors for AS kinases. Ideally, these bumped ATP/bumped inhibitors will only affect the function of engineered kinases with analog-sensitive mutation, but not the activity of corresponding wildtype kinase (Figure 1).

With this chemical genetic approach, I have attempted to dissect the cellular signaling role of ErbB3 using bumped ATP/bumped inhibitors on analog-sensitive ErbB3 mutant (and using wildtype ErbB3 as a control group). As shown in the main text, full length ErbB3 with analog sensitive mutation (T768G) fully retains signaling ability of ligand induced ErbB autophosphorylation (in BaF3 cells, Figure 1.10A) and Akt activation (in CHO cells, Figure 1.11), suggesting that its signaling function is intact. Unfortunately, the analog-sensitive mutation (T768G) causes aggregation of recombinant protein of ErbB3 kinase overexpressed in sf9 cells, which makes it difficult to directly characterize the effect of bumped ATP/bumped inhibitors on analog sensitive ErbB3 kinase mutant *in vitro*. To circumvent this problem, homologous EGFR kinase has been used as a model system to validate this approach since the equivalent analog-sensitive mutation (T766G) is well tolerated in recombinant EGFR intracellular protein and does not affect its solubility/activity. The preliminary studies with EGFR have yielded some encouraging results, and warrant further investigation of ErbB signaling using this approach.

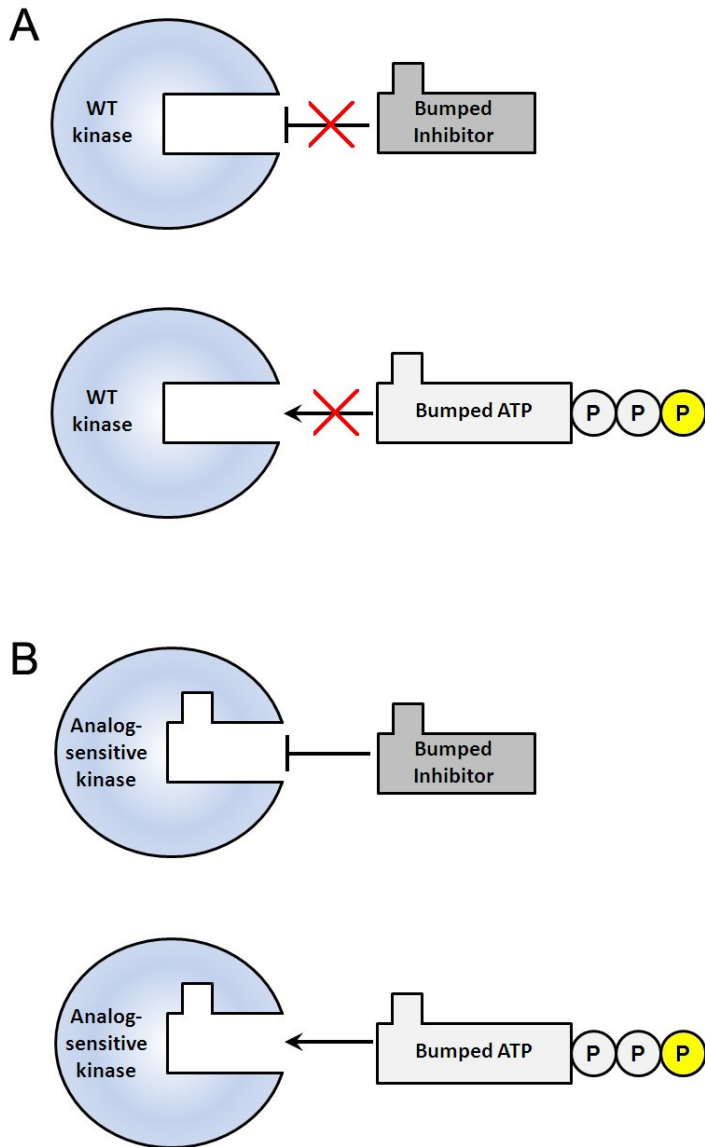


Figure 1: Diagram of the chemical genetic approach to study cellular signaling of kinases. **(A)** Due to the steric hindrance of ATP binding pockets, wildtype kinases cannot bind effectively to ‘bumped inhibitors’ or ‘bumped ATPs’. **(B)** Mutating the gatekeeper residue in the kinase of interest results in a analog-sensitive kinase that can effectively utilize the ‘bumped ATPs’ or bind to ‘bumped inhibitors’ with high affinity.

2.1 Using Bumped Inhibitors to Selectively Inhibit Cellular Signaling by Analog-sensitive ErbB Mutant.

Due to the lack of inhibitors specific for wildtype ErbB3 kinase, we investigated whether bumped inhibitors can serve as specific inhibitors for analog-sensitive (T768G) ErbB3 in cellular studies. We have obtained four membrane-permeable bumped inhibitors from the Shokat lab (1-NA-PP1, 1-NM-PP1, 2-NA-PP1 and 2-NM-PP1). Their chemical structures are shown in Figure 2A. The ideal bumped inhibitor shall selectively inhibit analog-sensitive kinase mutant in the assay and at the same time have minimal influence on the activity of wildtype kinase. Since ErbB3 signaling requires other ErbB kinases in the heterodimer, a successful candidate inhibitor for my study shall not inhibit any wildtype ErbB kinases (not only ErbB3 kinase).

Thus, before applying the bumped inhibitors in the cellular assays, we need to first make sure that (1) bumped inhibitors only binds to analog-sensitive ErbB3 kinase but not wildtype ErbB3 kinase; and (2) bumped inhibitors do not compromise the kinase activity of other ErbB family RTKs (especially ErbB2) that form heterodimer with ErbB3. Unfortunately, recombinant proteins of either wildtype ErbB2 kinase domain or T768G-mutated ErbB3 kinase domain form total aggregates when overexpressed in sf9 cells, which prevents the characterization of their binding to bumped inhibitors *in vitro*. Therefore, we cannot directly test whether both conditions (1) and (2) are fully satisfied in our chemical genetic approach. On the other hand, both wildtype and analog-sensitive (T766G) EGFR kinase domains can be easily purified as recombinant protein. Therefore,

we decided to use EGFR kinase as a model for testing the effect of bumped inhibitors on ErbB family kinases.

Using an *in vitro* radioactive [γ - ^{32}P]ATP kinase assay, we have investigated whether the bumped inhibitors can selectively inhibit analog-sensitive EGFR kinase but not wildtype EGFR kinase. 10 μM of each inhibitor is used in the kinase assay with purified recombinant EGFR kinases and the kinase activity is monitored as incorporation of ^{32}P into substrates (Figure 2B). The results suggest that, while all four inhibitors are able to inhibit analog-sensitive (T766G) EGFR kinase, three of them are also strong inhibitor for wildtype EGFR kinase. Only 2-NM-PP1 meets our criteria of a selective inhibitor for analog sensitive ErbB kinase, and it will be used in our subsequent cellular assays.

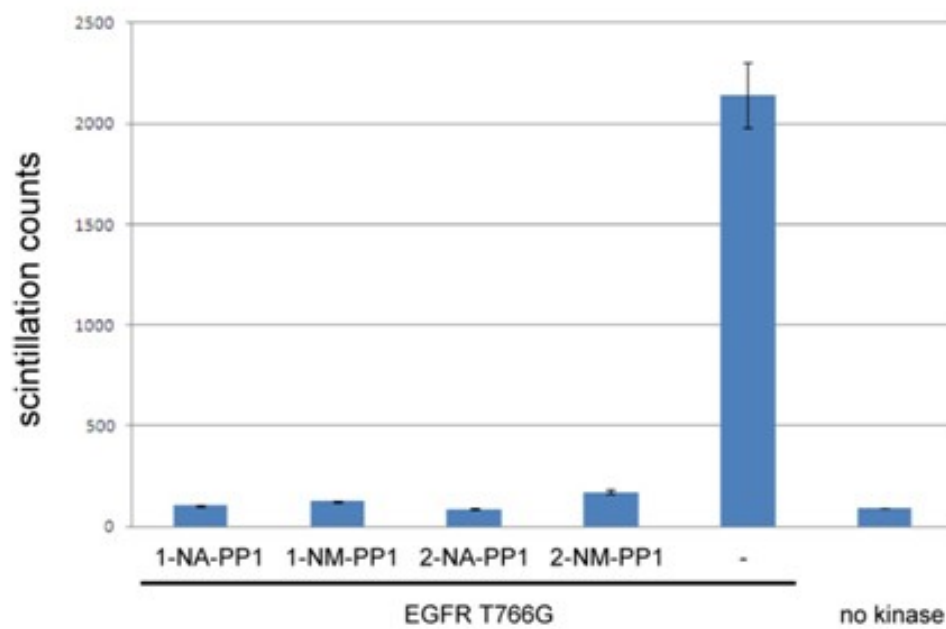
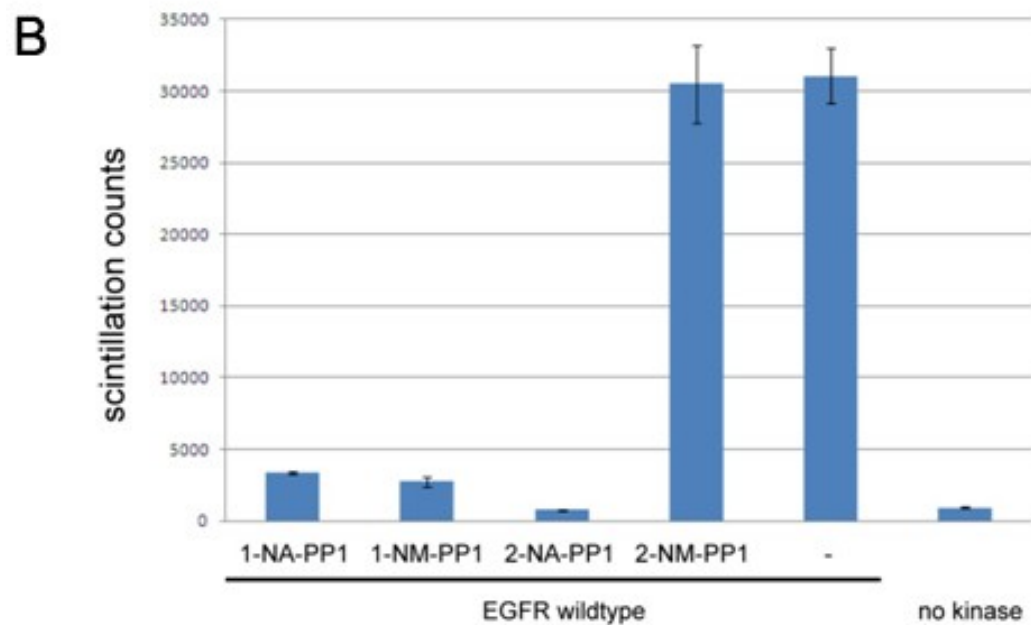
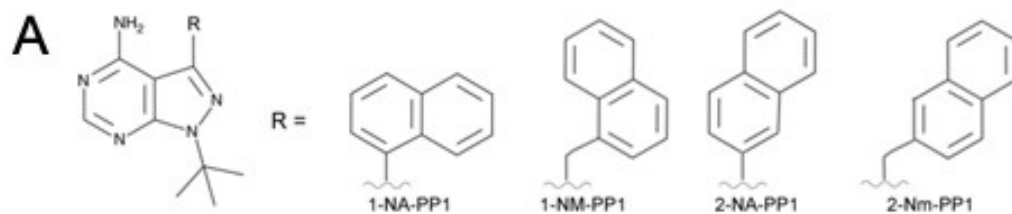


Figure 2: Inhibitory effect of bumped inhibitors on EGFR kinases. **(A)** Chemical structures of bumped inhibitors (Bishop, Kung et al. 1999). **(B)** Selectivity of bumped inhibitors to EGFR kinase (wildtype or analog-sensitive). In the kinase assays, 0.5 μM EGFR kinase domain (wildtype or T766G) is incubated with 100 μM ATP, $\sim 1 \mu\text{Ci}$ [γ - ^{32}P]ATP, 200 μM poly GluTyr peptide substrate, 5 mM MgCl_2 and 10 μM indicated inhibitor or DMSO control (-) for 5 minutes at room temperature. The reactions are stopped with 100mM EDTA and spotted onto nitrocellulose paper for washing and scintillation counting to measure the incorporation of ^{32}P . A no kinase control is also included. The measurements shown are the average values from duplicated experiments and the error bar indicates the high and low values. A maximum of $<7\%$ of total ^{32}P is incorporated in the assays.

Next, we applied 2-NM-PP1 on transfected CHO cells expressing either wildtype or analog-sensitive EGFR protein, and showed that this bumped inhibitor can selectively inhibit the kinase activity of analog-sensitive EGFR in CHO cells (Figure 3). Ligand-induced autophosphorylation of analog-sensitive (T766G) EGFR was nearly abolished at the presence of 3 μM 2-NM-PP1. On the other hand, the activity of wildtype EGFR was not affected by 2-NM-PP1 until the concentration of the inhibitor was raised by 10 fold (30 μM). Therefore, 2-NM-PP1 can be used as a selective inhibitor for analog-sensitive EGFR at low micromolar concentration.

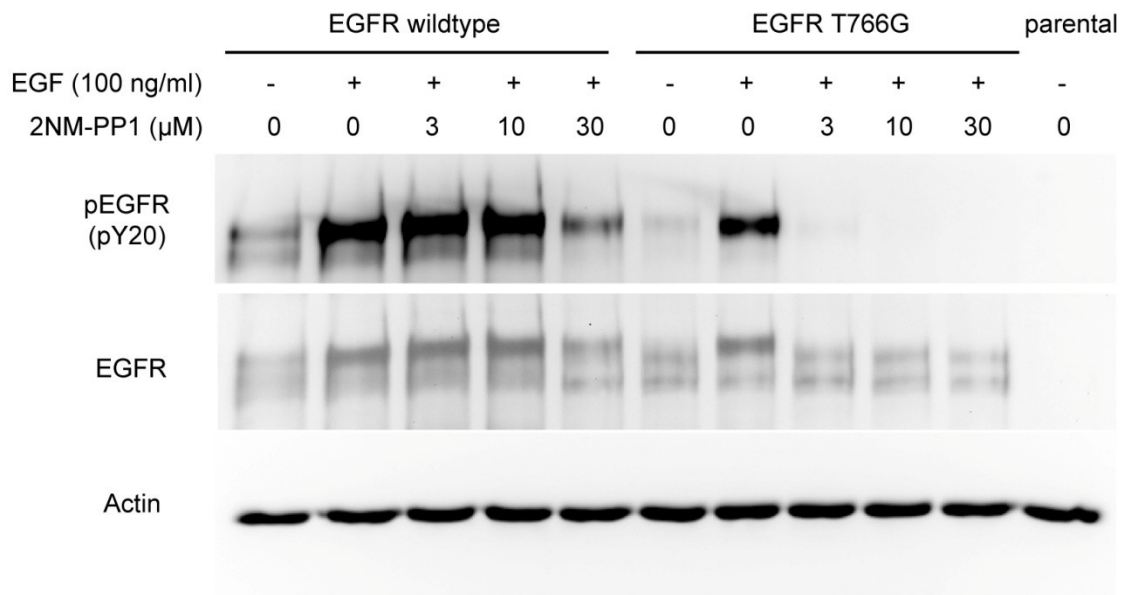


Figure 3: 2-NM-PP1 preferentially inhibits cellular signaling by EGFR with analog-sensitive mutation. CHO cells were grown in 12 well dishes, transiently transfected with pcDNA3.1-EGFR (full-length, wildtype or T766G) constructs and serum-starved overnight. 48 hours post transfection, 2NM-PP1 was added to each well with indicated final concentrations from a 10 mM stock solution (in DMSO) and cells were maintained in 37 °C for one additional hour. Afterwards, cells were placed on ice and stimulated with 100 ng/ml final concentration of EGF. Cells were then washed with PBS and lysed in RIPA buffer and subjected to western blotting. PhosphoEGFR was detected by pY20 anti-phosphotyrosine antibody; total EGFR were monitored by anti-EGFR Ab12 (labvision) and anti-Actin blots were used as loading controls. Experiments were performed in duplicates.

We then applied the 2NM-PP1 in our cellular assay for ErbB3 kinase, and investigated whether the bumped inhibitor can affect signaling by analog-sensitive ErbB3 mutant. In BaF3 cells co-expressing ErbB2/ErbB3, adding 2NM-PP1 resulted in decreased level of ligand-induced ErbB autophosphorylation in both cell lines carrying wildtype or T768G-mutated ErbB3 (Figure 4A). The decrease of ErbB autophosphorylation in wildtype ErbB2/ErbB3 applied with 2NM-PP1 suggested the presence of off-target effect. Although, comparing to cells carrying wildtype ErbB3, the decrease of autophosphorylation seemed more prominent in cells carrying T768G-mutated ErbB3, such effect is not statistically significant in our subsequent repeats. Therefore, we cannot conclude whether the cellular effect we observed is due to inhibition of ErbB3 kinase by 2-NM-PP1 or its off-target effect. Similarly, in CHO cells expressing wildtype or T768G-mutated ErbB3, no apparent effect is observed for ligand-induced Akt activation when 2NM-PP1 is applied (Figure 4B). It is too early to draw any conclusion from these results, since (1) we do not know whether 2-NM-PP1 binds preferentially to analog-sensitive ErbB3 and (2) we used the same cellular assays as in Chapter 1.4, in which the kinase-compromised ErbB3 mutants showed little effect. However, this bumped inhibitor approach is still promising for a more comprehensive study of ErbB3 kinase signaling using a proteomic approach, such as SILAC, at the absence of specific ErbB3 inhibitors.

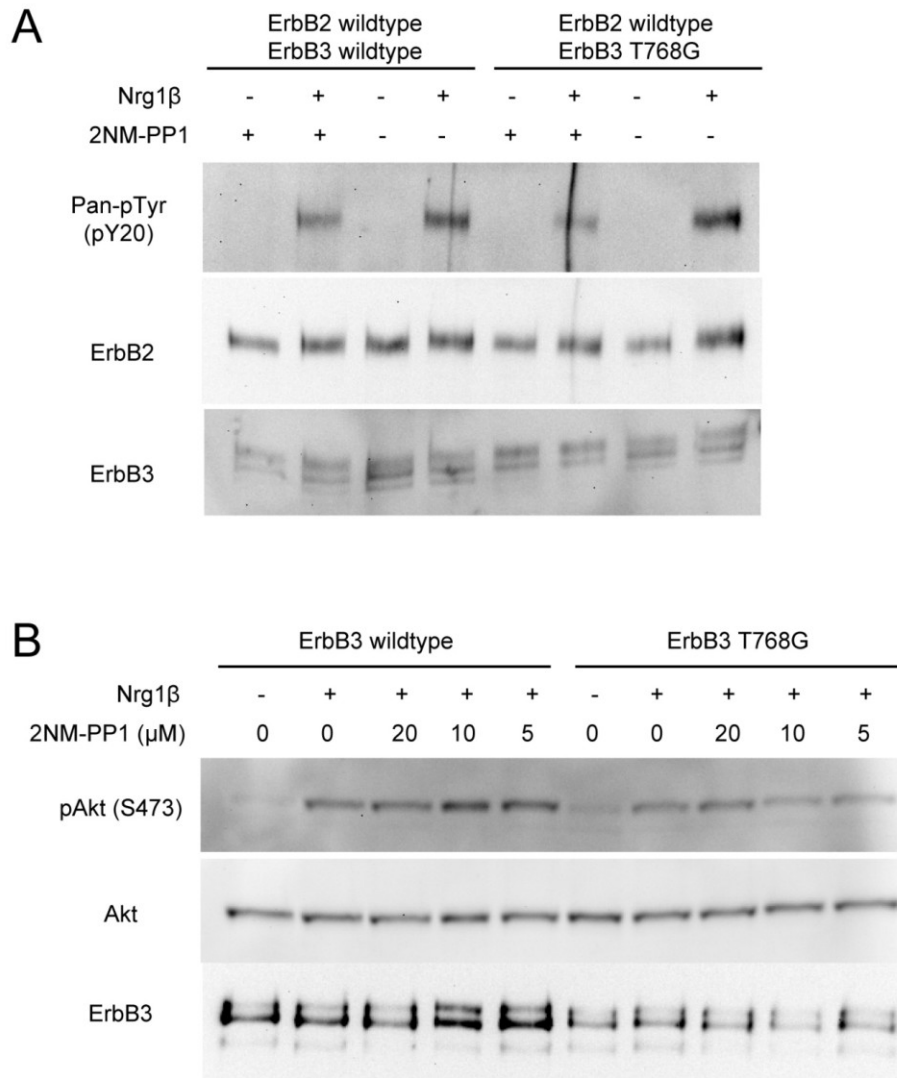


Figure 4: Application of 2-NM-PP1 on cellular signaling of analog-sensitive ErbB3 mutant. **(A)** BaF3 cells stably co-expressing ErbB2 wildtype and either ErbB3 wildtype or analog-sensitive (T768G) ErbB3 mutant were serum-starved for 4 hours, then further incubated with 8 μ M 2-NM-PP1 or DMSO control for 2 hours. Cells were then resuspended in PBS and stimulated with Nrg1 β on ice for 10 minutes. **(B)** CHO cells were transiently transfected with pcDNA plasmids containing either ErbB3 wildtype or analog-sensitive (T768G) ErbB3 mutant. 24 hours after transfection, CHO cells were serum-starved overnight, and then incubated with indicated amount of 2-NM-PP1 for 1 hour before stimulated with 5 ng/ml of Nrg1 β for 20 minutes at 37 $^{\circ}$ C. Samples were prepared in the same way as described in Experimental Procedures.

2.2 Using Bumped ATPs as Preferred Substrates for Analog-sensitive ErbB Kinase

Bumped ATPs have been used in multiple studies to identify the direct physiologic substrate of the engineered analog-sensitive kinase as well as study substrate specificity in cells (Elphick, Lee et al. 2007). Briefly, a ^{32}P -label can be incorporated into the γ phosphate group of bumped ATP. Then the ^{32}P label can be used to trace the substrates that are directly phosphorylated by this analog sensitive kinase in cells, since (at least in an ideal situation) only the engineered analog-sensitive kinase, but not the wildtype kinases, can utilize the ^{32}P labeled bumped ATP as substrate. As a proof of principle, we first used this approach to study EGFR kinase (as it is ~ 1000 fold more active than ErbB3 kinase). The goal is to investigate whether ^{32}P labeled bumped ATP can be used to identify the physiological substrate of EGFR kinase in cells. This study can be broken down into four stages:

- 1) Generation of bumped ATP
- 2) Test whether analog-sensitive EGFR kinase can effectively utilize bumped ATP
- 3) Development of membrane permeabilization method that allows bumped ATP to pass through plasma membrane and enter cytosol
- 4) Using bumped ATP to trace protein phosphorylation mediated directly by EGFR

1) Generation of γ - ^{32}P labeled bumped ATP ($[\gamma$ - $^{32}\text{P}]$ N6-Bn-ATP)

Due to the relative short half life (~ 14 days) of ^{32}P , γ - ^{32}P labeled bumped ATP needs to be generated shortly before the cellular assay. This is achieved by transferring γ - ^{32}P phosphate from fresh $[\gamma$ - $^{32}\text{P}]$ ATP onto bumped-ADP using purified recombinant yeast

nucleoside diphosphate kinase (γ NDPK) (Figure 5A). Briefly, the γ - ^{32}P phosphate is first transferred from ATP to a histidine side chain on γ NDPK protein to form an unstable phosphate-protein intermediate and ADP. ADP can be washed away and bumped ADP is then added to take the γ - ^{32}P phosphate from γ NDPK to form $[\gamma$ - $^{32}\text{P}]$ bumped-ATP. Using this method, we have generated $[\gamma$ - $^{32}\text{P}]$ N6-Benzyl-ATP ($[\gamma$ - $^{32}\text{P}]$ N6-Bn-ATP), the most commonly used bumped ATP, with a protocol adapted from (Elphick et al. ACS Chemical Biology 2007). The radioactivity generated by each step is monitored by scintillation counter (Figure 5B).

- Immobilize 0.1mg purified, recombinant γ NDPK (6x His tagged) with 20ul NiNTA beads in 1ml resuspension buffer (RSB: 20 mM Tris-HCl pH 8.0, 200 mM NaCl, 5% Glycerol), and wash once with RSB.
- Incubate the beads with 50uCi ^{32}P -ATP in 1ml RSB, and continue mixing on nutator for 5 min.
- Spin down NiNTA beads at 500 g, remove the solution. (Figure 5B column 1 shows the remaining $[\gamma$ - $^{32}\text{P}]$ ATP in solution *after* incubation with γ NDPK.)
- Wash three times with RSB + 1x phosphate (10 mM Na_2HPO_4 , 2 mM KH_2PO_4). (Figure 5B column 2-4)
- Wash once with RSB + 1x phosphate + 10 μM adenosine. (Figure 5B column 5)
- Wash twice with RSB without phosphate. (Figure 5B column 6)
- Incubate with 5nmol of N6-Bn-ADP in 200ul RSB + 10mM MgCl_2 for 5 min. Spin down the beads and transfer the solution to another tube. The solution contains the newly generated $[\gamma$ - $^{32}\text{P}]$ N6-Bn-ATP, which has incorporated $\sim 60\%$ of the initial ^{32}P .

(Figure 5B column 7 shows the radioactivity of $[\gamma\text{-}^{32}\text{P}]\text{N6-Bn-ATP}$, column 8 shows the remaining ^{32}P left on NiNTA beads)

- Make aliquots and freeze in $-20\text{ }^{\circ}\text{C}$.

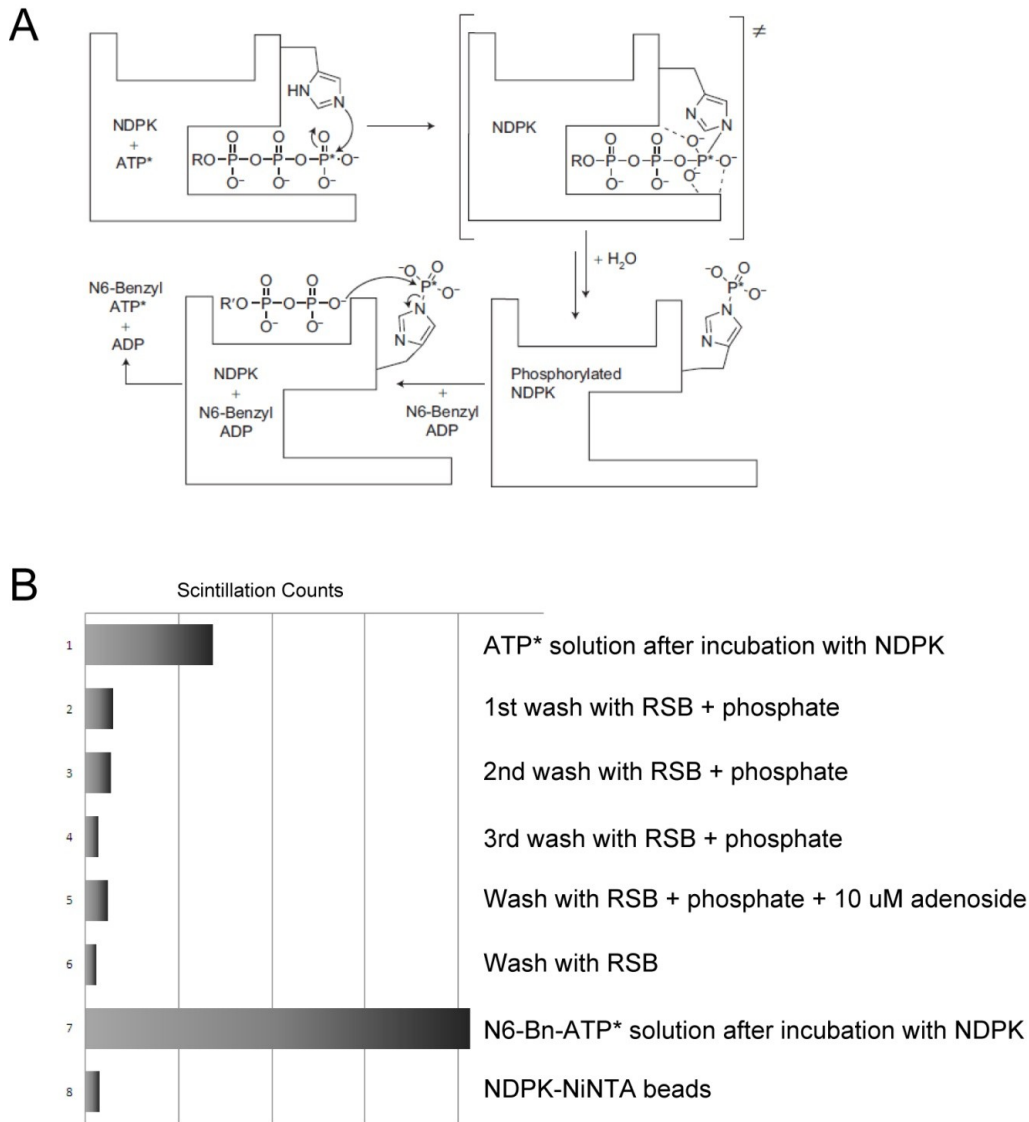


Figure 5 Generation of radioactive bumped ATP. (A) Diagram showing the transfer of $[\gamma\text{-}^{32}\text{P}]$ from ATP to bumped ATP using γNDPK (adapted from (Elphick, Lee et al. 2007)). (B) Tracking the radioactive signal generated in each step during a typical preparation. 1% of the solution from each step is used to monitor its radioactivity using scintillation counter. Numbers are averaged from duplicated measurements.

2) Test whether analog-sensitive EGFR kinase can effectively utilize bumped ATP

EGFR kinase is used as a model to investigate whether the chemical genetic approach with bumped ATP can be applied to ErbB kinases. In an *in vitro* radioactive kinase assay, both wildtype and T766G-mutated EGFR kinase can effectively utilize $[\gamma\text{-}^{32}\text{P}]\text{ATP}$ as substrate, whereas only analog-sensitive (T766G) EGFR kinase can utilize $[\gamma\text{-}^{32}\text{P}]\text{N}^6\text{-Bn-ATP}$ (Figure 6). Based on the readings from scintillation counter, we conclude that T766G-mutated EGFR kinase utilizes $[\gamma\text{-}^{32}\text{P}]\text{N}^6\text{-Bn-ATP}$ >100 times more efficiently than wildtype EGFR kinase.

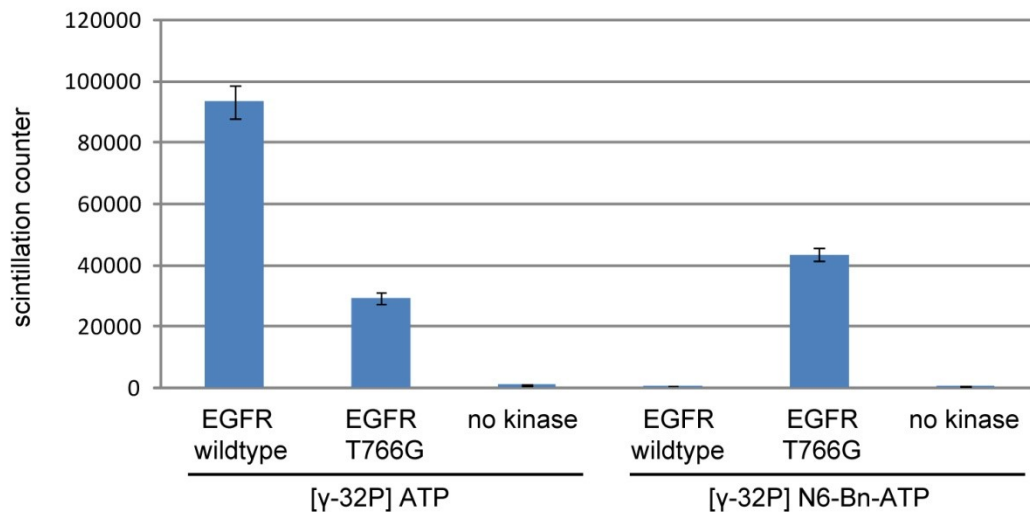


Figure 6: Bumped ATP (N6-Bn-ATP) can only be utilized by analog sensitive EGFR kinase but not wildtype EGFR kinase. In the kinase assays, 1 μM purified recombinant EGFR kinase domain (wildtype or T766G) is incubated with 100 μM ATP, ~ 1 μCi $[\gamma\text{-}^{32}\text{P}]\text{ATP}$ (or $[\gamma\text{-}^{32}\text{P}]\text{N}^6\text{-Bn-ATP}$), 200 μM poly GluTyr peptide substrate and 5 mM MgCl_2 for 5 minutes at room temperature. The reactions are stopped with

100mM EDTA and spotted onto nitrocellulose paper for washing and scintillation counting to measure the incorporation of ^{32}P . A no kinase control is also included. The measurements shown are the average values from duplicated experiments and the error bars represent one standard deviation. A maximal of 20% of total ^{32}P is incorporated in the assays.

3) Development of membrane permeabilization method that allows bumped ATP to pass through plasma membrane and enter into cytosol.

Permeabilization of cell membrane is needed for the negatively charged $[\gamma\text{-}^{32}\text{P}]\text{N6-Bn-ATP}$ to enter into cytosol and be utilized by kinases. At the same time, the disruption of cell membrane shall not interfere with ligand-induced ErbB dimerization/activation. We have shown that digitonin-permeabilization can meet such requirements, as demonstrated in both ErbB3 activation in T47D cells (Figure 7A) and EGFR activation in CHO cells (Figure 7B). In these experiments, cell pellets were mixed with equal volume of PBS (for intact cells) or cell lysis buffer (CLB, for permeabilized cells) containing 10 mM Tris pH 7.4, 150mM NaCl, protease inhibitors (1 mM PMSF, 10 μM leupeptin and 10 μM aprotinin), phosphatase inhibitors (25 mM NaF, 5 mM Na_2MoO_4 and 0.2 mM Na_3VO_4) and varying amount of digitonin (CALBIOCHEM Cat# 300410). Cell permeabilization was then verified by trypan blue staining and followed with ligand stimulation experiments. Reactions were stopped with 100 mM EDTA pH 8.0, and samples were prepared for SDS-PAGE and Western blotting.

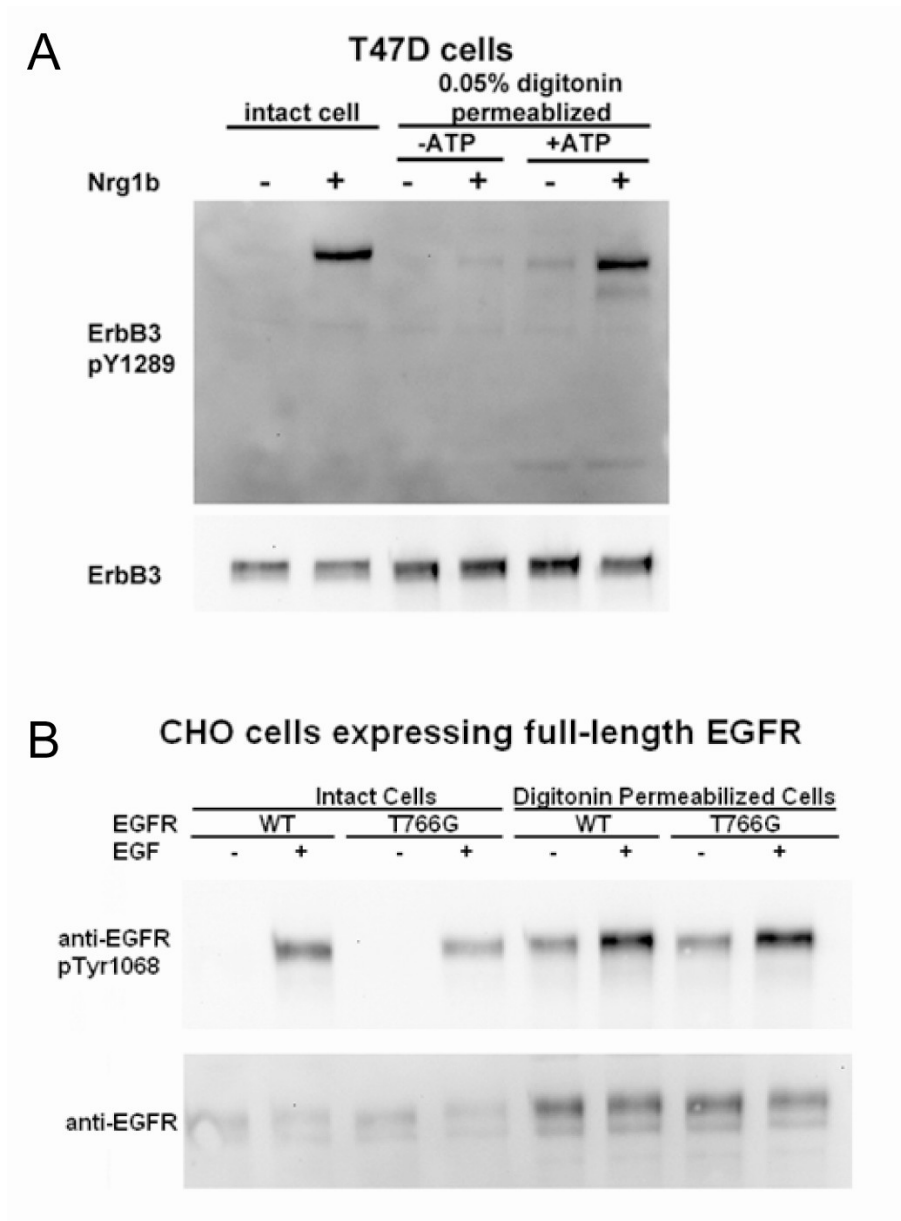


Figure 7 Permeabilization of cell membrane with digitonin does not affect ligand induced ErbB signaling. **(A)** Parental T47D cells were serum-starved overnight, detached from flasks with PBS+EDTA, washed in PBS, and then resuspended in cold PBS (for intact cells) or CLB buffer containing 0.05% (m/v) digitonin (for permeabilized cells). The volume of the resuspension buffer is equal to the volume of the cell pellet. Then 5mM MgCl₂ and optional 1 mM ATP were added to permeabilized cells. Cells were then stimulated with Nrg1β (40 ng/ml) for 5 minutes on ice and processed for Western blotting. **(B)** CHO cells transiently

transfected with EGFR (wildtype or T766G) were serum-starved overnight, washed and resuspended in cold PBS (for intact cells) or CLB buffer containing 0.01% (m/v) digitonin, 5mM MgCl₂ and 0.5 mM ATP. Cells were then stimulated with EGF (100 ng/ml) for 5 minutes on ice (for intact cells) or 3 minutes at room temperature (for permeabilized cells) and processed for Western blotting.

4) Using bumped ATP to trace protein phosphorylation mediated directly by EGFR

We have applied [γ -³²P]N6-Bn-ATP to permeabilized cells expressing wildtype or analog-sensitive (T766G) EGFR mutant and, after ligand stimulation experiment, used a radioactive phospho-image gel to look for protein substrates that carried the ³²P phosphate. Unfortunately, we could not identify any unique (or preferred) protein substrates in cells expressing T766G-mutated EGFR yet, due to the high background ³²P signals (many non-specifically labeled bands on the SDS-PAGE gel) in the assay. The main reasons for the high background signal are (a) many endogenous wildtype kinases can still utilize the bumped ATP as substrate at appreciable rates and (b) the γ -³²P phosphate on [γ -³²P]N6-Bn-ATP can be rapidly transferred onto other nucleotide diphosphate (NDPs) by endogenous NDPK in cells, which can then be effectively utilized by wildtype kinases.

Bibliography

- Adams, J. A. (2001). "Kinetic and catalytic mechanisms of protein kinases." Chemical Reviews **101**(8): 2271-2290.
- Alaimo, P. J., M. A. Shogren-Knaak, et al. (2001). "Chemical genetic approaches for the elucidation of signaling pathways." Current Opinion in Chemical Biology **5**(4): 360-367.
- Alaoui-Jamali, M. A., D. J. Song, et al. (2003). "Regulation of multiple tumor microenvironment markers by overexpression of single or paired combinations of ErbB receptors." Cancer Research **63**(13): 3764-3774.
- Arnold, K., L. Bordoli, et al. (2006). "The SWISS-MODEL workspace: a web-based environment for protein structure homology modelling." Bioinformatics **22**(2): 195-201.
- Azios, N. G., F. J. Romero, et al. (2001). "Expression of herstatin, an autoinhibitor of HER-2/neu, inhibits transactivation of HER-3 by HER-2 and blocks EGF activation of the EGF receptor." Oncogene **20**(37): 5199-5209.
- Baker, N. E. (1987). "MOLECULAR-CLONING OF SEQUENCES FROM WINGLESS, A SEGMENT POLARITY GENE IN DROSOPHILA - THE SPATIAL-DISTRIBUTION OF A TRANSCRIPT IN EMBRYOS." Embo Journal **6**(6): 1765-1773.
- Bandaranayake, R. M., D. Ungureanu, et al. (2012). "Crystal structures of the JAK2 pseudokinase domain and the pathogenic mutant V617F." Nat Struct Mol Biol **19**(8): 754-759.
- Baselga, J. and S. M. Swain (2009). "Novel anticancer targets: revisiting ERBB2 and discovering ERBB3." Nat. Rev. Cancer **9**: 463-475
- Bedard, P., F. Cardoso, et al. (2009). "Stemming Resistance to HER-2 Targeted Therapy." Journal of Mammary Gland Biology and Neoplasia **14**(1): 55-66.
- Bedard, P. L., F. Cardoso, et al. (2009). "Stemming Resistance to HER-2 Targeted Therapy." Journal of Mammary Gland Biology and Neoplasia **14**(1): 55-66.
- Benkert, P., M. Biasini, et al. "Toward the estimation of the absolute quality of individual protein structure models." Bioinformatics.
- Berger, M. B., J. M. Mendrola, et al. (2004). "ErbB3/HER3 does not homodimerize upon neuregulin binding at the cell surface." FEBS Lett. **569**: 332-336.
- Bishop, A. C., C.-y. Kung, et al. (1999). "Generation of Monospecific Nanomolar Tyrosine Kinase Inhibitors via a Chemical Genetic Approach." Journal of the American Chemical Society **121**(4): 627-631.
- Bonkowsky, J. L., S. Yoshikawa, et al. (1999). "Axon routing across the midline controlled by the Drosophila Derailed receptor." Nature **402**(6761): 540-544.
- Boudeau, J., D. Miranda-Saavedra, et al. (2006). "Emerging roles of pseudokinases." Trends Cell Biol. **16**: 443-452.
- Boudeau, J., J. W. Scott, et al. (2004). "Analysis of the LKB1-STRAD-MO25 complex." Journal of Cell Science **117**(26): 6365-6375.
- Brennan, D. F., A. C. Dar, et al. (2011). "A Raf-induced allosteric transition of KSR stimulates phosphorylation of MEK." Nature **472**(7343): 366-U134.

- Brünger, A. T., P. D. Adams, et al. (1998). "Crystallography & NMR system: A new software suite for macromolecular structure determination." Acta Crystallogr. D Biol. Crystallogr. **54**(Pt 5): 905-21.
- Buck, E., A. Eyzaguirre, et al. (2006). "Inactivation of Akt by the epidermal growth factor receptor inhibitor erlotinib is mediated by HER-3 in pancreatic and colorectal tumor cell lines and contributes to erlotinib sensitivity." Molecular Cancer Therapeutics **5**(8): 2051-2059.
- Burgess, A. W., H.-S. Cho, et al. (2003). "An Open-and-Shut Case? Recent Insights into the Activation of EGF/ErbB Receptors." Molecular Cell **12**(3): 541-552.
- Bush, J. O. and P. Soriano (2010). "Ephrin-B1 forward signaling regulates craniofacial morphogenesis by controlling cell proliferation across Eph-Ephrin boundaries." Genes & Development **24**(18): 2068-2080.
- Callahan, C. A., J. L. Bonkovsky, et al. (1996). "derailed is required for muscle attachment site selection in Drosophila." Development **122**(9): 2761-2767.
- Callahan, C. A., M. G. Muralidhar, et al. (1995). "CONTROL OF NEURONAL PATHWAY SELECTION BY A DROSOPHILA RECEPTOR PROTEIN-TYROSINE KINASE FAMILY MEMBER." Nature **376**(6536): 171-174.
- Castaneda, C., H. Cortes-Funes, et al. (2010). "The phosphatidyl inositol 3-kinase/AKT signaling pathway in breast cancer." Cancer and Metastasis Reviews **29**(4): 751-759.
- CCP4 (Collaborative Computational Project Number 4) (1994). "The CCP4 suite: Programs for protein crystallography." Acta Crystallogr. D Biol. Crystallogr. **50**: 760-763.
- Chan, T. O., J. Zhang, et al. (2011). "Resistance of Akt kinases to dephosphorylation through ATP-dependent conformational plasticity." Proceedings of the National Academy of Sciences of the United States of America **108**(46): E1120-E1127.
- Chen, F. L., W. L. Xia, et al. (2008). "Acquired Resistance to Small Molecule ErbB2 Tyrosine Kinase Inhibitors." Clinical Cancer Research **14**(21): 6730-6734.
- Cheng, K. and J. G. Koland (1998). "Nucleotide-binding properties of kinase-deficient epidermal-growth-factor-receptor mutants." Biochem. J. **330**: 353-359.
- Choi, S. H., J. M. Mendrola, et al. (2007). "EGF-independent activation of cell-surface EGF receptors harboring mutations found in gefitinib-sensitive lung cancer." Oncogene **26**: 1567-1576.
- Citri, A., K. B. Skaria, et al. (2003). "The deaf and the dumb: the biology of ErbB-2 and ErbB-3." Exp. Cell. Res. **284**(1): 54-65.
- Cleland, W. W. and A. C. Hengge (1995). "Mechanisms of phosphoryl and acyl transfer." Faseb Journal **9**(15): 1585-1594.
- Clevers, H. and R. Nusse (2012). "Wnt/b-Catenin Signaling and Disease." Cell **149**(6): 1192-1205.
- Cobb, M. H., B. C. Sang, et al. (1989). "Autophosphorylation activates the soluble cytoplasmic domain of the insulin receptor in an intermolecular reaction." J. Biol. Chem. **264**: 18701-18706.
- Coker, K. J., J. V. Staros, et al. (1994). "A KINASE-NEGATIVE EPIDERMAL GROWTH-FACTOR RECEPTOR THAT RETAINS THE CAPACITY TO

- STIMULATE DNA-SYNTHESIS." Proceedings of the National Academy of Sciences of the United States of America **91**(15): 6967-6971.
- Cole, P. A., A. D. Courtney, et al. (2003). "Chemical approaches to reversible protein phosphorylation." Accounts of Chemical Research **36**(6): 444-452.
- Cole, P. A., M. R. Grace, et al. (1995). "The role of the catalytic base in the protein tyrosine kinase Csk." J. Biol. Chem. **270**: 22105-22108.
- Dall'Acqua, W. and P. Carter (2000). "Substrate-assisted catalysis: Molecular basis and biological significance." Protein Science **9**(1): 1-9.
- Dann, C. E., J.-C. Hsieh, et al. (2001). "Insights into Wnt binding and signalling from the structures of two Frizzled cysteine-rich domains." Nature **412**(6842): 86-90.
- Dawson, J. P., M. B. Berger, et al. (2005). "Epidermal Growth Factor Receptor Dimerization and Activation Require Ligand-Induced Conformational Changes in the Dimer Interface." Molecular and Cellular Biology **25**(17): 7734-7742.
- De, A. (2011). "Wnt/Ca²⁺ signaling pathway: a brief overview." Acta Biochimica Et Biophysica Sinica **43**(10): 745-756.
- DeLano, W. L. (2002). The PyMOL Molecular Graphics System. Palo Alto, CA, USA, DeLano Scientific
- Dura, J. M., E. Taillebourg, et al. (1995). "THE DROSOPHILA LEARNING AND MEMORY GENE LINOTTE ENCODES A PUTATIVE RECEPTOR TYROSINE KINASE HOMOLOGOUS TO THE HUMAN RYK GENE-PRODUCT." Febs Letters **370**(3): 250-254.
- Elphick, L. M., S. E. Lee, et al. (2007). "Using Chemical Genetics and ATP Analogues To Dissect Protein Kinase Function." ACS Chemical Biology **2**(5): 299-314.
- Emsley, P. and K. Cowtan (2004). "Coot: model-building tools for molecular graphics." Acta Crystallogr. D Biol. Crystallogr. **60**(Pt 12 Pt 1): 2126-32.
- Engelman, J. A., P. A. Janne, et al. (2005). "ErbB-3 mediates phosphoinositide 3-kinase activity in gefitinib-sensitive non-small cell lung cancer cell lines." Proceedings of the National Academy of Sciences of the United States of America **102**(10): 3788-3793.
- Engelman, J. A., K. Zejnullahu, et al. (2007). "MET amplification leads to gefitinib resistance in lung cancer by activating ERBB3 signaling." Science **316**(5827): 1039-1043.
- Faltus, T., J. P. Yuan, et al. (2004). "Silencing of the HER2/neu gene by siRNA inhibits proliferation and induces apoptosis in HER2/neu-overexpressing breast cancer cells." Neoplasia **6**(6): 786-795.
- Fan, Y.-X., L. Wong, et al. (2005). "EGFR kinase possesses a broad specificity for ErbB phosphorylation sites, and ligand increases catalytic-centre activity without affecting substrate binding affinity." Biochem. J. **392**(3): 417-423.
- Favelyukis, S., J. H. Till, et al. (2001). "Structure and autoregulation of the insulin-like growth factor 1 receptor kinase." Nat. Struct. Mol. Biol. **8**: 1058-1063.
- Ferguson, K. M., P. J. Darling, et al. (2000). "Extracellular domains drive homo- but not heterodimerization of erbB receptors." Embo Journal **19**(17): 4632-4643.
- Ferretti, G., A. Felici, et al. (2007). "HER2/neu role in breast cancer: from a prognostic foe to a predictive friend." Current Opinion in Obstetrics & Gynecology **19**(1): 56-62.

- Fradkin, L. G., J. N. Noordermeer, et al. (1995). "THE DROSOPHILA WNT PROTEIN DWNT-3 IS A SECRETED GLYCOPROTEIN LOCALIZED ON THE AXON TRACTS OF THE EMBRYONIC CNS." Developmental Biology **168**(1): 202-213.
- Fradkin, L. G., M. van Schie, et al. (2004). "The Drosophila Wnt5 protein mediates selective axon fasciculation in the embryonic central nervous system." Developmental Biology **272**(2): 362-375.
- Furdui, C. M., E. D. Lew, et al. (2006). "Autophosphorylation of FGFR1 kinase is mediated by a sequential and precisely ordered reaction." Mol. Cell **21**: 711-717.
- Gibbs, C. S. and M. J. Zoller (1991). "Rational scanning mutagenesis of a protein kinase identifies functional regions involved in catalysis and substrate interactions." J. Biol. Chem. **266**: 8923-8931.
- Grillenzoni, N., A. Flandre, et al. (2007). "Respective roles of the DRL receptor and its ligand WNT5 in Drosophila mushroom body development." Development **134**(17): 3089-3097.
- Guy, P. M., J. V. Platko, et al. (1994). "Insect cell-expressed p180erbB3 possesses an impaired tyrosine kinase activity." Proc. Natl. Acad. Sci. U. S. A. **91**(17): 8132-6.
- Halford, M. M., J. Armes, et al. (2000). "Ryk-deficient mice exhibit craniofacial defects associated with perturbed Eph receptor crosstalk." Nature Genetics **25**(4): 414-418.
- Halford, M. M., A. C. Oates, et al. (1999). "Genomic structure and expression of the mouse growth factor receptor related to tyrosine kinases (Ryk)." Journal of Biological Chemistry **274**(11): 7379-7390.
- Halford, M. M. and S. A. Stacker (2001). "Revelations of the RYK receptor." Bioessays **23**(1): 34-45.
- Hamburger, A. W. (2008). "The role of ErbB3 and its binding partners in breast cancer progression and resistance to hormone and tyrosine kinase directed therapies." Journal of Mammary Gland Biology and Neoplasia **13**(2): 225-233.
- Hanks, S. K., A. M. Quinn, et al. (1988). "The protein kinase family: conserved features and deduced phylogeny of the catalytic domains." Science **241**: 42-52.
- Harris, K. E. and S. K. Beckendorf (2007). "Different Wnt signals act through the Frizzled and RYK receptors during Drosophila salivary gland migration." Development **134**(11): 2017-2025.
- Hellyer, N. J., K. Cheng, et al. (1998). "ErbB3 (HER3) interaction with the p85 regulatory subunit of phosphoinositide 3-kinase." Biochemical Journal **333**: 757-763.
- Hellyer, N. J., M.-S. Kim, et al. (2001). "Heregulin-dependent Activation of Phosphoinositide 3-Kinase and Akt via the ErbB2/ErbB3 Co-receptor." Journal of Biological Chemistry **276**(45): 42153-42161.
- Holbro, T., R. R. Beerli, et al. (2003). "The ErbB2/ErbB3 heterodimer functions as an oncogenic unit: ErbB2 requires ErbB3 to drive breast tumor cell proliferation." Proc. Natl. Acad. Sci. U. S. A. **100**: 8933-8938.
- Holbro, T. and N. E. Hynes (2004). "ErbB receptors: Directing key signaling networks throughout life." Annual Review of Pharmacology and Toxicology **44**: 195-217.

- Honegger, A. M., T. J. Dull, et al. (1987). "Point mutation at the ATP binding site of EGF receptor abolishes protein-tyrosine kinase activity and alters cellular routing." Cell **51**: 199-209.
- Honegger, A. M., R. M. Kris, et al. (1989). "EVIDENCE THAT AUTOPHOSPHORYLATION OF SOLUBILIZED RECEPTORS FOR EPIDERMAL GROWTH-FACTOR IS MEDIATED BY INTERMOLECULAR CROSS-PHOSPHORYLATION." Proceedings of the National Academy of Sciences of the United States of America **86**(3): 925-929.
- Honegger, A. M., A. Schmidt, et al. (1990). "EVIDENCE FOR EPIDERMAL GROWTH-FACTOR (EGF)-INDUCED INTERMOLECULAR AUTOPHOSPHORYLATION OF THE EGF RECEPTORS IN LIVING CELLS." Molecular and Cellular Biology **10**(8): 4035-4044.
- Hovens, C. M., S. A. Stacker, et al. (1992). "RYK, A RECEPTOR TYROSINE KINASE-RELATED MOLECULE WITH UNUSUAL KINASE DOMAIN MOTIFS." Proceedings of the National Academy of Sciences of the United States of America **89**(24): 11818-11822.
- Hsieh, J.-C., L. Kodjabachian, et al. (1999). "A new secreted protein that binds to Wnt proteins and inhibits their activities." Nature **398**(6726): 431-436.
- Hu, J., H. Yu, et al. (2011). "Mutation that blocks ATP binding creates a pseudokinase stabilizing the scaffolding function of kinase suppressor of Ras, CRAF and BRAF." Proceedings of the National Academy of Sciences **108**(15): 6067-6072.
- Hubbard, S. R., M. Mohammadi, et al. (1998). "Autoregulatory mechanisms in protein-tyrosine kinases." Journal of Biological Chemistry **273**(20): 11987-11990.
- Huse, M. and J. Kuriyan (2002). "The conformational plasticity of protein kinases." Cell **109**(3): 275-282.
- Hynes, N. E. and G. MacDonald (2009). "ErbB receptors and signaling pathways in cancer." Curr. Opin. Cell Biol. **21**: 177-184.
- Ikeya, M. and S. Takada (1998). "Wnt signaling from the dorsal neural tube is required for the formation of the medial dermomyotome." Development **125**(24): 4969-4976.
- Iyer, G. H., S. Garrod, et al. (2005). "Catalytic independent functions of a protein kinase as revealed by a kinase-dead mutant: study of the Lys72His mutant of cAMP-dependent kinase." J. Mol. Biol. **351**: 1110-1122.
- Janda, C. Y., D. Waghray, et al. "Structural Basis of Wnt Recognition by Frizzled." Science.
- Janda, C. Y., D. Waghray, et al. (2012). "Structural Basis of Wnt Recognition by Frizzled." Science **337**(6090): 59-64.
- Jura, N., N. F. Endres, et al. (2009). "Mechanism for activation of the EGF receptor catalytic domain by the juxtamembrane segment." Cell **137**: 1293-1307.
- Jura, N., Y. Shan, et al. (2009). "Structural analysis of the catalytically inactive kinase domain of the human EGF receptor 3." Proc. Natl. Acad. Sci. U. S. A. **106**: 21608-21613.
- Kamitori, K., M. Tanaka, et al. (2005). "Receptor related to tyrosine kinase RYK regulates cell migration during cortical development." Biochemical and Biophysical Research Communications **330**(2): 446-453.

- Katoh, M. and M. Katoh (2007). "WNT Signaling Pathway and Stem Cell Signaling Network." Clinical Cancer Research **13**(14): 4042-4045.
- Katso, R. M., R. B. Russell, et al. (1999). "Functional analysis of H-Ryk, an atypical member of the receptor tyrosine kinase family." Molecular and Cellular Biology **19**(9): 6427-6440.
- Katso, R. M. T., S. Manek, et al. (1999). "Overexpression of H-Ryk in mouse fibroblasts confers transforming ability in vitro and in vivo: Correlation with up-regulation in epithelial ovarian cancer." Cancer Research **59**(10): 2265-2270.
- Keeble, T. R., M. M. Halford, et al. (2006). "The Wnt receptor Ryk is required for Wnt5a-mediated axon guidance on the contralateral side of the corpus callosum." Journal of Neuroscience **26**(21): 5840-5848.
- Kim, K. and P. A. Cole (1997). "Measurement of a Bronsted nucleophile coefficient and insights into the transition state for a protein tyrosine kinase." Journal of the American Chemical Society **119**(45): 11096-11097.
- Kim, K. and P. A. Cole (1998). "Kinetic analysis of a protein tyrosine kinase reaction transition state in the forward and reverse directions." Journal of the American Chemical Society **120**(28): 6851-6858.
- Kraus, M. H., W. Issing, et al. (1989). "Isolation and characterization of ERBB3, a third member of the ERBB/epidermal growth factor receptor family: evidence for overexpression in a subset of human mammary tumors." Proc. Natl. Acad. Sci. U. S. A. **86**: 9193-9197.
- Krissinel, E. and K. Henrick (2004). "Secondary-structure matching (SSM), a new tool for fast protein structure alignment in three dimensions." Acta Crystallographica Section D-Biological Crystallography **60**: 2256-2268.
- Kurayoshi, M., H. Yamamoto, et al. (2007). "Post-translational palmitoylation and glycosylation of Wnt-5a are necessary for its signalling." Biochemical Journal **402**: 515-523.
- Lammers, R., E. Vanobberghen, et al. (1990). "TRANSPHOSPHORYLATION AS A POSSIBLE MECHANISM FOR INSULIN AND EPIDERMAL GROWTH-FACTOR RECEPTOR ACTIVATION." Journal of Biological Chemistry **265**(28): 16886-16890.
- Lee-Hoeflich, S. T., L. Crocker, et al. (2008). "A central role for HER3 in HER2-amplified breast cancer: implications for targeted therapy." Cancer Research **68**(14): 5878-5887.
- Lemmon, M. A. (2009). "Ligand-induced ErbB receptor dimerization." Exp. Cell Res. **315**: 638-648
- Lemmon, M. A. and J. Schlessinger (2010). "Cell Signaling by Receptor Tyrosine Kinases." Cell **141**(7): 1117-1134.
- Li, L., B. I. Hutchins, et al. (2009). "Wnt5a Induces Simultaneous Cortical Axon Outgrowth and Repulsive Axon Guidance through Distinct Signaling Mechanisms." Journal of Neuroscience **29**(18): 5873-5883.
- Liepinsh, E., L. Banyai, et al. (2006). "NMR structure of the WIF domain of the human Wnt-inhibitory factor-1." Journal of Molecular Biology **357**(3): 942-950.
- Lin, K., J. Lin, et al. (2012). "An ATP-Site On-Off Switch That Restricts Phosphatase Accessibility of Akt." Science signaling **5**(223): ra37.

- Liu, Y. B., J. Shi, et al. (2005). "Ryk-mediated Wnt repulsion regulates posterior-directed growth of corticospinal tract." Nature Neuroscience **8**(9): 1151-1159.
- Logan, C. Y. and R. Nusse (2004). "The Wnt signaling pathway in development and disease." Annual Review of Cell and Developmental Biology **20**: 781-810.
- Lu, W. G., V. Yamamoto, et al. (2004). "Mammalian Ryk is a Wnt coreceptor required for stimulation of neurite outgrowth." Cell **119**(1): 97-108.
- Lyu, J., R. L. Wesselschmidt, et al. (2009). "Cdc37 Regulates Ryk Signaling by Stabilizing the Cleaved Ryk Intracellular Domain." Journal of Biological Chemistry **284**(19): 12940-12948.
- Lyu, J., V. Yamamoto, et al. (2008). "Cleavage of the Wnt Receptor Ryk Regulates Neuronal Differentiation during Cortical Neurogenesis." Developmental Cell **15**(5): 773-780.
- MacDonald, B. T., K. Tamai, et al. (2009). "Wnt/beta-Catenin Signaling: Components, Mechanisms, and Diseases." Developmental Cell **17**(1): 9-26.
- Malinauskas, T., A. R. Aricescu, et al. (2011). "Modular mechanism of Wnt signaling inhibition by Wnt inhibitory factor 1." Nature Structural & Molecular Biology **18**(8): 886-U43.
- Min, X. S., B. H. Lee, et al. (2004). "Crystal structure of the kinase domain of WNK1, a kinase that causes a hereditary form of hypertension." Structure **12**(7): 1303-1311.
- Moreau-Fauvarque, C., E. Taillebourg, et al. (1998). "The receptor tyrosine kinase gene *linotte* is required for neuronal pathway selection in the *Drosophila* mushroom bodies." Mechanisms of Development **78**(1-2): 47-61.
- Mukherjee, K., M. Sharma, et al. (2008). "CASK functions as a Mg²⁺-independent neurexin kinase." Cell **133**(2): 328-339.
- Nahta, R. and F. J. Esteva (2006). "Herceptin: mechanisms of action and resistance." Cancer Letters **232**(2): 123-138.
- Oates, A. C., J. L. Bonkovsky, et al. (1998). "Embryonic expression and activity of doughnut, a second RYK homolog in *Drosophila*." Mechanisms of Development **78**(1-2): 165-169.
- Otwinowski, Z. and W. Minor (1997). "Processing of X-ray diffraction data collected in oscillation mode." Methods Enzymol. **276**: 307-326.
- Park, J. W., R. A. Neve, et al. (2008). "Unraveling the Biologic and Clinical Complexities of HER2." Clinical Breast Cancer **8**(5): 392-401.
- Pettersen, E. F., T. D. Goddard, et al. (2004). "UCSF Chimera—A visualization system for exploratory research and analysis." Journal of Computational Chemistry **25**(13): 1605-1612.
- Plowman, G. D., G. S. Whitney, et al. (1990). "Molecular cloning and expression of an additional epidermal growth factor receptor-related gene." Proc. Natl. Acad. Sci. U. S. A. **87**: 4905-4909.
- Prigent, S. A. and W. J. Gullick (1994). "Identification of C-ErbB-3 Binding-Sites for Phosphatidylinositol 3'-Kinase and Shc Using an Egf Receptor C-ErbB-3 Chimera." Embo Journal **13**(12): 2831-2841.
- Qian, X. L., C. M. Levea, et al. (1994). "Heterodimerization of Epidermal Growth-Factor Receptor and Wild-Type or Kinase-Deficient Neu - a Mechanism of Interreceptor

- Kinase Activation and Transphosphorylation." Proceedings of the National Academy of Sciences of the United States of America **91**(4): 1500-1504.
- Qiu, C., M. K. Tarrant, et al. (2009). "In vitro enzymatic characterization of near full length EGFR in activated and inhibited states." Biochemistry **48**: 6624-6632.
- Qiu, C., M. K. Tarrant, et al. (2008). "Mechanism of activation and inhibition of the HER4/ErbB4 kinase." Structure **16**: 460-467.
- Red Brewer, M., S. H. Choi, et al. (2009). "The juxtamembrane region of the EGF receptor functions as an activation domain." Mol. Cell **34**: 641-651.
- Riese, D. J., 2nd, T. M. van Raaij, et al. (1995). "The cellular response to neuregulins is governed by complex interactions of the erbB receptor family." Mol. Cell. Biol. **15**(10): 5770-6.
- Riese, D. J., T. M. van Raaij, et al. (1995). "The cellular response to neuregulins is governed by complex interactions of the erbB receptor family." Molecular and Cellular Biology **15**(10): 5770-6.
- Sakurai, M., T. Aoki, et al. (2009). "Differentially Expressed Drl and Drl-2 Play Opposing Roles in Wnt5 Signaling during Drosophila Olfactory System Development." Journal of Neuroscience **29**(15): 4972-4980.
- Sala, G., S. Traini, et al. (2011). "An ErbB-3 antibody, MP-RM-1, inhibits tumor growth by blocking ligand-dependent and independent activation of ErbB-3/Akt signaling." Oncogene **31**(10): 1275-1286.
- Schaefer, G., L. Haber, et al. (2011). "A Two-in-One Antibody against HER3 and EGFR Has Superior Inhibitory Activity Compared with Monospecific Antibodies." Cancer Cell **20**(4): 472-486.
- Schlessinger, J. (2000). "Cell signaling by receptor tyrosine kinases." Cell **103**(2): 211-25.
- Schmitt, A. M., J. Shi, et al. (2006). "Wnt-Ryk signalling mediates medial-lateral retinotectal topographic mapping." Nature **439**(7072): 31-37.
- Schoeberl, B., A. C. Faber, et al. (2010). "An ErbB3 Antibody, MM-121, Is Active in Cancers with Ligand-Dependent Activation." Cancer Research **70**(6): 2485-2494.
- Sergina, N. V., M. Rausch, et al. (2007). "Escape from HER-family tyrosine kinase inhibitor therapy by the kinase-inactive HER3." Nature **445**(7126): 437-441.
- Sharma, S. V., D. W. Bell, et al. (2007). "Epidermal growth factor receptor mutations in lung cancer." Nat. Rev. Cancer **7**: 169-181.
- Sharma, S. V., D. W. Bell, et al. (2007). "Epidermal growth factor receptor mutations in lung cancer." Nat Rev Cancer **7**(3): 169-181.
- Shen, K., A. C. Hines, et al. (2005). "Protein kinase structure and function analysis with chemical tools." Biochimica Et Biophysica Acta-Proteins and Proteomics **1754**(1-2): 65-78.
- Shi, F. and M. A. Lemmon (2011). "KSR Plays CRAF-ty." Science **332**(6033): 1043-1044.
- Shi, F., S. E. Telesco, et al. (2010). "ErbB3/HER3 intracellular domain is competent to bind ATP and catalyze autophosphorylation." Proceedings of the National Academy of Sciences **107**(17): 7692-7697.
- Shrout, A. L., D. J. Montefusco, et al. (2003). "Template-directed assembly of receptor signaling complexes." Biochemistry **42**: 13379-13385.

- Sierke, S. L., K. Cheng, et al. (1997). "Biochemical characterization of the protein tyrosine kinase homology domain of the ErbB3 (HER3) receptor protein." Biochem. J. **322 (Pt 3)**: 757-63.
- Sithanandam, G. and L. M. Anderson (2008). "The ERBB3 receptor in cancer and cancer gene therapy." Cancer Gene Therapy **15(7)**: 413-448.
- Soler, M., F. Mancini, et al. (2009). "HER3 is required for the maintenance of neuregulin-dependent and -independent attributes of malignant progression in prostate cancer cells." International Journal of Cancer **125(11)**: 2565-2575.
- Soltoff, S. P., K. L. Carraway, et al. (1994). "ERBB3 IS INVOLVED IN ACTIVATION OF PHOSPHATIDYLINOSITOL 3-KINASE BY EPIDERMAL GROWTH-FACTOR." Molecular and Cellular Biology **14(6)**: 3550-3558.
- Stamos, J., M. X. Sliwkowski, et al. (2002). "Structure of the epidermal growth factor receptor kinase domain alone and in complex with a 4-anilinoquinazoline inhibitor." Journal of Biological Chemistry **277(48)**: 46265-46272.
- Taillebourg, E., C. Moreau-Fauvarque, et al. (2005). "In vivo evidence for a regulatory role of the kinase activity of the linotte/derailed receptor tyrosine kinase, a *Drosophila* Ryk ortholog." Development Genes and Evolution **215(3)**: 158-163.
- Takada, R., Y. Satomi, et al. (2006). "Monounsaturated Fatty Acid Modification of Wnt Protein: Its Role in Wnt Secretion." Developmental Cell **11(6)**: 791-801.
- Tice, D. A., J. S. Biscardi, et al. (1999). "Mechanism of biological synergy between cellular Src and epidermal growth factor receptor." Proceedings of the National Academy of Sciences of the United States of America **96(4)**: 1415-1420.
- Till, J. H., M. Becerra, et al. (2002). "Crystal structure of the MuSK tyrosine kinase: insights into receptor autoregulation." Structure **10**: 1187-1196.
- Travis, A., S. E. Pinder, et al. (1996). "C-erbB-3 in human breast carcinoma: Expression and relation to prognosis and established prognostic indicators." British Journal of Cancer **74(2)**: 229-233.
- Trivier, E. and T. S. Ganesan (2002). "RYK, a catalytically inactive receptor tyrosine kinase, associates with EphB2 and EphB3 but does not interact with AF-6." Journal of Biological Chemistry **277(25)**: 23037-23043.
- van Amerongen, R., A. Mikels, et al. (2008). "Alternative Wnt Signaling Is Initiated by Distinct Receptors." Science Signaling **1(35)**: 5.
- van der Horst, E. H., M. Murgia, et al. (2005). "Anti-HER-3 MAbs inhibit HER-3-mediated signaling in breast cancer cell lines resistant to anti-HER-2 antibodies." International Journal of Cancer **115(4)**: 519-527.
- Villa, F., P. Capasso, et al. (2009). "Crystal structure of the catalytic domain of Haspin, an atypical kinase implicated in chromatin organization." Proceedings of the National Academy of Sciences of the United States of America **106(48)**: 20204-20209.
- Wang, Y. (2009). "Wnt/Planar cell polarity signaling: A new paradigm for cancer therapy." Molecular Cancer Therapeutics **8(8)**: 2103-2109.
- Willert, K., J. D. Brown, et al. (2003). "Wnt proteins are lipid-modified and can act as stem cell growth factors." Nature **423(6938)**: 448-452.
- Williams, D. M., D. X. Wang, et al. (2000). "Chemical rescue of a mutant protein-tyrosine kinase." Journal of Biological Chemistry **275(49)**: 38127-38130.

- Winn, M. D., M. N. Isupov, et al. (2001). "Use of TLS anisotropic displacements in macromolecular refinement." *Acta Crystallogr. D Biol. Crystallogr.* **57**: 122–133.
- Wood, E. R., A. T. Truesdale, et al. (2004). "A Unique Structure for Epidermal Growth Factor Receptor Bound to GW572016 (Lapatinib)." *Cancer Research* **64**(18): 6652-6659.
- Wouda, R. R., M. Bansraj, et al. (2008). "Src family kinases are required for WNT5 signaling through the Derailed/RYK receptor in the Drosophila embryonic central nervous system." *Development* **135**(13): 2277-2287.
- Xu, X., H. Nagarajan, et al. (2011). "The genomic sequence of the Chinese hamster ovary (CHO)-K1 cell line." *Nat Biotech* **29**(8): 735-741.
- Yao, Y., Y. Wu, et al. (2007). "Antagonistic roles of Wnt5 and the Drl receptor in patterning the Drosophila antennal lobe." *Nature Neuroscience* **10**(11): 1423-1432.
- Yarden, Y. and M. X. Sliwkowski (2001). "Untangling the ErbB signalling network." *Nat. Rev. Mol. Cell. Biol.* **2**(2): 127-37.
- Yee, K., T. R. Bishop, et al. (1993). "ISOLATION OF A NOVEL RECEPTOR TYROSINE KINASE CDNA EXPRESSED BY DEVELOPING ERYTHROID PROGENITORS." *Blood* **82**(4): 1335-1343.
- Yokoyama, H., T. Maruoka, et al. "Different Requirement for Wnt/beta-Catenin Signaling in Limb Regeneration of Larval and Adult Xenopus." *Plos One* **6**(7).
- Yoo, J. Y. and A. W. Hamburger (1998). "The use of the yeast two hybrid system to evaluate ErbB-3 interactions with SH2 domain containing proteins." *Biochemical and Biophysical Research Communications* **251**(3): 903-906.
- Yoshikawa, S., J. L. Bonkowsky, et al. (2001). "The Derailed guidance receptor does not require kinase activity in vivo." *Journal of Neuroscience* **21**(1): art. no.-RC119.
- Yoshikawa, S., R. D. McKinnon, et al. (2003). "Wnt-mediated axon guidance via the Drosophila derailed receptor." *Nature* **422**(6932): 583-588.
- Zhang, X., J. Gureasko, et al. (2006). "An allosteric mechanism for activation of the kinase domain of epidermal growth factor receptor." *Cell* **125**: 1137-1149.
- Zhang, X. W., J. Gureasko, et al. (2006). "An allosteric mechanism for activation of the kinase domain of epidermal growth factor receptor." *Cell* **125**(6): 1137-1149.
- Zhong, J., H.-T. Kim, et al. (2011). "The Wnt receptor Ryk controls specification of GABAergic neurons versus oligodendrocytes during telencephalon development." *Development* **138**(3): 409-419.